REPUBLIC OF TURKEY

YILDIZ TECHNICAL UNIVERSITY

GRADUATE SCHOOL OF NATURAL AND APPLIED SCIENCES

SIMULATION AND EXPERIMENTAL ANAYSIS OF DOUBLY-FED INDUCTION GENERATOR UNDER GRID FAULTS

YUSUF YAŞA

MSc. THESIS
DEPARTMENT OF ELECTRICAL ENGINEERING
PROGRAM OF ELECTRICAL MACHINES AND POWER ELECTRONICS

ADVISER

ASSOC. PROF. DR. ERKAN MEŞE

ISTANBUL, 2013

REPUBLIC OF TURKEY

YILDIZ TECHNICAL UNIVERSITY

GRADUATE SCHOOL OF NATURAL AND APPLIED SCIENCES

SIMULATION AND EXPERIMENTAL ANAYSIS OF DOUBLY-FED INDUCTION GENERATOR UNDER GRID FAULTS

A thesis submitted by Yusuf YAŞA in partial fulfillment of the requirements for the degree of **MASTER OF SCIENCE** is approved by the committee on 17.05.2013 in Department of Electrical Engineering, Electrical Machines and Power Electronics Program.

Thesis Adviser

Assoc. Prof. Dr. Erkan MEŞE

Yıldız Technical University

Approved By the Examining Committee

Assoc. Prof. Dr. Erkan MEŞE

Yıldız Technical University_____________________

Assoc. Prof. Dr. A. Faruk BAKAN, Member

Yıldız Technical University_____________________

Assoc. Prof. Dr. Hakan HOCAOĞLU, Member

Gebze Institute of Technology_____________________

ACKNOWLEDGEMENTS

This thesis presents the analysis of wind turbine systems with using embedded control techniques. The study is implemented with simulation and experimental. The thesis theoretical part of the thesis was studied in University of AKRON, USA and experimental setup was implemented in both the University of Akron and Yıldız Technical University. I should appreciate to Assist. Prof. Dr. Yılmaz SÖZER in electrical engineering department at University of Akron/USA and to my adviser Assoc. Prof. Dr. Erkan MEŞE for their support, patience and for their technical briefings. Also I should thank to my close friends Assist. Prof. Dr. Evren İŞEN, Tausif HUSAIN and Mr. Erik RINALDO for their supports during installation of experimental setup in University of Akron.

Furthermore, I should appreciate my family for their patience and tolerance during my intensive study.

April, 2013

Yusuf YAŞA

TABLE OF CONTENTS

Page

LIST OF SYMBOLS

d	d axis component
f	Voltage, current or flux linkage
i	Current
Ks	Transformation matrix
L	Inductance
Lm	Mutual inductance
Lr	Rotor self-inductance
Ls	Stator self-inductance
M	Mutual inductance
n	Sector number
nmech	Mechanical speed (rpm)
ns	Synchronous speed (rpm)
Pmech	Mechanical power
Pr	Rotor electrical power
Ps	Stator electrical power
p	Derivative
r	Resistance
s	Slip
Tmech	Mechanical torque
Ts	Switching period
v	Voltage
Vdc	DC bus voltage
q	q axis component
λ	Flux linkage
Өr	Rotor position
ω	Radial speed
x	Reactance
ψ	Flux linkage

LIST OF ABBREVIATIONS

DFIG	Doubly Fed Induction Generator
PMSG	Permanent Magnet Synchronous Generator
SGSC	Series Grid Side Converter
EMF	Electromotive Force
DPPC+	Dynamic Programming Power Control Plus
LVRT	Low-Voltage Ride Through
GSC	Grid Side Converter
RSC	Rotor Side Converter
SVPWM	Space Vector Pulse Width Modulation
SPWM	Sinusoidal Pulse Width Modulation
PLL	Phase Locked Loop
FE	Finite Element
FEA	Finite Element Analysis
FFT	Fast Fourier Transform
FEM	Finite Element Model
ADC	Analog Digital Converter
DSP	Digital Signal Processor
NO	Normally Open
NC	Normally Closed

LIST OF FIGURES

Page

LIST OF TABLES

ABSTRACT

SIMULATION AND EXPERIMENTAL ANALYSIS OF DOUBLY-FED INDUCTION GENERATOR UNDER GRID FAULTS

Yusuf YAŞA

Department of Electrical Engineering

MSc. Thesis

Adviser: Assoc. Prof. Dr. Erkan MEŞE

The percentage of wind power in electrical power systems worldwide is increasing rapidly every year because of the some important advantages of wind power. Wind power is not a new energy source in the world. Wind power has been existed since the world was created. Firstly, people started to use wind power with windmills by the 9th century but not for getting electrical power until July 1887. After this date, the popularity of getting electrical power from wind power has been continuously increased in academia and in industry. Especially in a few decades, by means of power electronics, wind turbines and wind farms became widespread. The reports in 2010 show that recently 21% of electricity production in Denmark, 18% in Portugal, 16% in Spain and 8% in Germany are provided by the wind power [1].These countries have the highest rate in wind power. For Turkey, this rate is around at 2% which is very low compare to wind power capacity of the country that is 58 GW. This power is more than the country's installed electric power capacity (55.4 GW)[2].

The last few years, there are so many appeal for installing wind power turbine or farm in Turkey [3]. But because of the limited capacity of interconnected system, the taking appeal is stopped for some time to organize interconnected system again.

The wind power technology in world tends to variable speed wind power technology because it has so many advantages compare to fixed speed systems such as less mechanical stress, higher efficiency, higher power quality, less reactive power consumption and so on. In variable speed technology, two generator types are generally used; doubly-fed induction generator (DFIG) and permanent magnet synchronous generator (PMSG). These two generator types have some advantages and disadvantages between each other. In this thesis, DFIG was selected to analyze the wind power turbine system.

The analysis of wind turbine systems consists of two situations; under healthy condition and under fault condition. The wind turbine system model is created in simulation softwares. Simulation results are obtained from coupled simulation that is modeling of turbine components in different simulation softwares and combining all these components together. Analyzing wind turbine systems in coupled simulation is a unique study in the literature. The advantage of this study that provides more realistic results compare to use only one software. Some important parameters are obtained for improving control technique of DFIG during fault condition. The simulation results are also verified with experimental study. Finally, results are discussed and future study is explained.

Key words: Wind turbine, doubly fed induction generator, fault analysis of wind turbine, control of DFIG

YILDIZ TECHNICAL UNIVERSITY

GRADUATE SCHOOL OF NATURAL AND APPLIED SCIENCES

ÖZET

ŞEBEKE HATA DURUMUNDA ÇİFT BESLEMELİ ASENKRON GENERATÖRÜN SİMULASYON VE DENEYSEL ANALİZİ

Yusuf YAŞA

Elektrik Mühendisliği Anabilim Dalı

Yüksek Lisans Tezi

Tez Danışmanı: Doç. Dr. Erkan MEŞE

Rüzgâr enerji sistemlerinin elektrik güç sistemlerindeki payı her yıl, rüzgâr enerjisinin bazı avantajlarından dolayı hızla artmaktadır. Rüzgâr enerjisi kaynağı Dünya'da yeni oluşan bir enerji kaynağı değildir. Rüzgâr enerjisi Dünya yaratıldığından beri var olmuştur. İlk olarak insanlar 9. yüzyılda rüzgâr enerjisini yel değirmenlerinde kullanmaya başlamış, Temmuz 1887 'ye kadar bu enerjiden elektrik üretmek mümkün olmamıştır. Bu tarihten sonra, rüzgâr enerjisinden elektrik üretmenin akademik ve endüstride yaygınlığı sürekli artmıştır. Özellikle son birkaç on yılda, güç elektroniği sayesinde, rüzgâr türbinleri ve rüzgâr çiftlikleri çok yaygınlaşmıştır. 2010 yılında yayınlanan rapora göre hâlihazırda elektrik üretimi Danimarka'da %21, Portekiz'de %18, İspanya'da %16 ve Almanya'da %8 oranında rüzgâr enerjisinden sağlanmaktadır [1]. Bu ülkeler Dünya'da rüzgâr enerjisinde en yüksek orana sahip ülkelerdir. Türkiye için bu oran %2 civarındadır. Bu oran Türkiye'nin 58 GW rüzgâr gücü kapasitesi düşünüldüğünde çok düşük kalmaktadır. Bu güç, şu anki Türkiye'nin kurulu gücünden (55,4 GW) daha fazladır [2].

Son birkaç yılda, Türkiye'de rüzgâr türbini ya da çiftliği kurmak için birçok başvuru yapılmaktadır[3]. Fakat, enterkonnekte sistemin kapasite yetersizliğinden dolayı enterkonnekte sistemin tekrar yapılanması için bazen başvuru alımları durdurulmaktadır.

Dünyadaki rüzgâr enerjisi teknolojisi değişken hızlı rüzgâr türbini teknolojisine doğru kaymaktadır. Çünkü değişken hızlı rüzgar türbinleri sabit hızlı rüzgar türbinlerine göre birçok avantaj barındırmaktadır; daha az mekanik stres, yüksek verimlilik, yüksek kalitede güç, az reaktif güç vb. Değişken hızlı rüzgar türbinlerinde iki tür generatör tipi genellikle kullanılmaktadır; çift beslemeli asenkron generatör ve sabit mıknatıslı senkron generatör. Bu iki generatör tipinin birbirlerine göre avantajları ve dezavantajları vardır. Bu tezde rüzgâr türbini sisteminin analizinde çift beslemeli asenkron generatör seçilmiştir.

Rüzgâr türbini sisteminin analizi iki kısımdan oluşmaktadır; sağlıklı şartlar altında ve hata anında. Rüzgâr türbini sistem modeli simulasyon yazılımları ile oluşturulmuştur. Simulasyon sonuçları, rüzgar türbini elemanlarının ayrı ayrı simulasyon yazılımları kullanılarak modellenmesi ve birbirine entegre edilmesi ile elde edilmiştir. Rüzgar türbininin simulasyon yazılımlarının entegre edilmesi ile analizi literatürde yeni bir çalışmadır. Bu çalışmanın avantajı tek bir simulasyon yazılımına göre çok daha gerçekçi sonuç vermesidir. Bazı önemli parametreler, hata durumunda kontrol algoritması gerçeklemek için elde edilmiştir. Simulasyon sonuçları deneysel olarak da doğrulanmıştır. Sonuç olarak sonuçlar tartışılmış ve gelecekte yapılacak çalışma hakkında bilgi verilmiştir.

Anahtar Kelimeler: Rüzgâr turbini, çift beslemeli asenkron generatör, rüzgâr türbininde hata analizi, çift beslemeli asenkron generatörün kontrolü

YILDIZ TEKNİK ÜNİVERSİTESİ FEN BİLİMLERİ ENSTİTÜSÜ

CHAPTER 1

INTRODUCTION

1.1 Literature Review

1.1.1 About Modeling of System

In Pannell's study, the paper presents detailed analytical analysis of wind turbine DFIG grid-fault response. The paper states that, fault ride through systems must be designed to manage the large and potentially dangerous fault currents in both stator and rotor circuits. The European Union's electrical generation was 4% in 2008. But with this figure it can be expected to reach 12% by 2020. In rotor circuit, there is a DC-link capacitor maintains the dc-link voltage, providing a small energy buffer and permitting independent control of the two converters. It also states that, in medium and high power wind turbines (> 1 MW each) DFIGs dominate global installations. However the internal machine flux is exposed directly to the electrical grid and the DFIG is vulnerable to dips in supply voltage resulting from grid faults [4].

The Zhang's paper analyzes the influence of the crowbar resistors on the electrical behavior of the crowbar protected DFIG during the grid voltage dips. In the paper, it was reported that bigger by-pass resistance will produce smaller current magnitude and torque transients, but higher rotor voltage and slower decaying speed of the faulty currents. Based on the analysis, a resistance of 0.8 pu was found as the optimal value for the active crowbar design [5].

In Seman's study, 2 MW wind power DFIG is simulated under a short-term asymmetrical network disturbances. DFIG model was created by analytical and FEM-based methods. Then the model coupled with crowbar protection circuit. These two obtained models were compared to each other to check the machine modeling approaches during faults. Some significant differences were found especially when the grid fault has been introduced and rotor-side converter is restarted and when the fault is cleared. The reason is that FEM model takes into account the magnetic saturation in the stator and rotor inductances. So we can say FEM model is more accurate than the analytical model [6].

1.1.2 Solutions with Extra Hardware

The Wessels's paper investigated the dynamic voltage restorer connected to a wind turbine DFIG. Also paper claims this system allows the wind turbine an uninterruptible fault ride through of voltage dips. Simulation study was carried out for 2 MW system and experimental study was implemented for asymmetrical faults in 22 kW laboratory test bench. But this approach has cost disadvantage in wind turbine applications [7].

The Morren's paper describes the solution that is to limit the high current in rotor in order to protect the converter by using bypass resistors. The main difference from the other papers that mentioned about crowbar protection system is the converters still connected to the grid. Resistors take some currents from machine's rotor. So they prevent high current from converters. Therefore converters can still remain connected to grid. After grid fault clearance, the system can resume power generation immediately within a few hundred milliseconds [8].

The Abbey's paper presents a new method with integration of super capacitor to DFIG wind turbine to enhance LVRT capability. Super capacitors have short-term energy storage. So for instantaneous faults, it can damp short-term oscillations and can enhance the performance of DFIG and converters. On the other hand, it has cost disadvantage, since super capacitors are expensive [9].

The Flannery's paper presents modeling, analysis and control design of a DFIG wind turbine with a series grid-side converter (SGSC) that is for voltage sags. It should be noticed in the paper that the negative sequence component of the voltage seen at the DFIG terminals can reach up to 50% for the worst case under unbalanced condition. In this paper, the negative sequence component of the stator flux was trying to be kept zero with SGSC. But this study requires extra converter-hardware. This means that it has also cost disadvantage [10].

1.1.3 Solutions with Changing Algorithm

Xiang's study analyzes the effects of grid fault on DFIG and develops new control method that does not require any extra hardware. The paper states that the fundamental difficulty for the DFIG in ride-through is the electromotive force (EMF) induced in the machine rotor during the fault, which depends on dc and negative sequence components in the stator-flux linkage and the rotor speed. The algorithm was developed through the simulation and verified with experimental study [11]. This method depends strongly on the estimation of certain parameters [12]. So it requires significant effort to determine model parameters.

The Santos-Martin's paper analyzes the effect of unbalanced voltage in DFIG and proposed new control topology that is the dynamic programming power control plus (DPPC+) during fault. The paper introduces with some drawbacks of vector control like lack of robustness and linear nature when facing changes in operational conditions. Then it mentioned about direct torque and power control since they have high dynamics but have excessive torque and power ripple due to high bandwidth. In addition the paper states that PI controllers in stator-flux-vector-oriented control of DFIG leads to excessive oscillations. The proposed control technique was simulated and experimentally validated with 20-kW test bench [13].

In Gomis-Bellmunt's paper, the investigation of ride-through in DFIG during unbalanced voltage sag was carried out. Then new control strategy is proposed by changing current reference values in order to keep stable torque and dc bus voltage. It was reported that machine is extremely sensitive to voltage disturbances since the stator is directly connected to the electrical grid. In addition the mechanical speed does not change too much during fault can be seen from the paper. The simulation study was implemented to verify the control technique [14].

The Blaabjerg's study presents a new control technique for the rotor-side converter of DFIG wind turbine. The aim was to improve its low-voltage ride through (LVRT) capability. This method is based on designing an algorithm. So there is no extra hardware to perform the method. Also there are some references to other papers; the authors criticized the other methods such as the one made by Xiang et al. The method has some gains to improve capability though cannot be judged sufficient. Because the paper concludes so many assumptions in DFIG system like liner magnetic circuit of DFIG, negligible crossed terms of the rotor current and etc [12].

In Rodriguez study, a new power control technique is presented that is valid both in fault condition and in normal condition. One of the significant deductions is about the connection type of distribution transformer, which is usually of type Δy. They showed that it has influence on the grid fault occurring at power generation system such as wind turbine. Additionally, under unbalanced fault, on the wind turbine side of distribution transformer there will be negative-sequence component in the voltages. This causes double-frequency oscillations in the system. This paper has assumption that only the grid-side converter (GSC) is considered. In their method, active power is controlled while reactive power is disregarded and assumed to be zero [15].

The Mullane's paper has one new method to improve LVRT capability. This method is called feedback linearization technique and concludes nonlinear controller. Increased inverter currents during the fault may damage the converters. So the main objective of this technique is to reduce the current levels. The wind turbine conventional control systems are designed with linear controller while their behavior is nonlinear in nature. So this paper deals with modeling of the system as nonlinear but transforming parameters to linear plane [16].

In Mohseni's paper, to increase fault ride through capability of DFIG, PI controller in vector control is replaced with a vector based hysteresis current controller. Hysteresis current control technique has fast dynamic response and simple structure. But it has high frequency switching. So high power switching losses would occur. This disadvantage does not exist in the paper. Also there is no experimental result with this technique [17].

1.1.4 Grid Codes and Reports

In Aalborg University report, some definitions and classifications about events in electrical network have been made. Then these events were investigated for different countries in Europe and America. Then event survey was mentioned about in these countries. The important point is that one phase-to-ground fault type is the highest probability to occur worldwide. Additionally, most of the faults occurred in momentary time like 1-6 utility cycle duration of grid, located on 132 kV overhead lines according to the report. Then some simulation results are also given in this report [18].

The Tsili's paper gives the review of grid code technical requirements for large wind farms about their connection and stabilities. The paper concentrated on most important parameters for wind farms like active and reactive power regulation, voltage and frequency limits and wind farm behavior during grid disturbances. The most important point in this paper states that wind turbine should support the system voltage with increased reactive power generation, according to certain codes. Additionally, the paper gives the grid codes of some European countries such as Germany, Denmark and Ireland. These countries have the high penetration rate of wind turbines in their electrical networks [19].

In Erlich's study, wind turbines in the German transmission system were discussed and some important points are given. Despite several improvements, there are still fraught with uncertainty based on system stability in grid. The grid code was introduced in 2003 firstly in Germany. According to the code, during fault wind turbine should remain connected to the grid by introducing new technologies. Turbines have to guarantee reconnection and continuation of power generation. According to the paper, there are two reasons of necessities fault ride through of wind turbine; to provide active power continuously after fault clearance and wind turbine have to support grid voltage during and after the fault to reduce the size of voltage dip. For Germany grid code, this paper can be taken as a good reference [20].

In Kasem study, the paper states that electromagnetic torque will fluctuate which may cause mechanical stress on the drive train system. The fault ride through capability means that all generation plants, including wind, must have the ability to remain connected to the grid during low voltage conditions and faults. This required capability depends on countries energy department. Some countries dictate that the wind turbine must feed the reactive power during and after the fault. Also this paper gives detailed knowledge about Germany grid code which is the most known grid code. Besides that, crowbar selection is discussed [21].

The Erlich's study reports that in the past grid codes focused primary on protection of the wind turbines themselves and ignored the effects of wind turbines on power transmission lines during fault. Supporting the grid with a reactive power must be primary during the grid fault. Also it should be activated within very limited time like one utility cycle [22].

In Mohseni's study, the paper states that voltage sag conditions can be significantly different from one grid to another one because they depend on network characteristics and constraints. The authors say that DFIG concept suffers from the behavior during grid fault. The paper presents analysis of DFIG for both symmetrical and asymmetrical grid faults [23].

For symmetrical faults, huge current overshoots occur at the end of the fault. However they strongly depend on the circuit breaker activating time.

For Asymmetrical faults, continuous oscillations occur in rotor current and dc bus voltage.

Especially for the three phase fault, dc bus voltage has the highest peak during fault.

1.2 Objective of the Thesis

The objective of this thesis is to find out the behavior of DFIG wind turbine during healthy and fault conditions with a new approach which uses new simulation techniques and verifying the study with experimental results. Especially there is a need for extended study of the whole turbine system like mechanical parts of wind turbine, generator, converters, step-up transformer and grid interface during and after faults. This thesis presents detailed analysis of the DFIG based wind turbine system components.

1.3 Hypothesis

DFIG wind turbine system has been modeled and analyzed by finite element method which has quite realistic results. The simulation results show that there are meaningful changes during fault especially in DFIG internal parameters such as inductances and fluxes. These results will contribute to develop enhanced control technique to increase fault ride-through capability of wind turbine.

CHAPTER 2

THEORETICAL BACKGROUND

Doubly fed induction generator is a component of wind turbine that is used to convert mechanical rotational power to electrical power via electromagnetic field. This machine type has windings not only in the stator but also in the rotor. Doubly fed induction generator (DFIG) can give power to the grid from both rotor and stator windings. The power converters are connected to the rotor windings. Because of that only rotor power flows from power converters, the power converters can be designed for only rotor power. So it makes available to increase wind turbine power. In conclusion, DFIG is generally used in high power wind turbine applications.

2.1 Three-Phase Mathematical Model of DFIG

The DFIG has two winding sets in stator and rotor as shown in Figure 2.1.

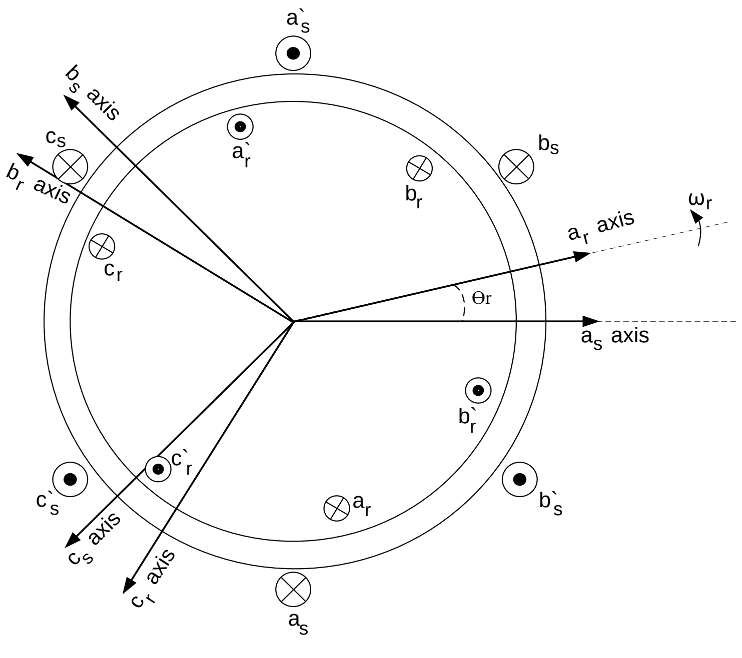

Figure 2.1Stator and rotor phase vectors of DFIG

If the windings have Y connection, the equivalent circuit will become as in Figure 2.2.

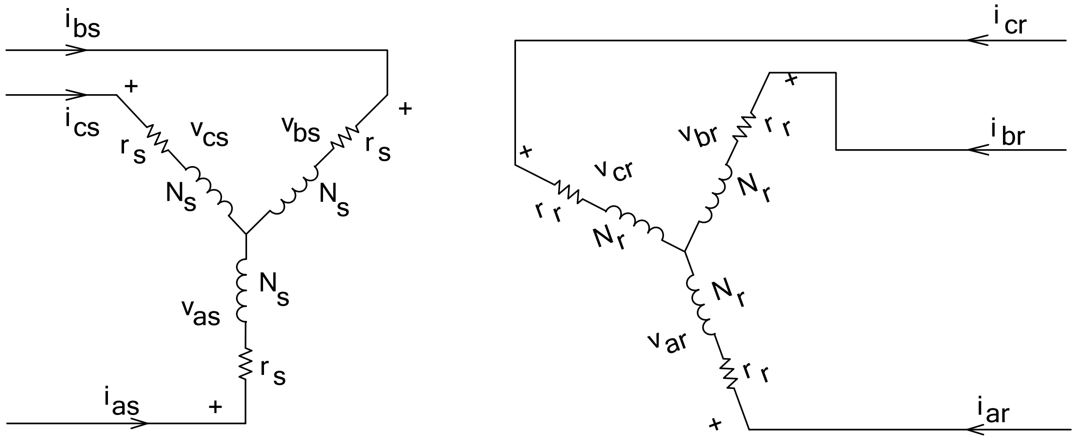

Figure 2.2 Stator and rotor Y connection of windings in DFIG

The equations of these circuits are,

$$v_{abcs} = p\lambda_{abcs} + r_s i_{abcs} \tag{2.1}$$

$$v_{abcr} = p\lambda_{abcr} + r_r i_{abcr} \tag{2.2}$$

In equations, v is the line-to-neutral voltage, p is a derivative symbol, λ is the flux linkage, r and i are the resistance and the current of each phases, respectively. The flux linkage has also formula λ=L.i that is proportional to the current and inductance of related phase.

It can be understood from inductance matrix that stator and rotor self-inductances are invariant to the rotor position Ɵr in (2.22), if we neglect slotting effect. On the other hand, the mutual inductances between stator and rotor windings are functions of rotor position. Hence modeling and analyzing the induction machine in 3–phase frame is not a simple task. Because of that, this undesirable difficulty should be eliminated with some techniques. Now, fortunately we can transform both stator and rotor variables to a common frame of reference [24].

$$\begin{aligned}\lambda_{as} &= L_s\, i_{as} + M_s\, i_{bs} + M_s\, i_{cs} \\ &\quad + M_{sr}\, i_{ar} \cos(\theta_r) + M_{sr}\, i_{br} \cos(\theta_r + 120^\circ) + M_{sr}\, i_{cr} \cos(\theta_r - 120^\circ)\end{aligned} \tag{2.3}$$

$$\begin{aligned}\lambda_{bs} &= M_s\, i_{as} + L_s\, i_{bs} + M_s\, i_{cs} \\ &\quad + M_{sr}\, i_{ar} \cos(\theta_r - 120^\circ) + M_{sr}\, i_{br} \cos(\theta_r) + M_{sr}\, i_{cr} \cos(\theta_r + 120^\circ)\end{aligned} \tag{2.4}$$

$$\lambda_{cs} = M_s\, i_{as} + M_s\, i_{bs} + L_s\, i_{cs} + M_{sr}\, i_{ar} \cos(\theta_r - 120^\circ) + M_{sr}\, i_{br} \cos(\theta_r) + M_{sr}\, i_{cr} \cos(\theta_r + 120^\circ) \tag{2.5}$$

For stator windings, we assume that,

$$i_{as} + i_{bs} + i_{cs} = 0 \tag{2.6}$$

$$L_{ss} = L_s - M_s \tag{2.7}$$

$$\lambda_{as} = L_s\, i_{as} + M_s\, (i_{bs} + i_{cs}) + M_{sr}\, i_{ar} \cos(\theta_r) + M_{sr}\, i_{br} \cos(\theta_r + 120^\circ) + M_{sr}\, i_{cr} \cos(\theta_r - 120^\circ) \tag{2.8}$$

$$\lambda_{bs} = M_s\, (i_{as} + i_{cs}) + L_s\, i_{bs} + M_{sr}\, i_{ar} \cos(\theta_r - 120^\circ) + M_{sr}\, i_{br} \cos(\theta_r) + M_{sr}\, i_{cr} \cos(\theta_r + 120^\circ) \tag{2.9}$$

$$\lambda_{cs} = M_s\, (i_{as} + i_{bs}) + L_s\, i_{cs} + M_{sr}\, i_{ar} \cos(\theta_r - 120^\circ) + M_{sr}\, i_{br} \cos(\theta_r) + M_{sr}\, i_{cr} \cos(\theta_r + 120^\circ) \tag{2.10}$$

For rotor windings, we assume that

$$i_{ar} + i_{br} + i_{cr} = 0 \tag{2.11}$$

$$L_{rr} = L_r - M_r \tag{2.12}$$

$$\lambda_{ar} = M_{sr}\, i_{as} \cos(\theta_r) + M_{sr}\, i_{bs} \cos(\theta_r - 120^\circ) + M_{sr}\, i_{cs} \cos(\theta_r + 120^\circ) + L_r\, i_{ar} + M_r\, (i_{br} + i_{cr}) \tag{2.13}$$

$$\lambda_{br} = M_{sr}\, i_{as} \cos(\theta_r + 120^\circ) + M_{sr}\, i_{bs} \cos(\theta_r) + M_{sr}\, i_{cs} \cos(\theta_r - 120^\circ) + L_r\, i_{br} + M_r\, (i_{ar} + i_{cr}) \tag{2.14}$$

$$\lambda_{cr} = M_{sr}\, i_{as} \cos(\theta_r + 120^\circ) + M_{sr}\, i_{bs} \cos(\theta_r) + M_{sr}\, i_{cs} \cos(\theta_r - 120^\circ) + L_r\, i_{cr} + M_r\, (i_{ar} + i_{br}) \tag{2.15}$$

The stator and rotor flux linkages are,

$$\lambda_{as} = L_{ss}\, i_{as} + M_{sr} \left[i_{ar} \cos(\theta_r) + i_{br} \cos(\theta_r + 120^\circ) + i_{cr} \cos(\theta_r - 120^\circ) \right] \tag{2.16}$$

$$\lambda_{bs} = L_{ss}\, i_{bs} + M_{sr}\left[i_{ar}\cos(\theta_r - 120^\circ) + i_{br}\cos(\theta_r) + i_{cr}\cos(\theta_r + 120^\circ) \right] \tag{2.17}$$

$$\lambda_{cs} = L_{ss}\, i_{cs} + M_{sr}\left[i_{ar}\cos(\theta_r + 120^\circ) + i_{br}\cos(\theta_r - 120^\circ) + i_{cr}\cos(\theta_r) \right] \tag{2.18}$$

$$\lambda_{ar} = M_{sr}\left[i_{as}\cos(\theta_r) + i_{bs}\cos(\theta_r - 120^\circ) + i_{cs}\cos(\theta_r + 120^\circ) \right] + L_{rr}\, i_{ar} \tag{2.19}$$

$$\lambda_{br} = M_{sr}\left[i_{as}\cos(\theta_r + 120^\circ) + i_{bs}\cos(\theta_r) + i_{cs}\cos(\theta_r - 120^\circ) \right] + L_{rr}\, i_{br} \tag{2.20}$$

$$\lambda_{cr} = M_{sr}\left[i_{as}\cos(\theta_r - 120^\circ) + i_{bs}\cos(\theta_r + 120^\circ) + i_{cs}\cos(\theta_r) \right] + L_{rr}\, i_{cr} \tag{2.21}$$

$$\begin{bmatrix} \lambda_{as} \\ \lambda_{bs} \\ \lambda_{cs} \\ \lambda_{ar} \\ \lambda_{ar} \\ \lambda_{ar} \end{bmatrix} = \begin{bmatrix} L_{ss} & 0 & 0 & & & \\ 0 & L_{ss} & 0 & & L_{sr} & \\ 0 & 0 & L_{ss} & & & \\ & & & L_{rr} & 0 & 0 \\ & L_{sr}^{T} & & 0 & L_{rr} & 0 \\ & & & 0 & 0 & L_{rr} \end{bmatrix} \begin{bmatrix} i_{as} \\ i_{bs} \\ i_{cs} \\ i_{ar} \\ i_{br} \\ i_{cr} \end{bmatrix} \tag{2.22}$$

$$L_{sr} = M_{sr} \begin{bmatrix} \cos(\theta_r) & \cos(\theta_r + 120^\circ) & \cos(\theta_r - 120^\circ) \\ \cos(\theta_r - 120^\circ) & \cos(\theta_r) & \cos(\theta_r + 120^\circ) \\ \cos(\theta_r + 120^\circ) & \cos(\theta_r - 120^\circ) & \cos(\theta_r) \end{bmatrix} \tag{2.23}$$

$$v_{as} = i_{as} r_s + \frac{d\lambda_{as}}{dt} \tag{2.24}$$

Equation (2.24) requires derivative operation of fluxes. For instance if we take the first row of flux linkage matrix

$$\frac{d\lambda_{as}}{dt} = \frac{d[\,first\ \text{raw of the flux matrix}]}{dt} \tag{2.25}$$

There is L_{sr} inductance which has trigonometric functions. The derivative of these functions is not straightforward.

2.2 **Reference Frame Theory**

In 1920 R. H. Park, introduced a new approach to electric machine analysis. He transformed the stator variables to a frame of reference that is rotating with rotor, is called Park transformation [25]. This transformation allows us to eliminate all time-varying inductances from the equations. The transformation can be written as,

$$f_{qd0s} = K_s f_{abcs} \tag{2.26}$$

$$\begin{bmatrix} \vec{f}_q \\ \vec{f}_d \end{bmatrix} = \begin{bmatrix} \cos(\theta - \theta_{sum}) \\ \sin(\theta - \theta_{sum}) \end{bmatrix} \begin{bmatrix} \vec{f}_{sum} \end{bmatrix} \tag{2.27}$$

In (2.27), f can be considered voltage, current or flux linkage. K_s is a transformation matrix that is equal to,

$$[K_s] = \frac{2}{3}\begin{bmatrix} \cos(\theta) & \cos(\theta - \frac{2\pi}{3}) & \cos(\theta + \frac{2\pi}{3}) \\ \sin(\theta) & \sin(\theta - \frac{2\pi}{3}) & \sin(\theta + \frac{2\pi}{3}) \\ \frac{1}{2} & \frac{1}{2} & \frac{1}{2} \end{bmatrix} \tag{2.28}$$

$$\theta = \int \omega dt \tag{2.29}$$

The space vectors that are related to Park transformation can be seen from Figure 2.3.

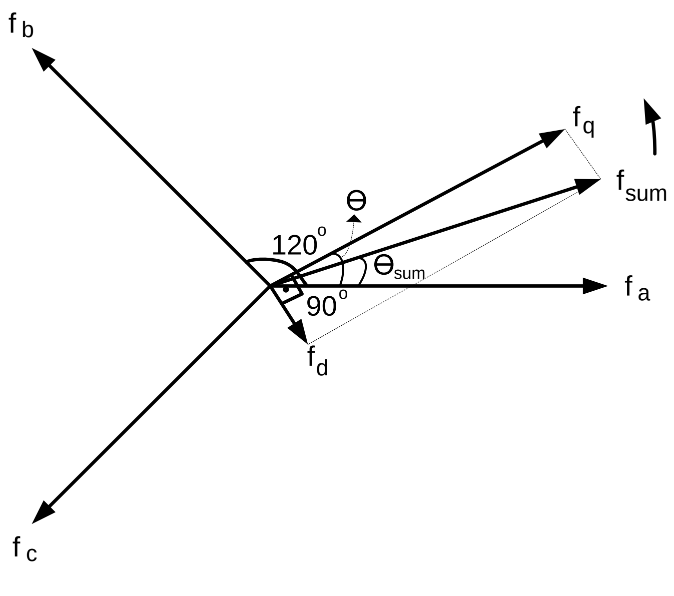

Figure 2.3 3-phase and 2-phase vectors

Q and D axis vectors rotate with ω rotational speed however three phase vectors do not rotate, however their amplitudes and directions do vary. But summation of these three phase vectors create one vector-f_{sum} that has constant magnitude and rotates with a rotational speed of ω similar to q and d axis vectors.

$$\vec{f}_{sum} = \vec{f}_a + \vec{f}_b + \vec{f}_c \tag{2.30}$$

$$\begin{bmatrix} \vec{f}_q \\ \vec{f}_d \end{bmatrix} = \begin{bmatrix} \cos(\theta - \theta_{sum}) \\ \sin(\theta - \theta_{sum}) \end{bmatrix} \begin{bmatrix} \vec{f}_{sum} \end{bmatrix} \tag{2.31}$$

2.3 Q and D Axis Mathematical Model of DFIG

Two phase mathematical model of DFIG can be obtained by using reference frame theory. After using K_s transformation matrix, q and d axis equations of DFIG are obtained from Figure 2.4.

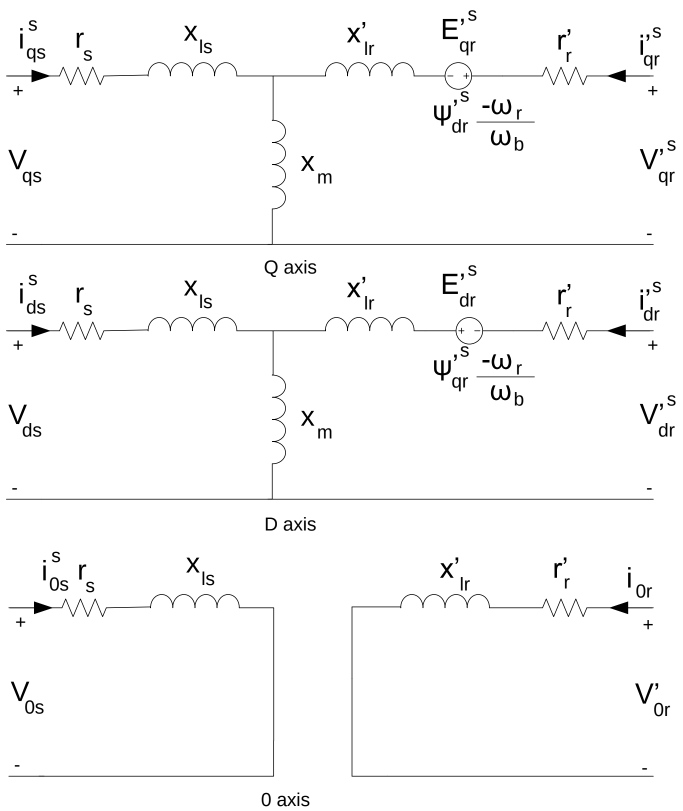

Figure 2.4 Q and D axis equivalent circuits of DFIG

$$v_{qs}{}^{e} = \frac{p}{\omega_b}\psi_{qs}{}^{e} + \frac{\omega_e}{\omega_b}\psi_{ds}{}^{e} + r_s i_{qs}{}^{e} \tag{2.32}$$

$$v_{ds}{}^{e} = \frac{p}{\omega_b}\psi_{ds}{}^{e} - \frac{\omega_e}{\omega_b}\psi_{qs}{}^{e} + r_s i_{ds}{}^{e} \tag{2.33}$$

$$v_{0s} = \frac{p}{\omega_b}\psi_{0s} + r_s i_{0s} \tag{2.34}$$

$$v_{qr}{}^{'e} = \frac{p}{\omega_b}\psi_{qr}{}^{'e} + \left(\frac{\omega_e - \omega_r}{\omega_b}\right)\psi_{dr}{}^{'e} + r_r{}^{'} i_{qr}{}^{'e} \tag{2.35}$$

$$v_{dr}{}^{'s} = \frac{p}{\omega_b}\psi_{dr}{}^{'e} - \left(\frac{\omega_e - \omega_r}{\omega_b}\right)\psi_{qr}{}^{'e} + r_r{}^{'} i_{dr}{}^{'e} \tag{2.36}$$

$$v_{0r}{}^{'} = \frac{p}{\omega_b}\psi_{0r}{}^{'} + r_r{}^{'} i_{0r}{}^{'} \tag{2.37}$$

ω_b : Base speed ($\omega_b=2\pi f_s$) rad/s

f_s : stator frequency Hz

p : pole pairs

ω_e : electrical speed ($\omega_e=2\pi f_s$) rad/s

ω_r : rotor mechanical speed rad/s

2.4 **Control of DFIG**

The control of DFIG is usually implemented with two-converters (back-to-back converters) that are shown in Figure 2.5.

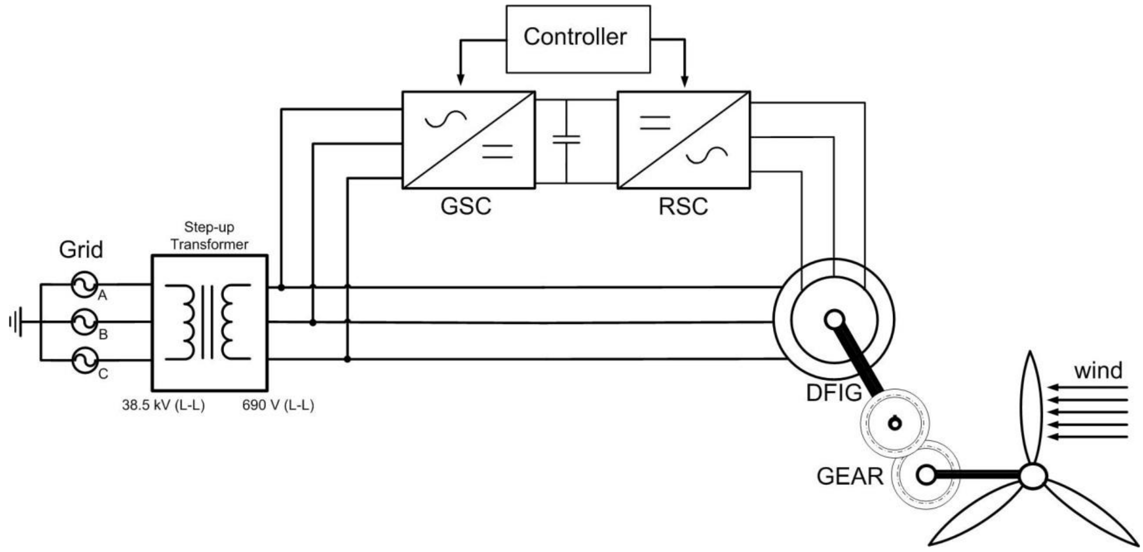

Figure 2.5 DFIG wind turbine components

Wind turbine components are rotor blades, gear, DFIG, rotor side converter (RSC), grid side converter (GSC), controller, step-up transformer and grid. The wind causes rotation in the rotor blades at low speed compared to DFIG speed. Then by means of gear, speed is boosted up to around synchronous speed.

2.5 The Principle of power conversion in DFIG

If a three phase induction machine has p pole pairs and its stator is connected to a source with frequency f, the synchronous speed can be calculated by (2.38) [26].

$$n_s = \frac{60 f_s}{p} \quad \text{rpm} \tag{2.38}$$

The slip speed and the slip is,

$$n_{slip} = n_s - n_{mech} \tag{2.39}$$

$$s = \frac{(n_s - n_{mech})}{n_s} \tag{2.40}$$

The slip is an important parameter in the operation of induction machine. Some particular values of the slip are,

s=1 : The machine stops

s=0 : The machine is at synchronous speed s>1 : The mechanical speed direction is opposite of produced rotating magnetic field by stator (generator operation below synchronous speed, braking operation in the opposite direction).

0<s<1 : The machine is at subsynchoronous operation (below synchronous speed).

-1<s<0 : The machine is at supersynchronous operation (above synchronous speed).

These values are the theoretical values for the induction machine. In practice, the s parameter is limited with some boundaries. The rotor slip frequency is calculated by (2.41).

$$f_{slip} = s.f_s \tag{2.41}$$

The rotor of induction machine should be supplied with this frequency. For squirrel cage induction machine, it is performed automatically with short-circuit bars. But for doubly fed induction generator (or wound rotor induction generator), the rotor windings must be excited with slip frequency. Additionally, to excite with slip frequency the rotor speed must be known. So it requires speed information which can be acquired with encoder or resolver.

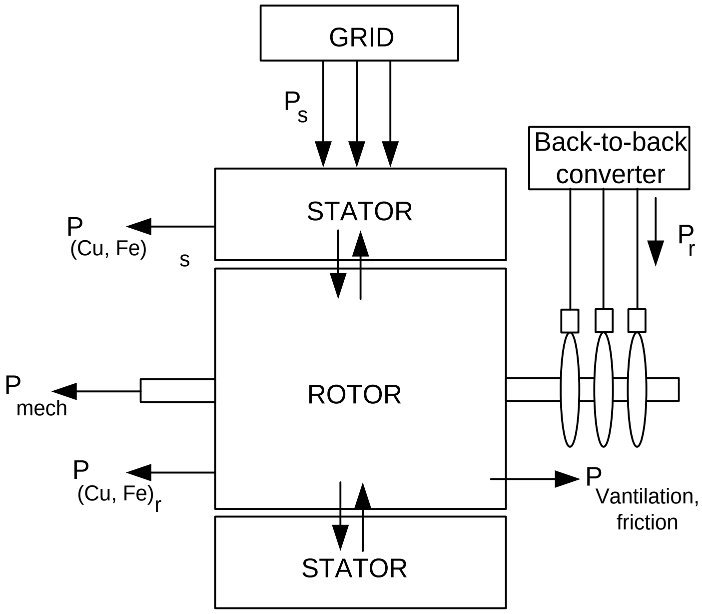

Figure 2.6 Power flow diagram of DFIG

The power diagram of DFIG is shown in Figure 2.6. The copper and iron losses in stator and rotor are represented with $P_{(Cu,Fe)s}$ and $P_{(Cu,Fe)r}$, respectively.

Mechanical input power,

$$P_{mech} = \frac{2\pi n_{mech}}{60} T_{mech} \tag{2.42}$$

Electrical stator power,

$$P_s = \frac{2\pi n_s}{60} T_{mech} \tag{2.43}$$

Electrical rotor power,

$$P_r = P_{mech} - P_s = \frac{2\pi (n_{mech} - n_s)}{60} T_{mech} \tag{2.44}$$

$$P_r = s.P_s \tag{2.45}$$

For generator operation, if the power flow directions in Figure 2.6 are taken reference point, the sign of mechanical power will be negative and the input torque T_{mech} will be negative. Stator power P_s will also be negative; this means DFIG gives power to grid from stator. In rotor, the power direction depends on speed difference between mechanical speed and synchronous speed. Below synchronous speed (n_{mech}<ns), P_r becomes positive. Rotor Side Converter (RSC) should supply the rotor windings. Whereas, above synchronous speed ($n_{mech}>n_s$), P_r becomes negative, RSC should take power from rotor windings. It is important to note that stator can give power to the grid not only in supersynchronous operation but also in subsynchronous operation. For rotor power, it is not the same. Rotor can give power from rotor to the back-to-back converter only in supersynchronous operation. Another important point is in (2.45) that the rotor power is proportional with slip.

2.6 **Field Oriented Control**

During the last few years, the 3-phase AC machine drives became more sophisticated. The reason is definitely perfect control strategies of this type of machine drives. It is known that best controllable machine type is DC machine. Because of the near 90 degrees relative angle between stator and rotor magnetic fluxes, both field (stator) and armature (rotor) magnetic fluxes can be controlled independently without affecting each other and it provides full control of the machine[27].

The field oriented control also called vector control is a simulation of control of AC machine to DC machine in general terms. The field orientation control process starts with vector transformation that is mentioned before. 3 phase currents are transformed to 2-phase q-d reference frame with Ks transformation matrix. In steady state condition, the q and d axis currents become DC. So the control algorithm can be built in DC frame like DC motor control. Typical control scheme for AC machine applications is shown in Figure 2.7.

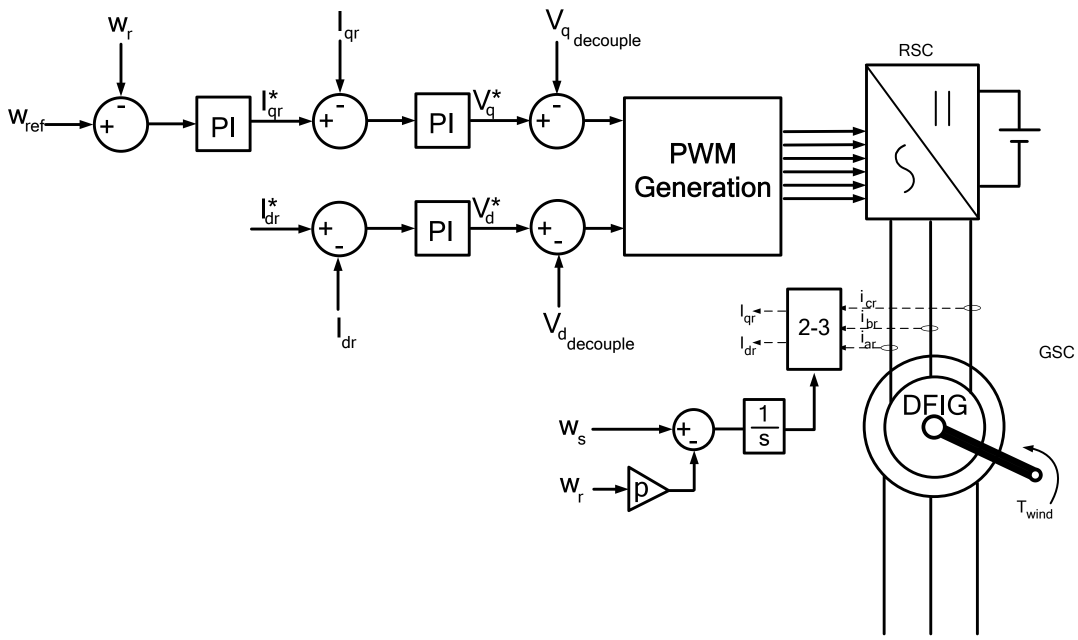

Figure 2.7 The vector control scheme of DFIG

2.7 **Space Vector Pulse Width Modulation (SVPWM)**

Space vector PWM is a technique that generates switching signals to drive switches. It has lots of advantages compared to Sinusoidal PWM (SPWM) and hysteresis control. 2-level 6 switches IGBT inverter basic scheme can be seen from Figure 2.8.

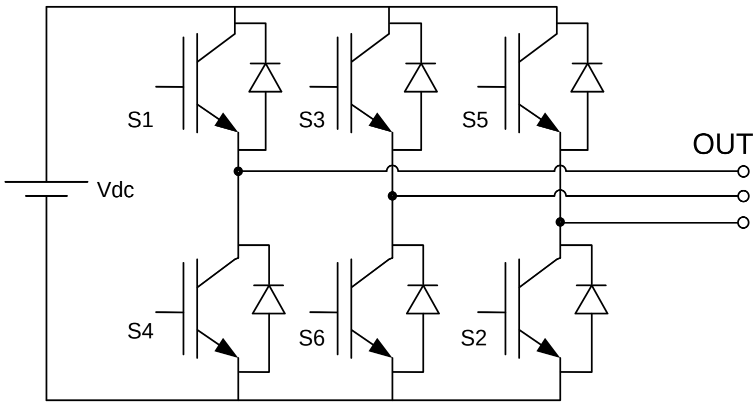

Figure 2.8 The circuit scheme of two level 6 switch inverter

The advantages of space vector PWM (SVPWM) can be listed as,

- More DC bus utilization than SPWM.
- Minimum switching loss with proper switching pattern selection
- Low harmonic content in output current with proper switching pattern selection

These three parameters are the most important features of general three phase inverters and we can achieve these advantages without adding any extra hardware device because switching technique only depends on control algorithm. These advantages become more important especially at high power applications like in wind turbine.

2.7.1 **SVPWM Algorithm**

The inputs of SVPWM are the q and d axis reference voltages, reference voltage vector angle and dc bus voltage; the outputs are three phase voltage references respectively can be seen from Figure 2.9.

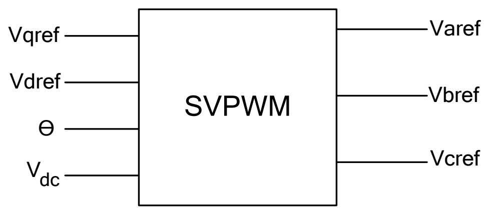

Figure 2.9 Inputs and the outputs of SVPWM

q and d axis reference voltages come from current PI regulators. The angle-Θ is the angle of reference rotating voltage in reference frame shown in Figure 2.10.

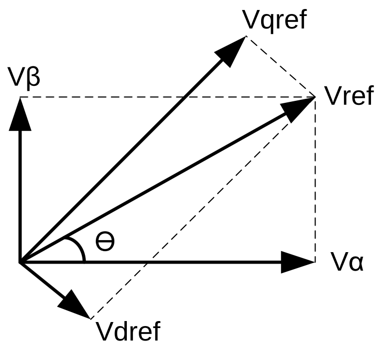

Figure 2.10 Reference frames of Vref

The output signal waveforms should be like in Figure 2.11 at steady state condition.

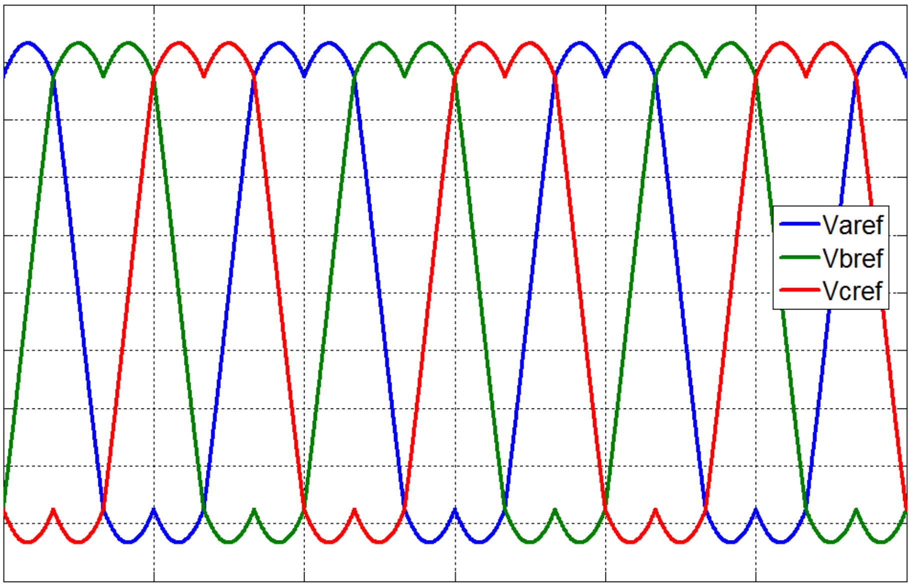

Figure 2.11 The regular outputs of SVPWM

Details of SVPWM algorithm will be presented as it is an important part of DFIG control. It should be noted that the following algorithm is also the optimized code of embedded system. The general control algorithm is shown in Figure 2.12.

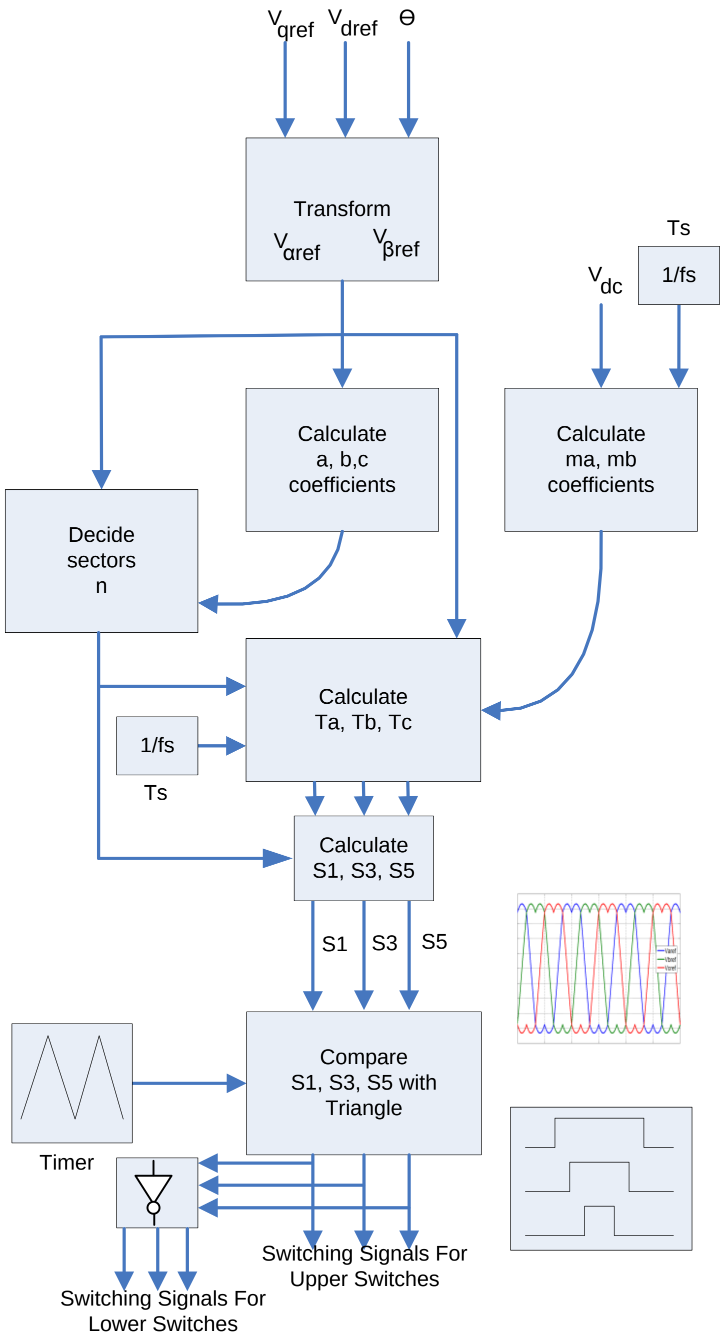

Figure 2.12 The flow chart of SVPWM algorithm

Firstly, the input q and d axis reference voltages are transformed to stationary reference frame $V_{\alpha ref}$ and $V_{\beta ref}$ as in Figure 2.10. Since same calculations will be used more than one time, they will be saved as a coefficients like a,b,c, ma and mb in Figure 2.12 to decrease calculation time in microcontroller. The coefficients calculations are the followings,

$$\begin{bmatrix} V_{\alpha ref} \\ V_{\beta ref} \end{bmatrix} = \begin{bmatrix} \cos(\theta) & \sin(\theta) \\ \sin(\theta) & -\cos(\theta) \end{bmatrix} \begin{bmatrix} V_{qref} \\ V_{dref} \end{bmatrix} \tag{2.46}$$

$$\mathrm{a} = \sqrt{3}.V_{\alpha ref} \tag{2.47}$$

$$b = -V_{\beta ref} \tag{2.48}$$

$$c = -a \tag{2.49}$$

After transforming to stationary reference frame and calculating the coefficients, let us give information about sector of reference voltage.

Two-level, three phase inverter has six switches as shown in Figure 2.8. The six switches have 2^3=8 possibility in combination in Table 2.1 [28].

Table 2.1 The combination of switching states and corresponding output voltages

a	**b**	**c**	$\mathbf{V_a}$	$\mathbf{V_b}$	$\mathbf{V_c}$	$\mathbf{V_{ab}}$	$\mathbf{V_{bc}}$	$\mathbf{V_{ca}}$
0	0	0	0	0	0	0	0	0
1	0	0	$2/3.V_{dc}$	$-1/3.V_{dc}$	$-1/3.V_{dc}$	1	0	-1
1	1	0	$1/3.V_{dc}$	$1/3.V_{dc}$	$-2/3.V_{dc}$	0	1	-1
0	1	0	$-1/3.V_{dc}$	$2/3.V_{dc}$	$-1/3.V_{dc}$	-1	1	0
0	1	1	$-2/3.V_{dc}$	$1/3.V_{dc}$	$1/3.V_{dc}$	-1	0	1
0	0	1	$-1/3.V_{dc}$	$-1/3.V_{dc}$	$2/3.V_{dc}$	0	-1	1
1	0	1	$1/3.V_{dc}$	$-2/3.V_{dc}$	$1/3.V_{dc}$	1	-1	0
1	1	1	0	0	0	0	0	0

In stationary reference frame, voltage reference vector rotates with ω radial speed as shown in Figure 2.3.

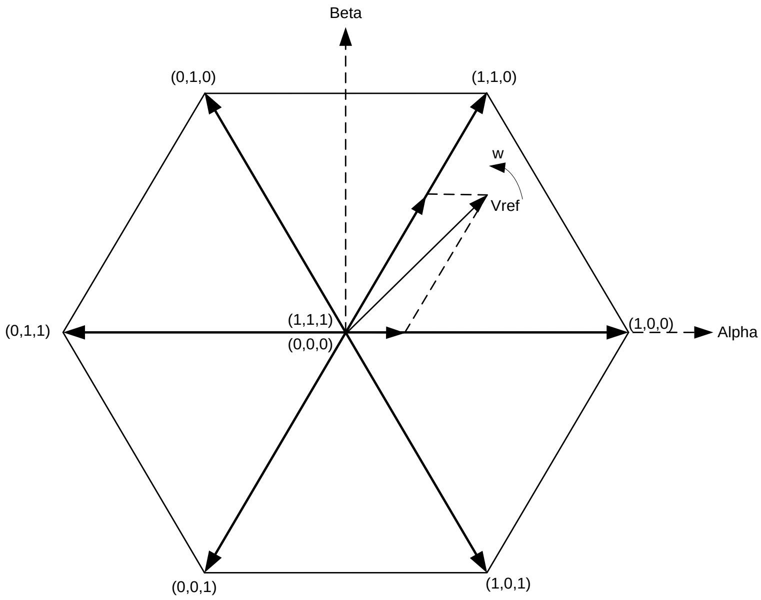

Figure 2.13 The basic space vectors and switching states

To obtain this reference voltage on machine phase windings, we should know where the reference voltage is. It can be understood from Table 2.1 that in six switches inverter there are 8 possibilities. Each combination of switches creates one space vector in Figure 2.13. The reference vector must be created with these space vectors and/or their combination. To generate reference vector, closest three space vectors should be applied to power switches. So these three vectors will be decided in every step time by means of sector (n).

In algorithm first step is definition of α and β vectors of reference vector as mentioned before. Then, the second step will be finding the sector of reference vector-V_{ref}. In this hexagonal shape there are 6 sectors in Figure 2.14.

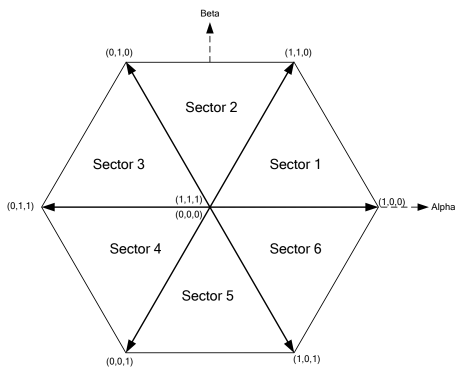

Figure 2.14 Sectors of inverter algorithm

To find which sector V_{ref} in, the algorithm in Figure 2.15 can be implemented.

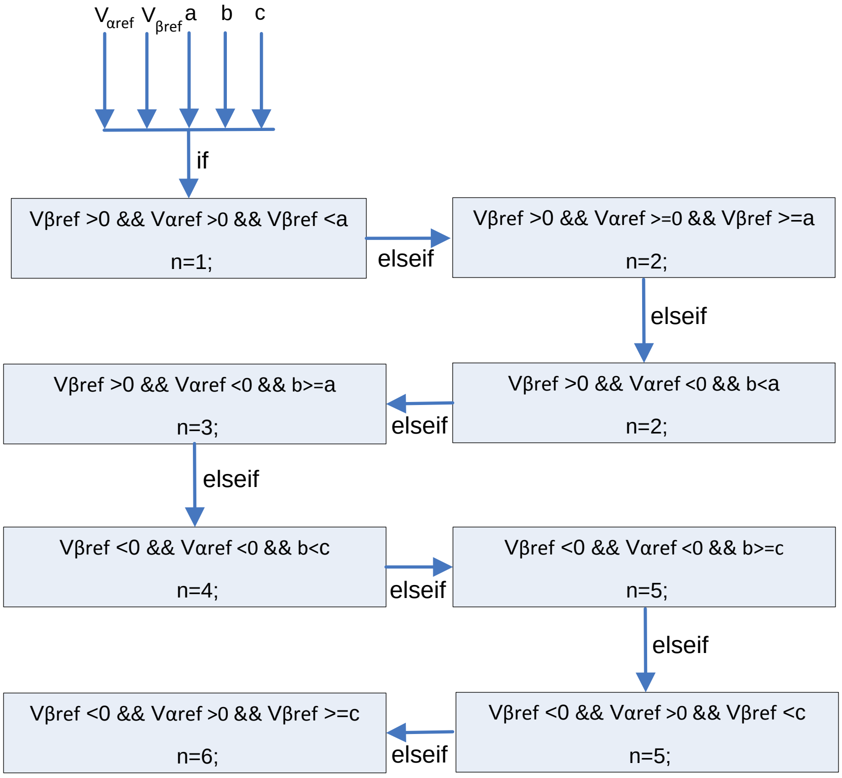

Figure 2.15 Algorithm of sector decision

After implementing this algorithm in Figure 2.15, the place of the reference vector in hexagonal shape will be known. After this step closest three vector is also known. For instance, if V_{ref} is in sector 2, closest three vectors are (1,1,0), (0,1,0) and (0,0,0) or (1,1,1). In this stage, we should calculate the time of each related vector that it should be applied. It will be the fourth step.

In third step, let us calculate the ma, mb modulation index of each vector that are nonzero vector's modulation indexes.

$$m_a = \frac{\sqrt{3}.Ts}{V_{dc}} \tag{2.50}$$

$$m_b = \frac{3}{2}\frac{Ts}{V_{dc}} \tag{2.51}$$

T_s is a switching time of inverter that is constant in algorithm. It is selected 100 µs in both simulation and experimental study. Beside that V_{dc} is a DC bus voltage.

In fourth step, the implementing time of each vector will be calculated. As expected, these time values (Ta, Tb and Tc) will be different for each sector. The calculation algorithm can be seen from Figure 2.16.

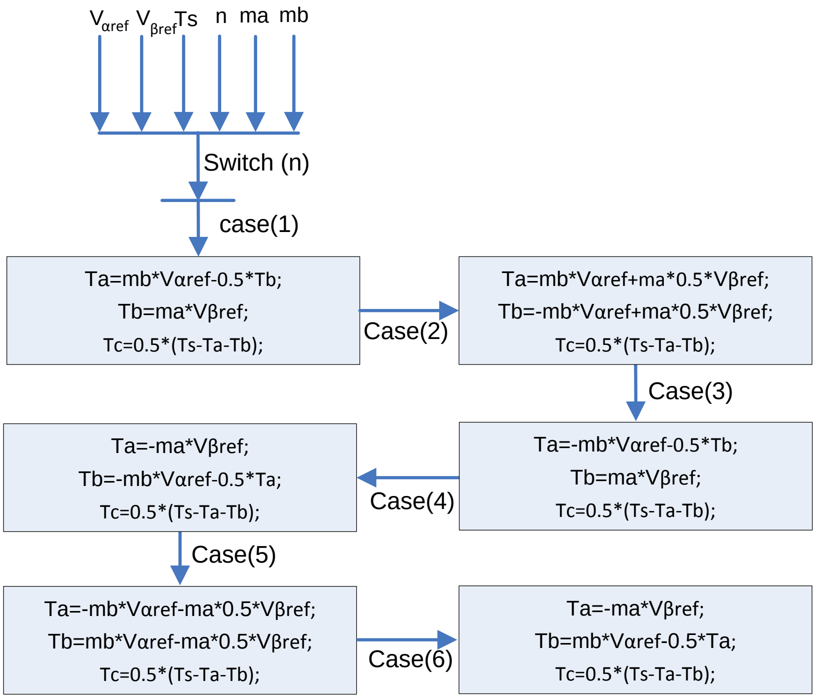

Figure 2.16 Calculation of implementation times of vectors shown as flow chart

It was mentioned before; in each sector, three space vectors are used to get V_{ref}. So these three time values that are calculated in Figure 2.16 are obtained for these three vectors.

It was mentioned, SVPWM has minimum switching loss advantage. The main reason of this advantage is definitely a sequence of switching.

The fifth step is a providing minimum switching loss. For this object the calculation in Figure 2.17 can be implemented. The output of algorithm that is carried out so far should be like in Figure 2.18.

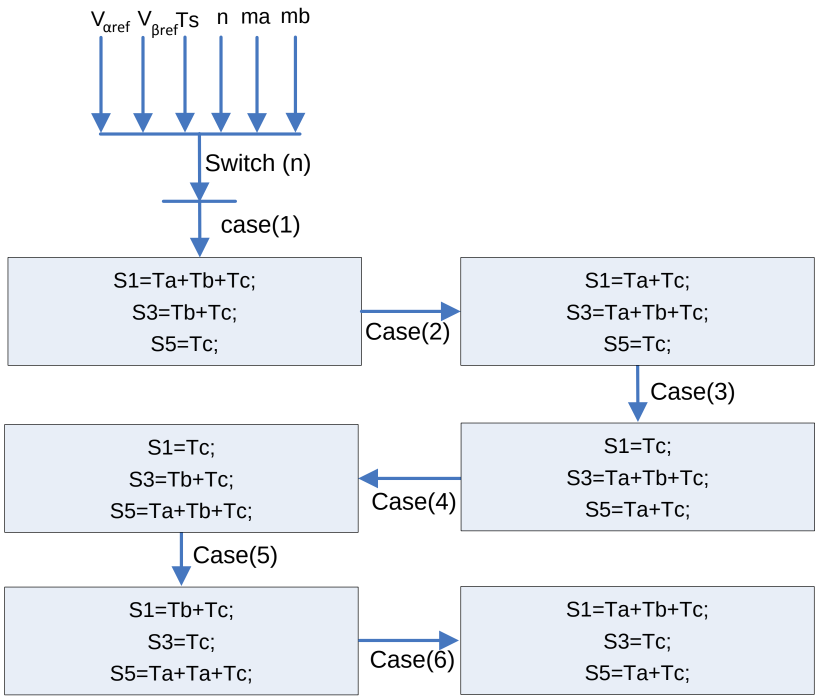

Figure 2.17 The flow chart of getting space vector wave shapes for upper switches

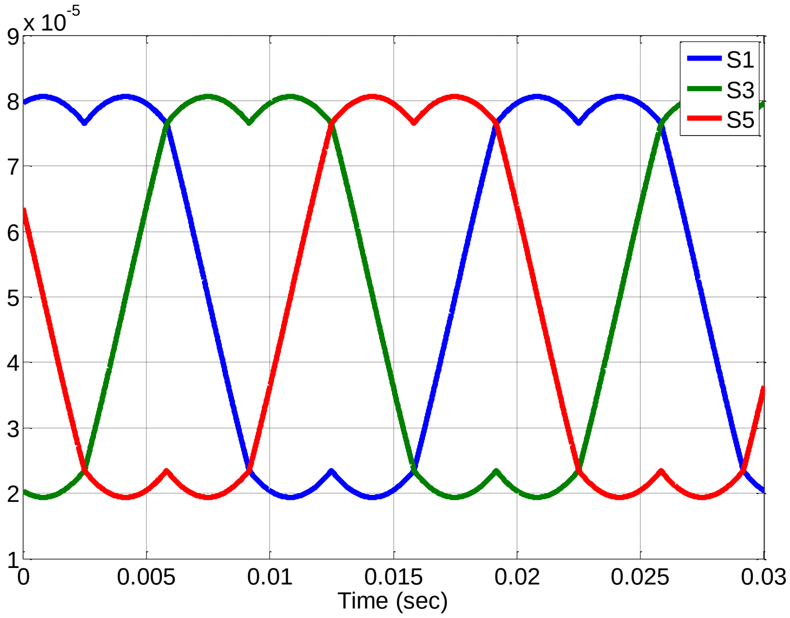

Figure 2.18 Application duration of each vectors in SVPWM

It should be noted that both x and y axes are time. If the modulation index becomes 1, the magnitudes of S1,S3 and S5 will be equal to Ts that is 100µs here. In practical, microcontroller timers are used to compare with these S1, S3, S5 waveshapes. In experimental, if timer period is chosen 7500, SVPWM outputs must multiply with $\frac{7500}{\mathrm{Ts}}$ to compare with this timer. After multiplying it is ready to compare.

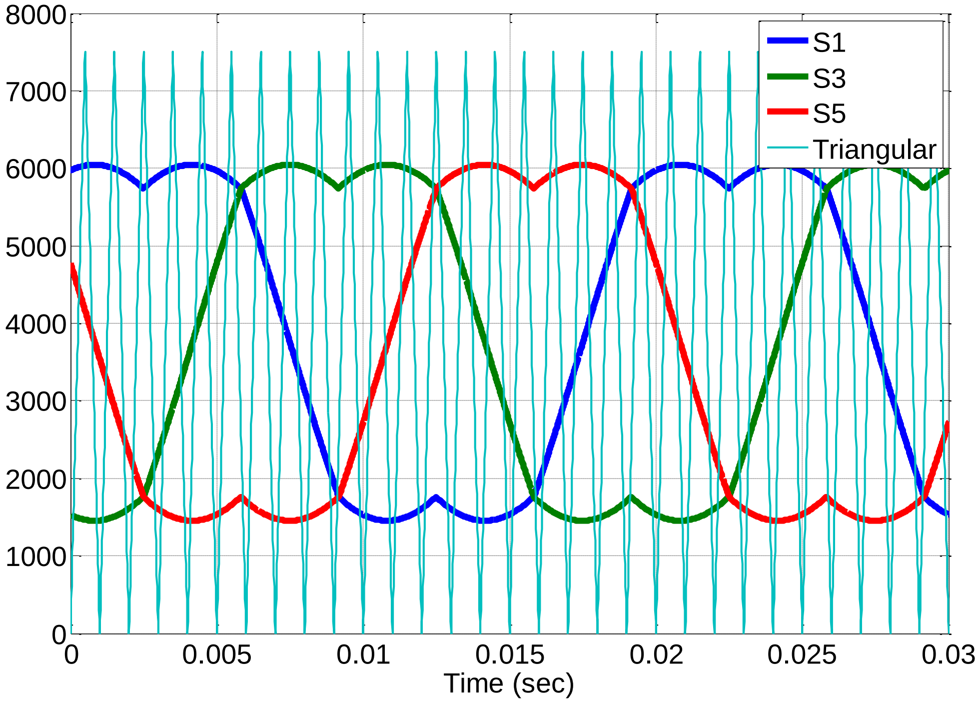

Figure 2.19 Comparing of space vectors with triangular

In Figure 2.19, the timer period was selected 1 msec to understand comparison in figure. After comparison Figure 2.20 wave shapes will be obtained. These three gate signals and their complementaries will go to the six power switches.

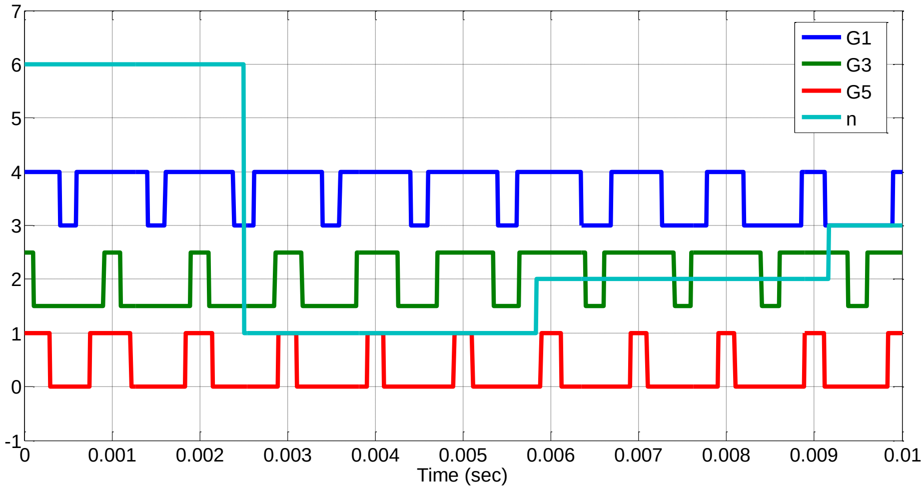

Figure 2.20 Gate signals for upper power switches

2.7.2 SVPWM Advantages

It can be understood from gate signals that only one switch will be active in each state. During one switching period (T_s), 6 times switching will be done. It provides minimum switching loss.

Also SVPWM has lower harmonic content in current and lower ripple in torque, according to [29]. The comparison results can be seen from Figure 2.21.

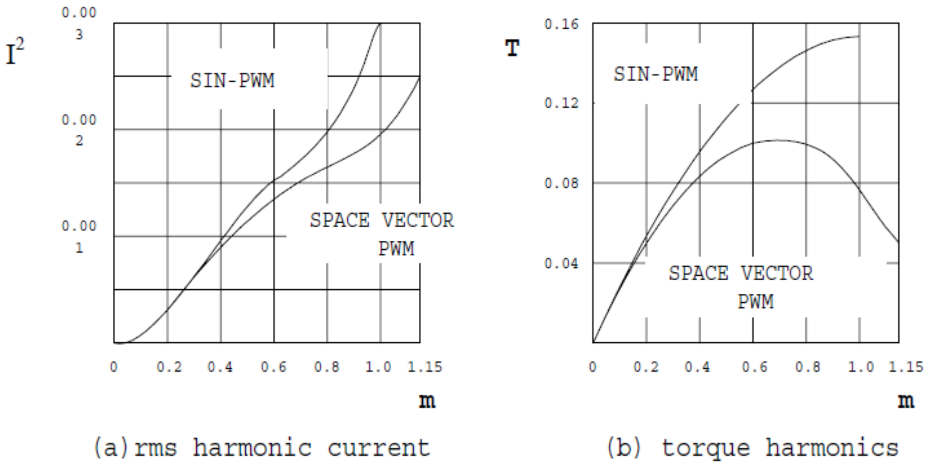

Figure 2.21 Comparison of Sin-PWM and SVPWM in terms of harmonic content [29]

Another advantage of SVPWM technique as mentioned before is more dc bus utilization in compare to Sin-PWM. It can be understood from Figure 2.22 that DC bus limit is the outer circle (blue) and SVPWM limit is the inner circle (red). The hexagonal shape can be achieved with applying square wave excitation.

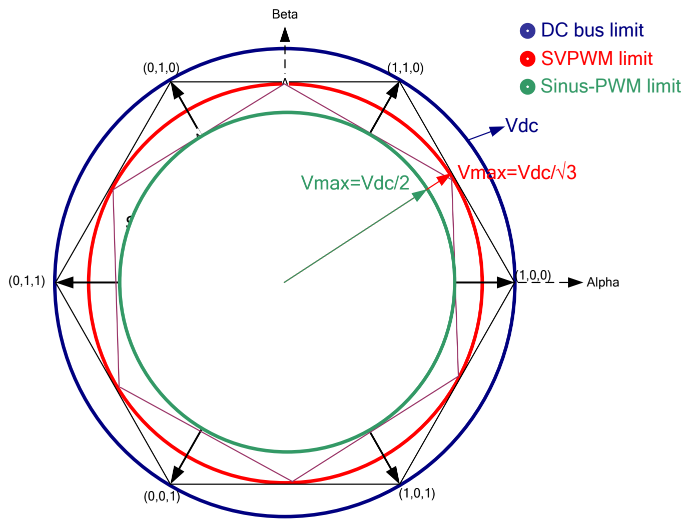

Figure 2.22 DC bus, SVPWM and sinus-PWM limits on output voltage

The available output voltage in SVPWM (red) will be equal to $\frac{\text{Vdc}}{\sqrt{3}} = 0.577.\text{Vdc}$, if the modulation index equals to 1. Whereas in sinus-PWM (green), the output voltage will be equal to $\frac{\text{Vdc}}{2}$ = 0.5.Vdc. So SVPWM has 15.4% more DC-bus utilization than sinus-PWM.

2.8 Control of Grid Connected Converter

The control of grid connected converter is also implemented with vector control topology. The main task of this converter in DFIG wind turbine application is an ability to obtain DC bus voltage control and reactive power flow control that comes from the grid or goes to the grid. The vector control scheme of converter is shown in

Figure 2.23.

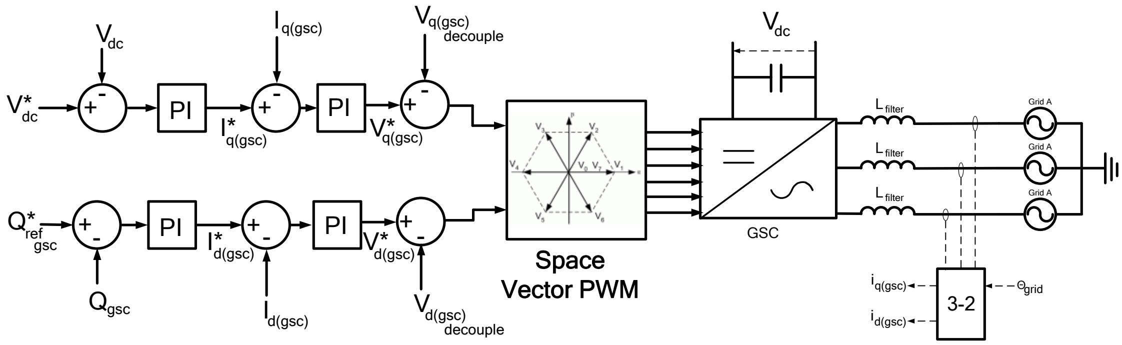

Figure 2.23 The vector control scheme of grid side converter (GSC)

As expected, the topology of GSC is the same as the topology of RSC. Only difference would be input parameters and angle that is used for generating reference space vector. This angle should be obtained from the grid voltages shown in Figure 2.24.

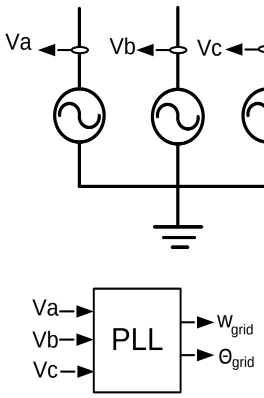

Figure 2.24 Obtaining of grid speed and angle

The grid angle will be used in vector transformation matrix. For GSC, the grid angle is quite important and it must be calculated with very good accuracy. For this reason, Phase locked loop (PLL) technique will be used in both simulation and experimental study.

Another technique to get angle could be to use equation (2.52). For simulation there would be no disadvantage, but in experimental work more calculating time is consumed in digital signal processor (DSP).

$$\Theta = \arctan\left(\frac{V_\beta}{V_\alpha}\right) \tag{2.52}$$

The RSC uses DC bus power during subsynchronous operation or gives power to DC bus during supersynchronous operation. So in both operations, RSC will cause instability on DC bus. So DC bus voltage will tend to decrease during subsynchronous operation and will tend to increase during supersynchronous operation. In conclusion, GSC must regulate the DC bus with high speed dynamic response in order to provide stability.

Also the GSC has responsibility to control reactive power with controlling d axis current.

2.9 Phase Locked Loop (PLL)

According to some reasons that were mentioned in the previous section, we need PLL technique. The PLL technique that will be given here will be analyzed in simulation and will be carried out in experimental. The PLL algorithm scheme can be seen from Figure 2.25.

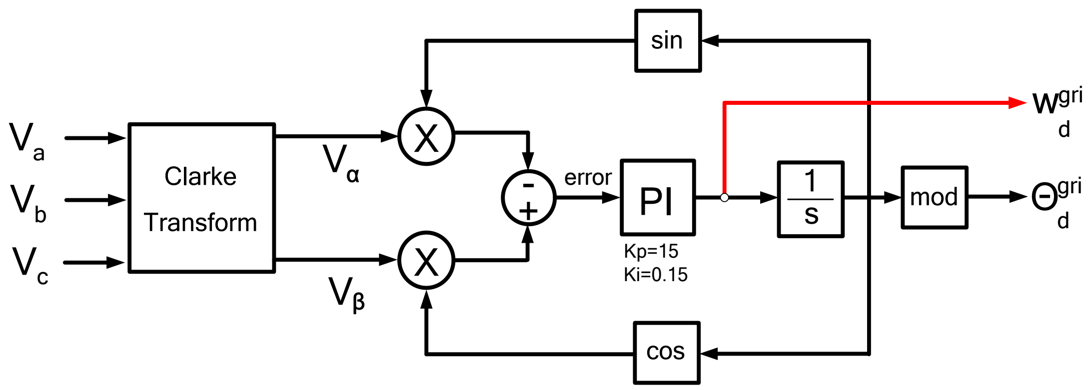

Figure 2.25 PLL control algorithm

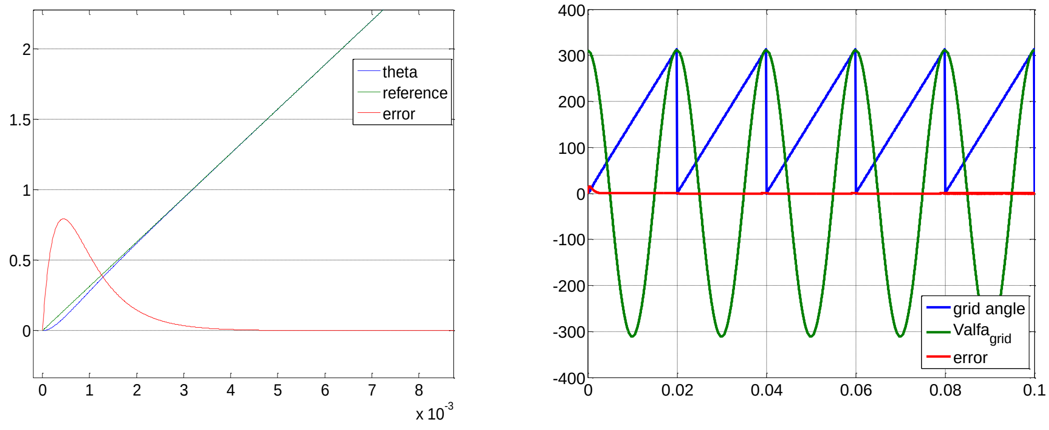

Figure 2.26 Grid angle acquisition from PLL and related data

In Figure 2.26, the PLL algorithm results are given for 50 Hz, 220 Vrms grid. It can be understood from the figure, the dynamic response of PLL is quite well, error reaches to zero around after 3.8 ms from initial where the grid period is 20 ms, and also steady state error is zero.

CHAPTER 3

SIMULATION STUDY

3.1 Modeling of DFIG

A sample DFIG from [30] is used to build finite element model. The aim of this thesis is not to present the design procedure of DFIG but rather to give its particular behavior under fault conditions. So only some design results will be shared to make sure modeled DFIG is reliable to use in the analysis. The efficiency curve of the DFIG can be seen in Figure 3.1.

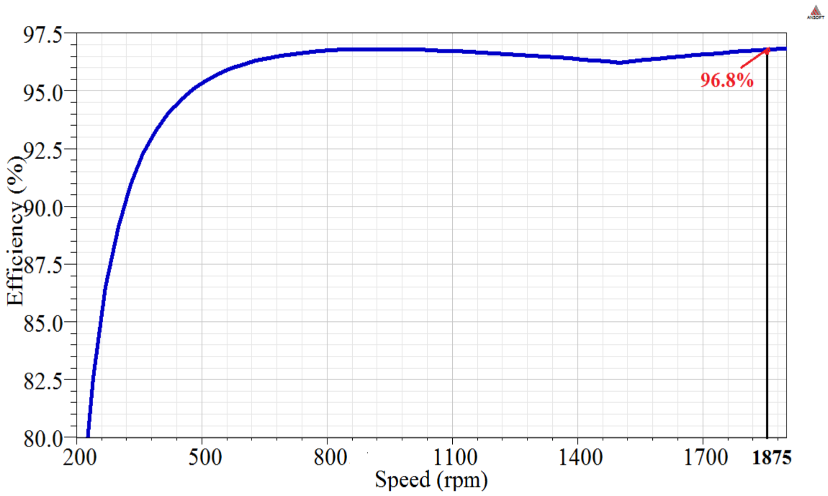

Figure 3.1 The efficiency curve of modeled DFIG

The efficiency of DFIG in nominal power is around 96.8% which is good for this 2.5 MW power level that is in IE3 high efficiency class according to CEMEP [31].

The stator, rotor and total output power variations depending on the speed can be seen in Figure 3.2. In nominal conditions, total output power consists of 500 kW rotor output and 2 MW stator output power where the slip is around -0.25.

Figure 3.3**Hata! Başvuru kaynağı bulunamadı.** gives some finite element (FE) design results. In this design, DFIG is assumed to be liquid cooled.

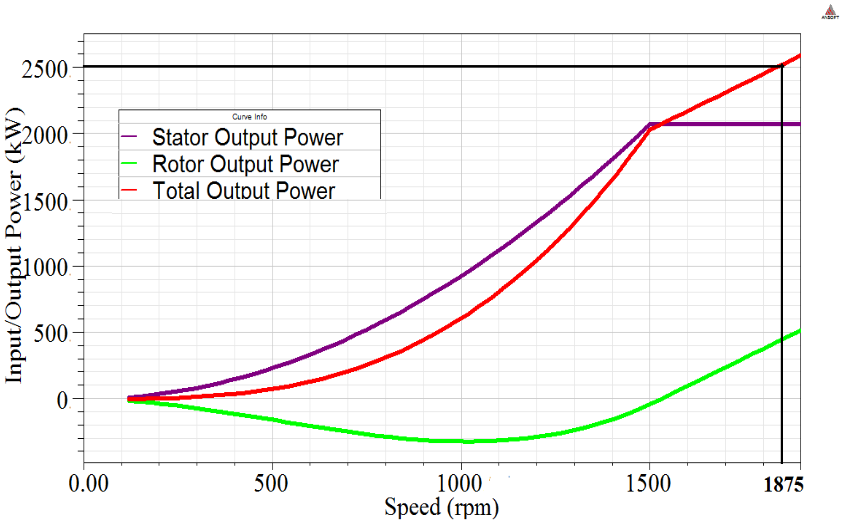

Figure 3.2 Variation of power outputs in response to speed variation

Table 3.1 Some DFIG design parameters

Parameter	**value**	**Unit**	**Parameter** (at full-load)	**value**	**unit**
Frequency	50	Hz	Stator-teeth flux density	1.268	Tesla
Rated voltage	690	V (L-L)	Stator-yoke flux density	1.548	Tesla
Rated speed	1500	rpm	Rotor-teeth flux density	1.835	Tesla
Rated output power	2000	kW	Rotor-yoke flux density	1.728	Tesla
Number of poles	4		Air gap flux density	0.753	Tesla
Number of stator slots	60		Stator phase current	1722	A
Number of rotor slots	48		Rotor phase current	2217	A
Winding type	Y3		Shaft Torque	13230	N.m.

The magnetic flux density distribution at 1.8 sec can be seen in Figure 3.3. There is a quarter model of the DFIG in Figure 3.4.

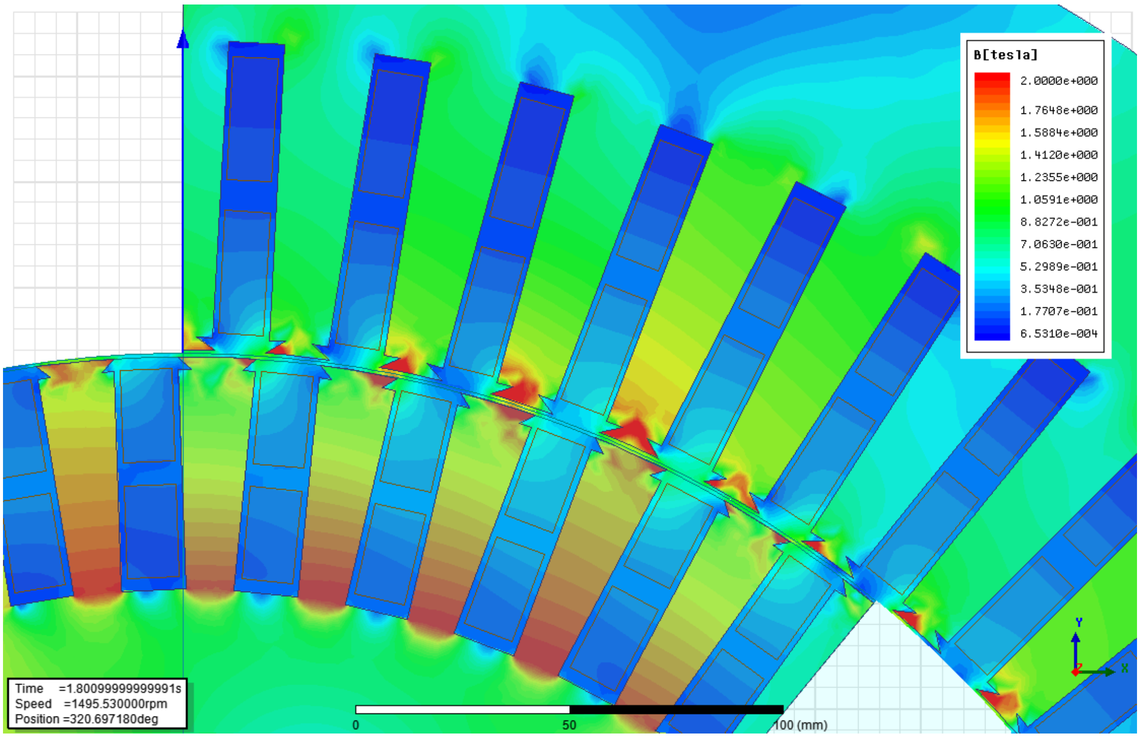

Figure 3.3 The flux density distribution in DFIG at 1.8 second

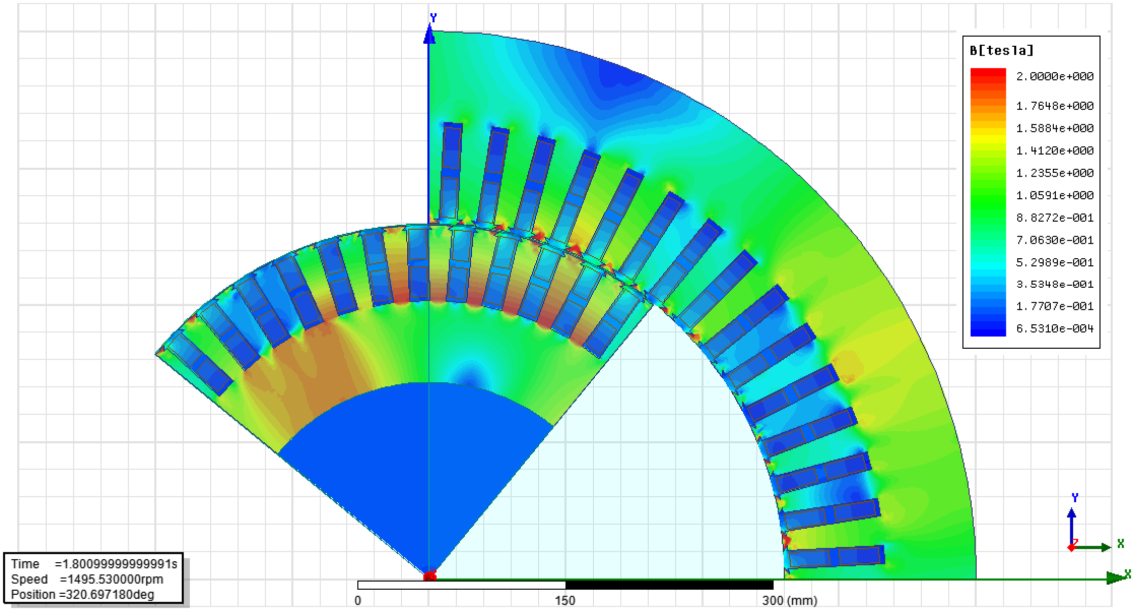

Figure 3.4 The flux density distribution in the quarter model of the DFIG at 1.8 second

The electromagnetic performance of the modeled DFIG seems to be satisfactory. So we can use these model results in the simulation platform.

3.2 Analysis of Healthy Condition

The simulation study is carried out with two different tools to make sure modeling of the system is quite reliable. The first of them is only Matlab-Simulink and the second one is Matlab-Simulink, Ansoft-Maxwell and Ansoft-Simplorer.

3.2.1 MATLAB-Simulink Simulation

In this section, the wind turbine components are modeled by using Matlab-Simulink power system toolbox as shown in Figure 3.5.

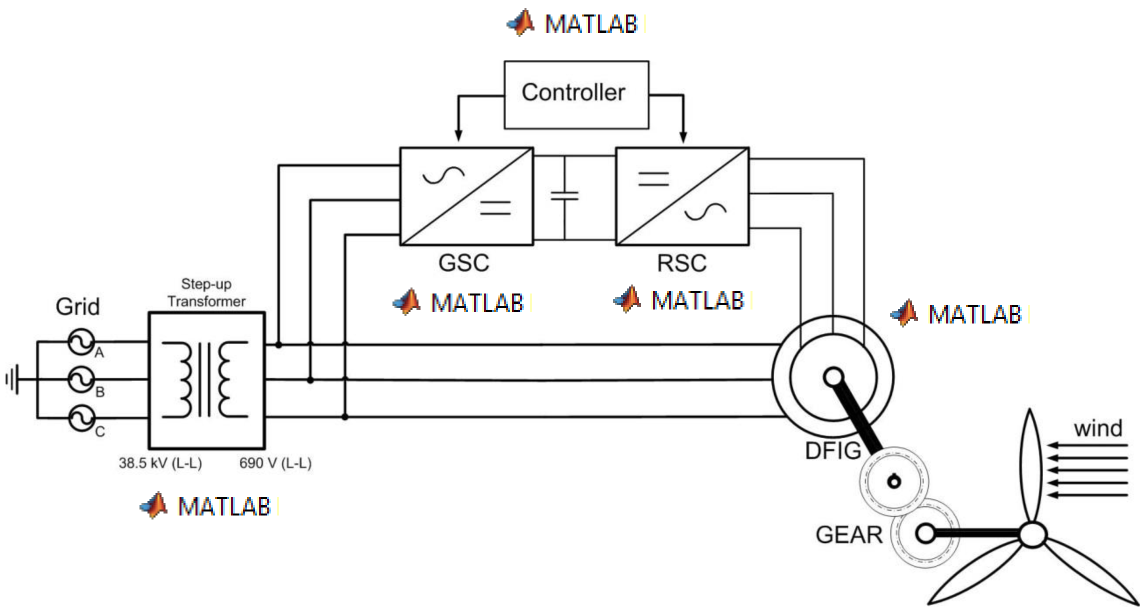

Figure 3.5 Wind turbine model implementing diagram with using Matlab-Simulink

The system components are turbine blades, gear, DFIG, RSC, GSC, controller, step-up transformer and grid. The mechanical parts that are blades and gear are modeled with wind turbine toolbox in Simulink is shown in Figure 3.6.

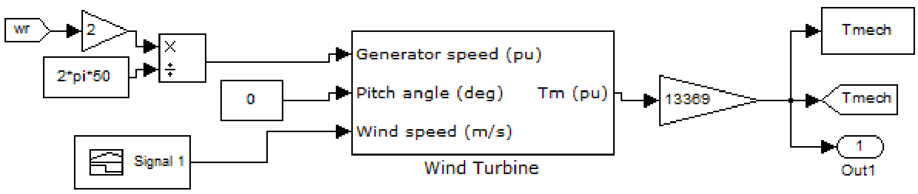

Figure 3.6 Wind turbine blades and gear modeling in Simulink

The DFIG of wind turbine is modeled in Ansoft-Maxwell finite element analysis (FEA) software. The design results are taken from FEA and are used in Simulink DFIG power system toolbox model as shown in Figure 3.7.

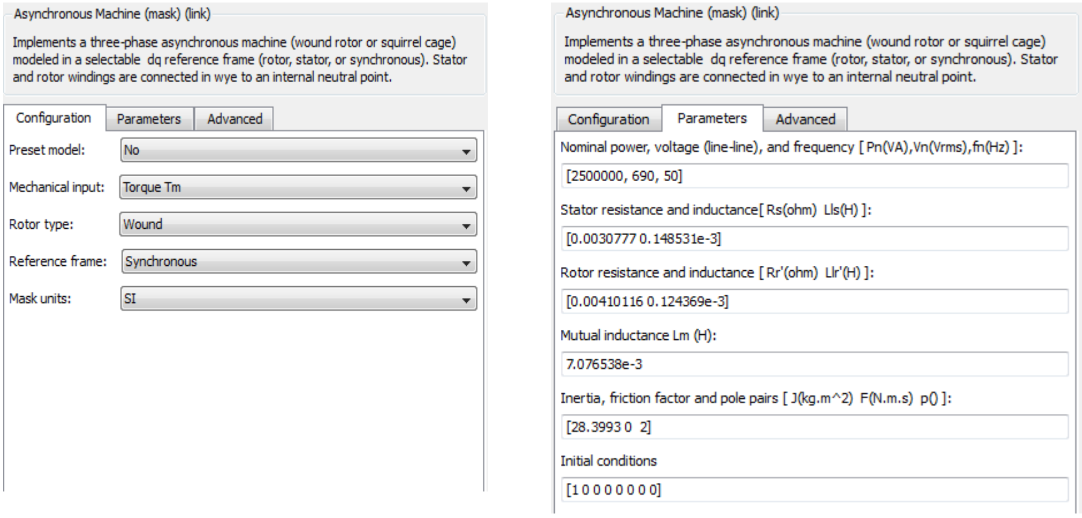

Figure 3.7 The modeling of DFIG in Matlab-Simulink.

The whole system model in Matlab-Simulink can be seen from Figure 3.8. The RSC and GSC model is created by using IGBT module toolbox. DC bus capacitor is selected 9.6mF with 0.18mΩ internal resistance. The L type filter on the output of GSC is 1mH with 6mΩ internal resistance. The power transmission line is modeled as shown in Figure 3.8. The simulation results in healthy condition are given below. The system specifications in MATLAB-Simulink are given in Table 3.2.

Table 3.2 Simulation specifications in MATLAB-Simulink

Grid Specifications			**Grid Side Converter(GSC) Specifications**		
Frequency	50	Hz	Filter inductance	1	mH
Voltage on stator side	690	V (L-L)	Filter inductance resistance	6	mΩ
Transformer winding type	Y3-Y3		DC bus capacitor	9.6	mF
DFIG Specifications			DC bus capacitor resistance	0.18	mΩ
Torque input type	ramp		DC bus voltages	1200	V
Turbine rotor inertia	28.399	Kgm^2	Switching frequency	2	kHz
Shaft Torque	13230	N.m.	**Rotor Side Converter(RSC) Specifications**		
Winding type	Y3		Switching frequency	2	kHz

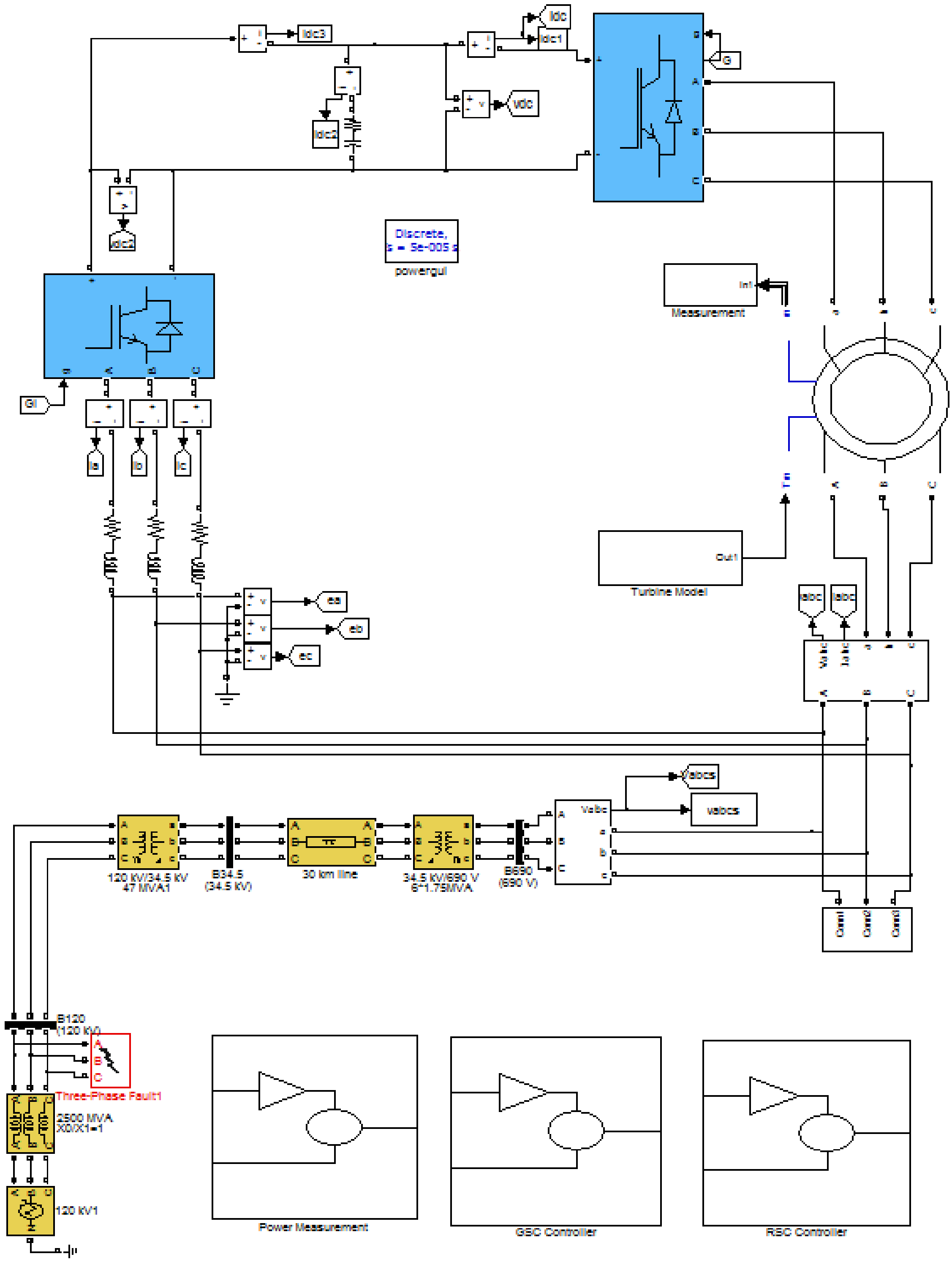

Figure 3.8 Matlab-Simulink model of DFIG wind turbine

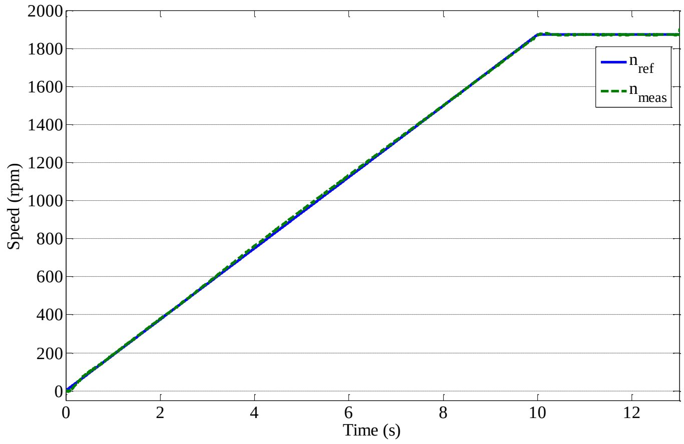

Figure 3.9 Reference and measured speed of DFIG

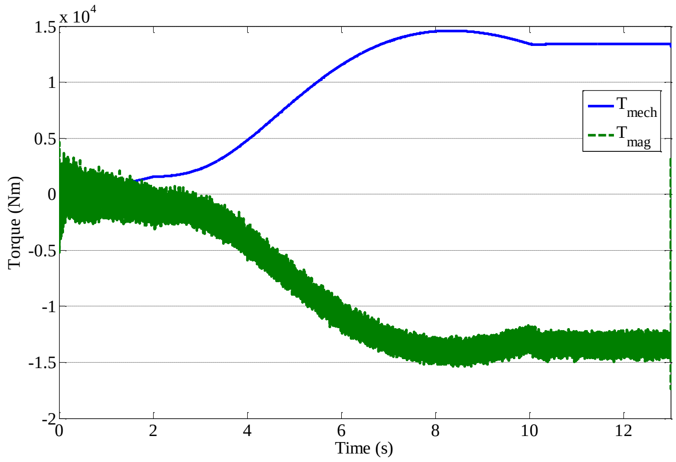

Figure 3.10 Mechanical and electromagnetic torque of DFIG

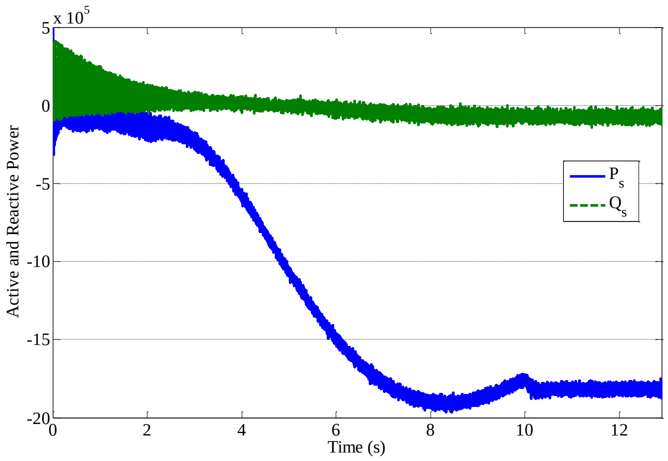

Figure 3.11 Stator active and reactive power of DFIG

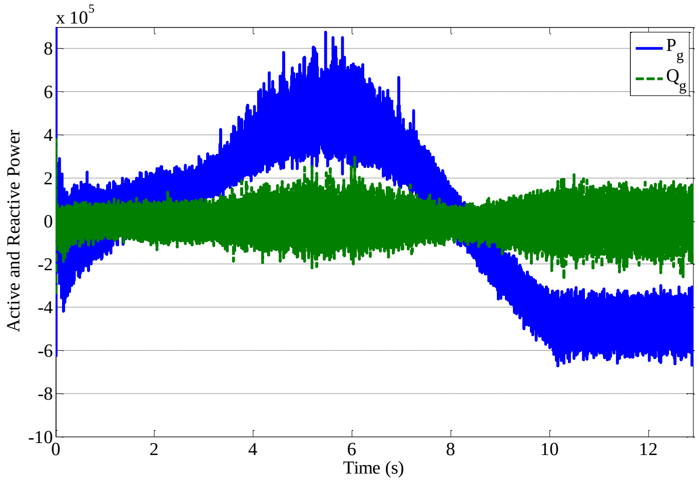

Figure 3.12 Active and reactive power of GSC

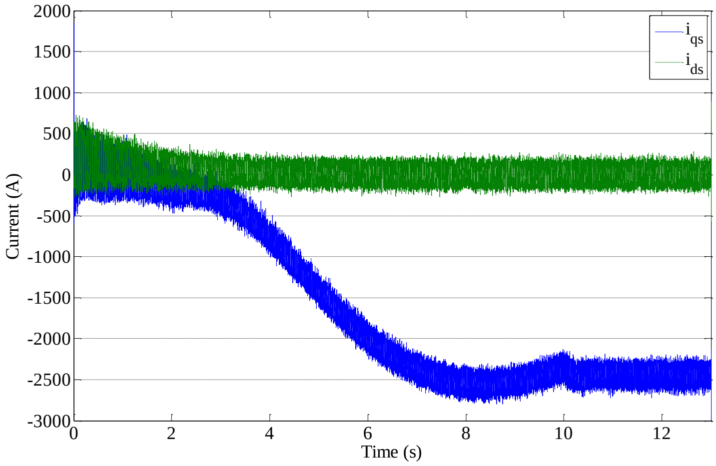

Figure 3.13 Stator q and d axis currents of DFIG

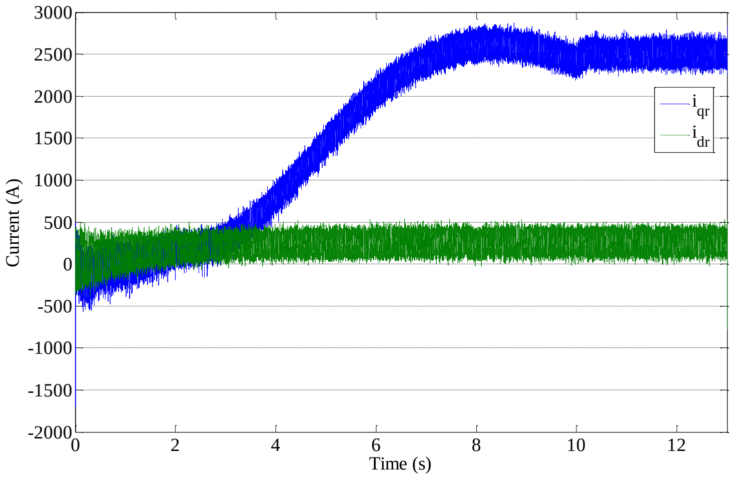

Figure 3.14 Q and d axis currents of RSC

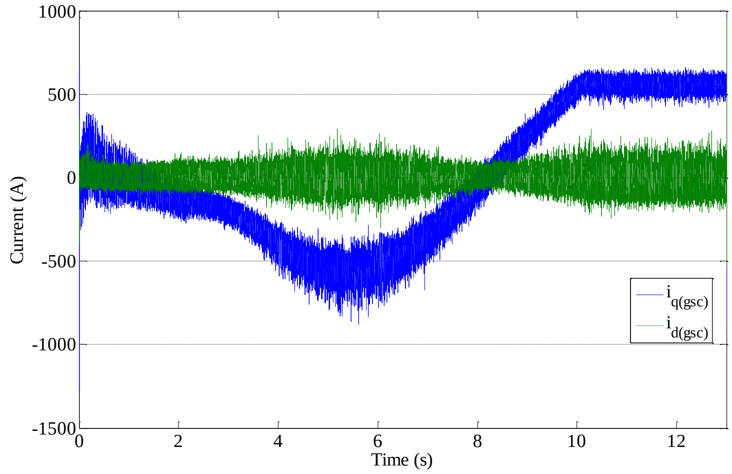

Figure 3.15 Q and d axis currents of GSC

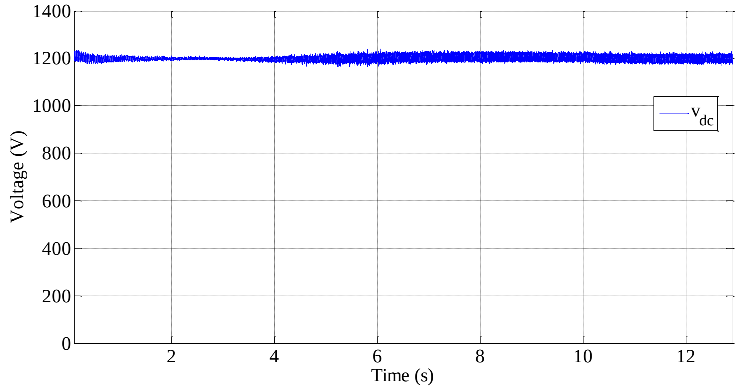

Figure 3.16 DC bus voltage of wind turbine

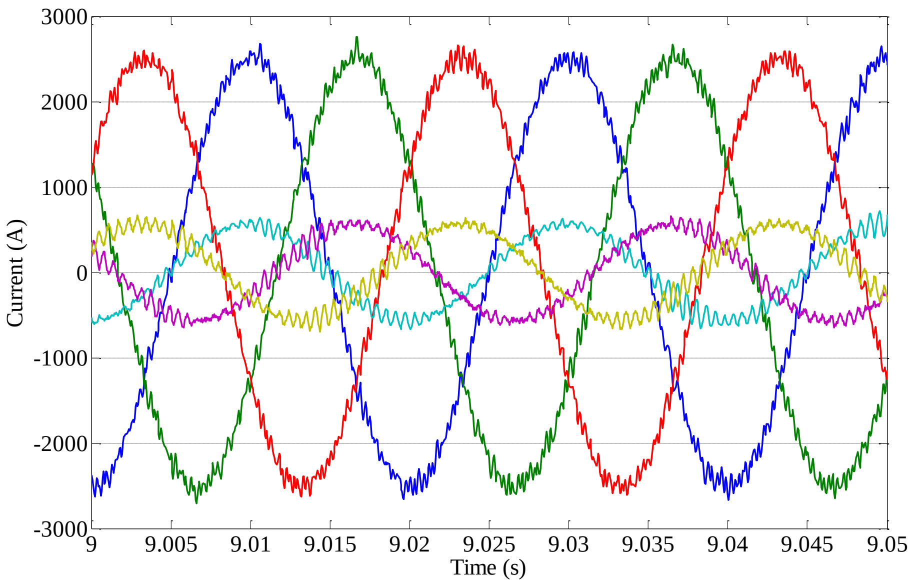

Figure 3.17 Stator currents (bigger) and voltages (smaller)

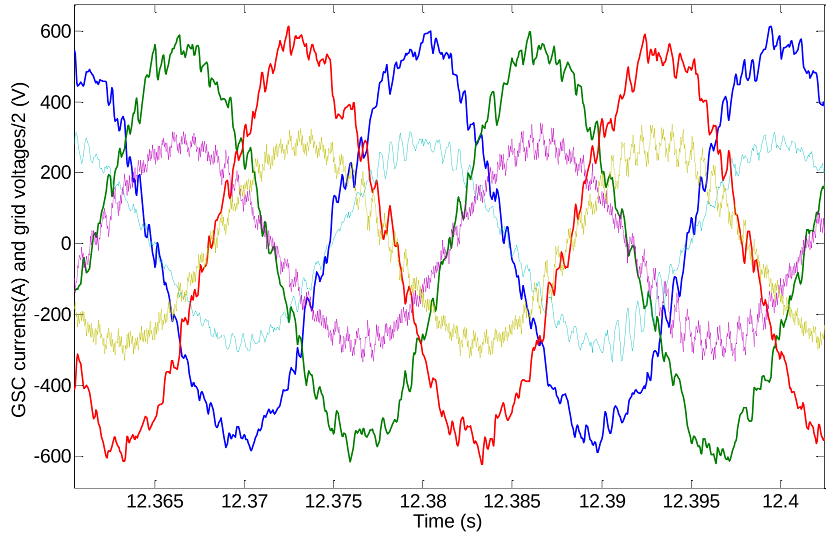

Figure 3.18 Grid voltages (bigger) and GSC currents/2 (smaller)

The MATLAB-Simulink simulation results show us that modeled DFIG wind turbine can reach nominal power in a 10 sec by controlling the power converters as shown from Figure 3.9 to Figure 3.12. In nominal case, stator can give around 2 MW active power and around zero reactive power whereas only the 500 kW active power flows through the rotor converters and this power enables the control of DFIG full power. The capacitors in DC bus provide required reactive power to the DFIG. These capacitors provide us to control RSC and GSC as independent controllers because large capacitors behave as a buffer. Corresponding stator q and d axis currents are shown in Figure 3.13. Power converters RSC and GSC currents are shown in Figure 3.14 and Figure 3.15, respectively.

The important point here that, RSC currents are higher than the GSC currents because induced voltage in the rotor windings is proportional to the slip;

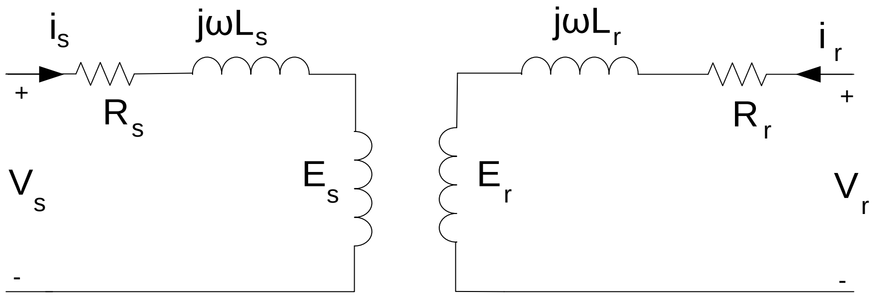

Figure 3.19 The equivalent one phase circuit diagram of DFIG

In nominal case, if we assume Vs=Es,

$$s.Es=Er \tag{3.1}$$

So the induced voltage in rotor windings at nominal case become Vs.(s)

$$Vs = 690/\sqrt{3}\ V \tag{3.2}$$

$$Er = 99.59\ V \tag{3.3}$$

Vs and Er are phase-to-neutral voltages.

In rotor windings; voltage level is lower than the stator voltage. So for 500 kW power, current must be higher in RSC. But for the GSC, the output voltage of the GSC is 690 V (line to line) and DC bus is 1200 V. So for this voltage level current will be low.

In Figure 3.15, the active power of rotor is positive below the synchronous speed because of the positive slip. It proves (2.45). It demonstrates that, below the synchronous speed rotor takes power from grid. Above synchronous speed, slip will be negative and power will flow from DFIG to the grid through power converters.

Figure 3.16 shows the DC bus voltage. DC bus voltage is controlled with GSC q axis current.

3.2.2 **Coupled Simulation**

Coupled simulation is an integration of two or more simulation platforms and a creation of a communication link between them to provide more realistic component and system simulation. Through using Matlab-Simulink, Ansoft-Simplorer and Ansoft-Maxwell 2D simulation packages, DFIG model with finite element method, inverter switches, step up transformer, and the control algorithm have been built and coupled together as shown in Figure 3.20. It is a new approach for analyzing a DFIG wind turbine in the literature.

Mechanical input of the generator is assumed to be constant at 12000 Nm. The step-up transformer and power converters are modeled in Ansoft-Simplorer. The control algorithm is created in MATLAB-Simulink as used before. DFIG is modeled through finite element technique by using Ansoft-Maxwell. Whole system components are integrated in Ansoft-Simplorer platform.

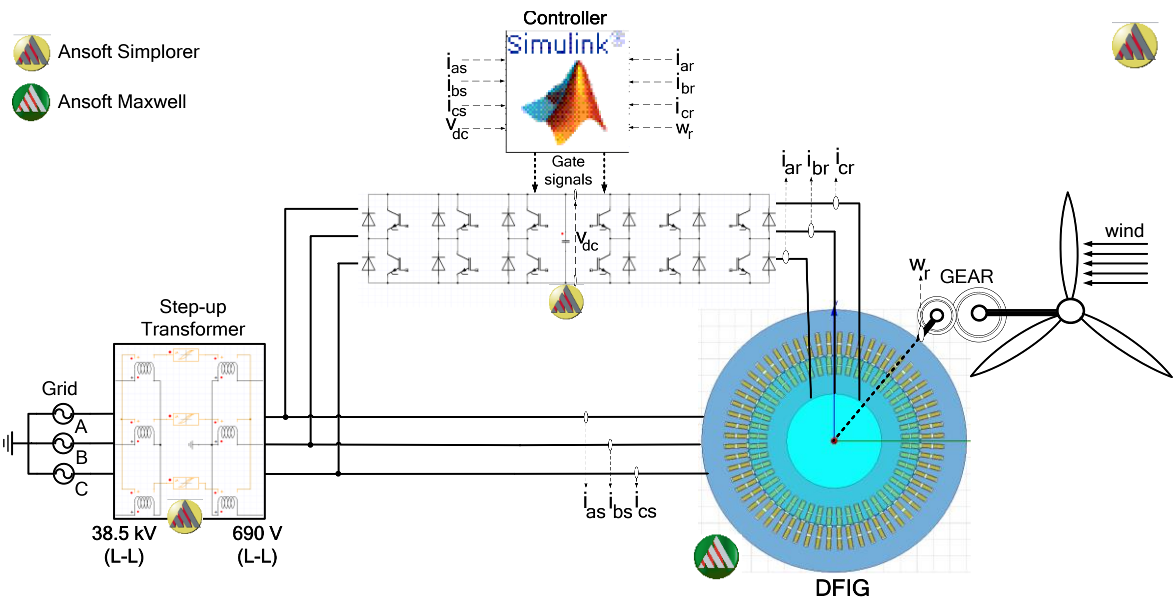

Figure 3.20 Schematic diagram of coupled simulation in wind turbine

3.2.2.1 **Modeling of Step-up Transformer**

The step-up transformer is used for connecting DFIG to the medium level voltage of the grid. The primary side of the transformer is connected to the DFIG with 690 V line-to-line voltages. The secondary side of the transformer is connected to the grid which has medium level 38.5 kV voltage. According to the survey [18]; faults are generally occurred at medium level voltage side. So it would be sufficient to consider one step-up transformer only.

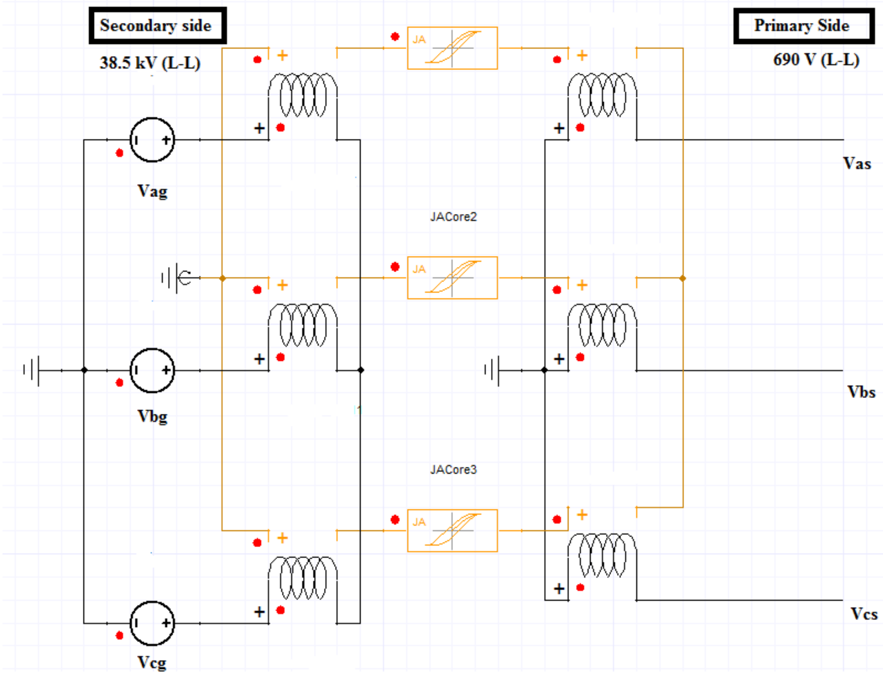

Figure 3.21 Model of step-up transformer

Figure 3.21 shows the model of used step-up transformer in analysis of wind turbine where the transformer is connected in star(Y). The good point of the model is that it takes into account not only mutual coupling but also transformer's magnetic hysteresis loop. So this means magnetic saturation of transformer is considered. This is very important aspect of analyzing DFIG behavior during grid fault.

3.2.2.2 **Modeling of Power Switches**

The power converters are modeled as a two level inverter and rectifier. One converter has six IGBTs. Every IGBT has parallel connected diode as shown in Figure 3.22. The modeled IGBT and diode has 1.25 V voltages drop during on state.

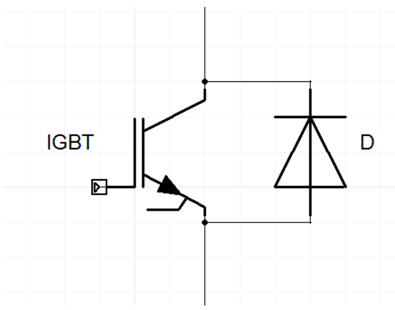

Figure 3.22 Power switch and diode

3.2.2.3 **Coupled Simulation Results**

The coupled simulation results for healthy condition are given below.

Figure 3.23 shows the variation of stator voltage and current. The power converters in rotor control the active and reactive power of stator. The variation shows that reactive power of stator is around zero. Only active power flows through to the grid from stator because stator voltage and current are in phase.

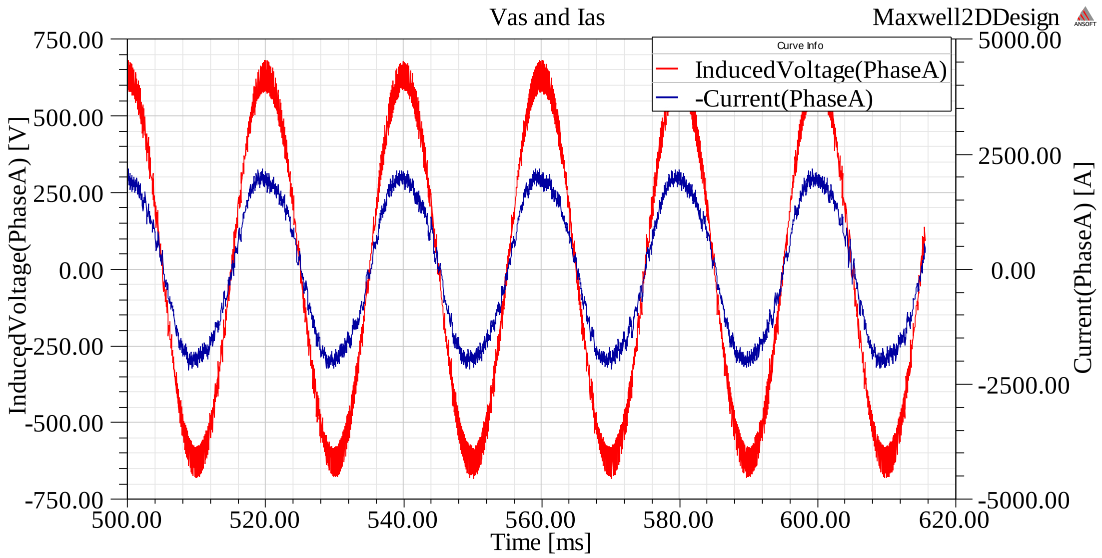

Figure 3.23 Stator voltage and current variation

The current caused some ripples on a grid voltage because of the magnetic and electrical effect of current. It demonstrates the realistic result.

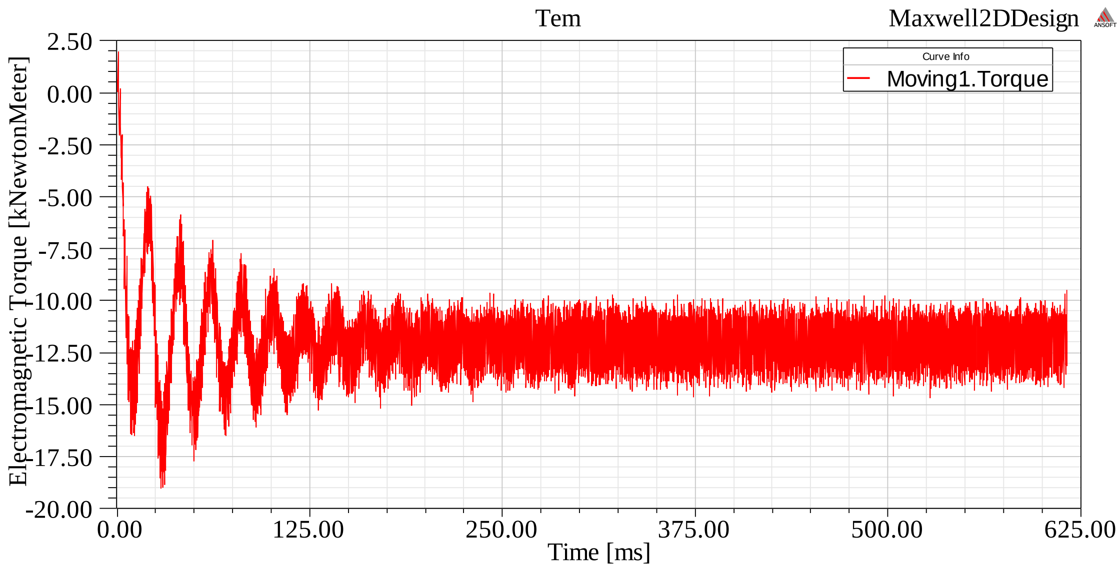

Figure 3.24 Electromagnetic torque variation

The variation of electromagnetic torque is shown in Figure 3.24. The transient time is kept short with tuning PI coefficients of power converters because of the long finite element analysis time. Because of that the transient response of generator is abnormal. The mechanical torque input is constant at 12500 Nm. So, in steady state, torque would be around 12500 Nm as shown in Figure 3.24.

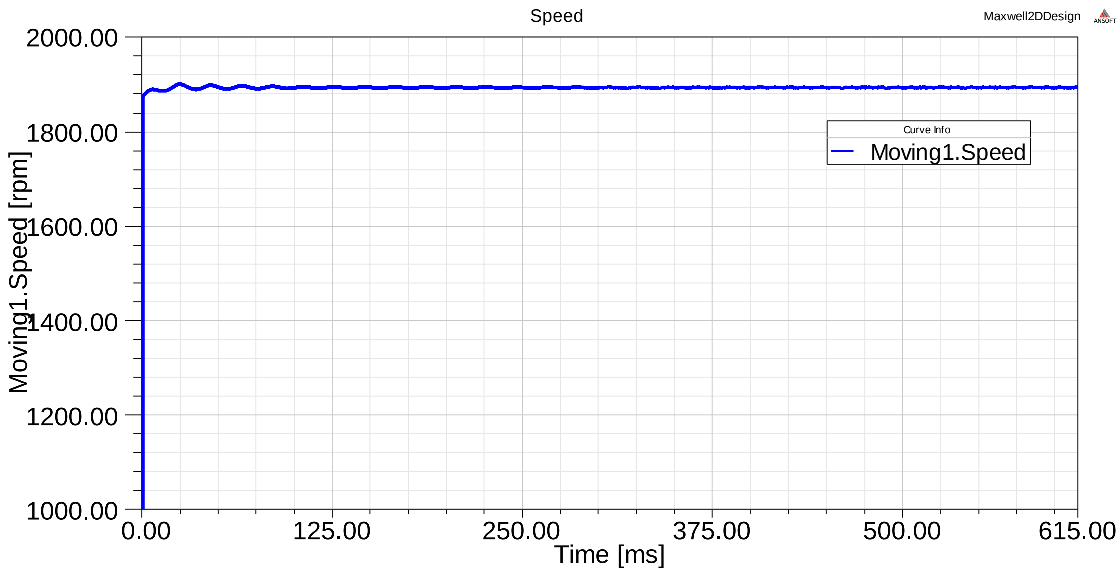

Figure 3.25 Mechanical speed variation

The mechanical speed variation of DFIG is shown in Figure 3.25. The mechanical speed is around 1875 rpm where the slip is -0.25 which is nominal point.

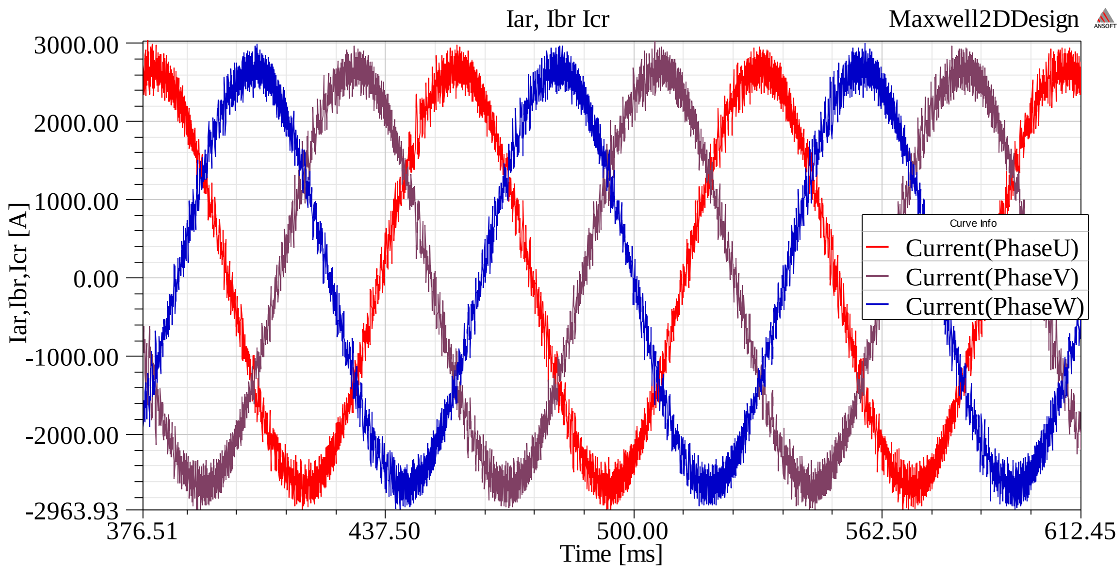

Figure 3.26 Rotor Side Converter(RSC) Currents

The RSC three phase currents can be seen from Figure 3.26. The switching frequency of RSC is selected 2 kHz for 500 kW power level. The three phase currents have low harmonic content as shown in figure.

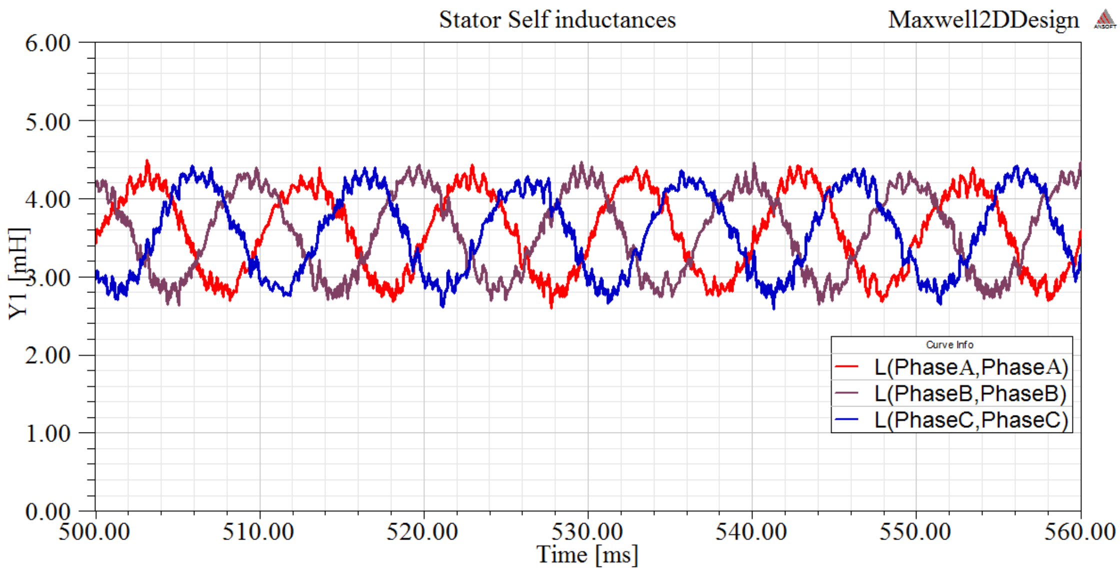

Figure 3.27 Stator self-inductances

The coupled simulation provides machine`s internal parameters such as inductances and fluxes. The self-inductances of stator and rotor windings are shown in Figure 3.27 and Figure 3.28, respectively.

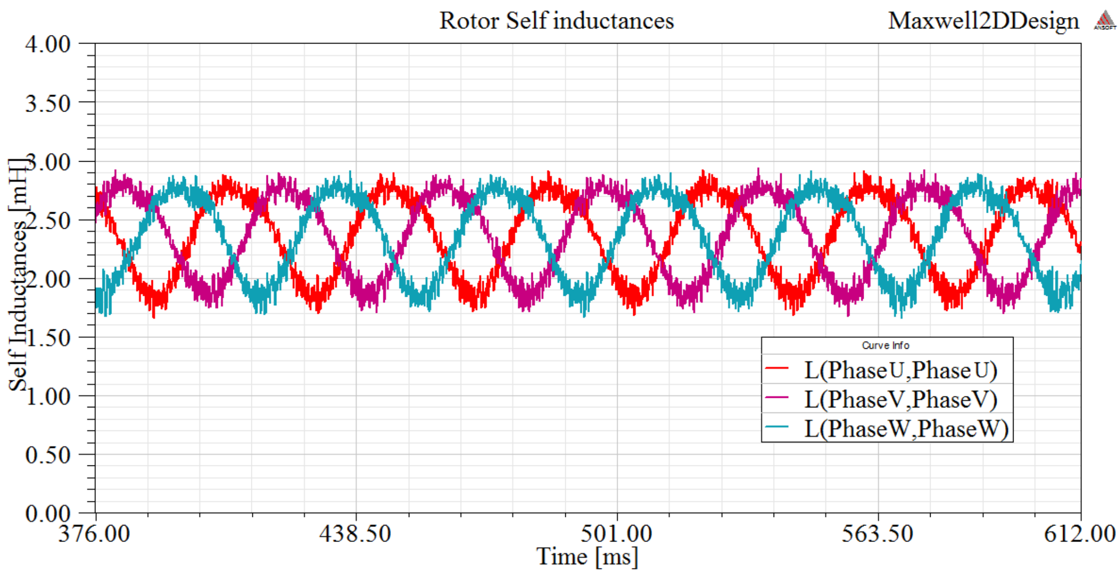

Figure 3.28 Rotor self-inductances

3.3 Analysis of Fault Condition

According to the Aalborg University`s report [18], the fault events in electrical network are mostly related to the voltage magnitude. The voltage magnitude may change in time durations from milliseconds up to hours in fault condition is called voltage sag. The report surveyed the fault events in different countries. The result is that single phase-to-ground fault type has the highest probability to occur in the electrical network. Additionally, most of faults occurred in momentary time like 1-6 utility cycle duration of grid, located on 132 kV overhead lines [18]. However to analyze DFIG in wind turbines, many papers [12],[15],[21] concentrated on symmetrical 3-phase faults which have very low probability to occur.

In this thesis, three fault types are analyzed to see the effects of grid fault on DFIG wind turbine. These three fault types are one phase-to-ground, two phase-to-ground and three phase-to-ground faults. The voltage magnitude in medium voltage level of grid when fault occurs is assumed to be zero which is the worst scenario for DFIG wind turbine. Every fault is assumed to have 150ms time duration which is the maximum permissible duration to stay connected for the zero magnitude voltage according to the German grid code in Figure 3.29 which is the reference code for other European and American countries.

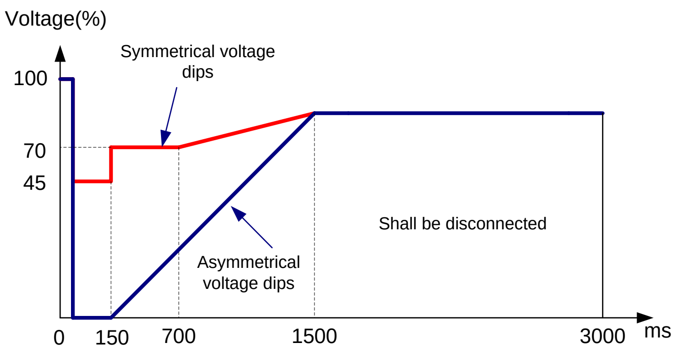

Figure 3.29 Voltage limit curves according to the Germany grid code

Figure 3.29 shows the German grid code. This figure determines the wind turbine required remain connected time duration to the grid. For instance, if the symmetrical fault like three phase-to-ground occurs, the wind turbine must remain connected to the grid when the voltage dip above 45% in 150 ms duration. Below that percentage, the wind turbine can be disconnected. For asymmetrical voltage dips, the wind turbine must be remaining connected even if the voltage of grid becomes zero for 150 ms. These percentage values are depend on country`s electrical network characteristics. So it varies from one country to another. We will analyze all these fault types with assuming zero voltage magnitude on medium voltage level side of the grid.

In the thesis; two simulation packages are used. Because of the nonlinear system components of wind turbine, the coupled simulation technique is probably more reliable than the only MATLAB-Simulink simulation. Hence DFIG model is created with finite element method and also step-up transformer, which is very important in the analysis, is modeled with saturable function (B-H hysteresis loop). The system model is also created in MATLAB-Simulink of which the results are not quite accurate and reliable. Therefore only the coupled simulation results will be shared in the thesis.

3.3.1 **One Phase-to-ground Fault implementation**

One phase-to-ground fault is implemented by applying zero voltage on secondary side of the phase-C. The voltages of primary side of the transformer are given in Figure 3.30 which is also stator winding voltages.

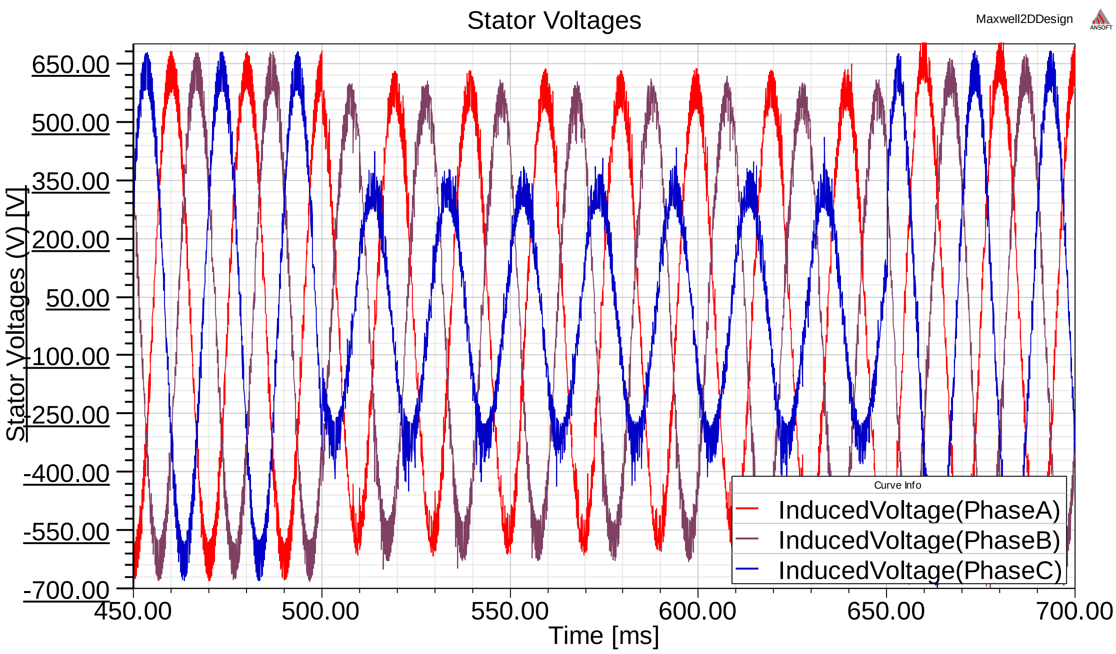

Figure 3.30 Variation of stator voltages in one phase-to-ground fault condition

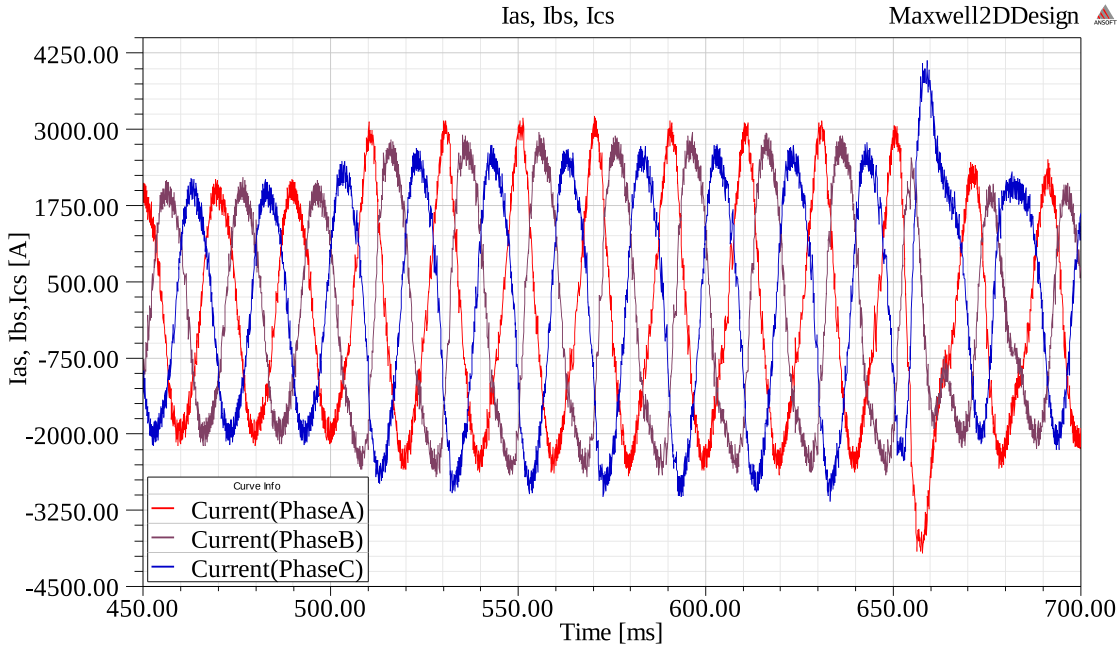

Figure 3.31 Variation of stator currents in one phase-to-ground fault condition

The stator currents variations during fault are given in Figure 3.31. The current which is around 2000 A in normal condition becomes two times higher in magnitude when one phase-to-ground fault occurs. The rotor currents are shown in Figure 3.32 also become two times higher in fault condition. These current levels are very high and problematic for power converters.

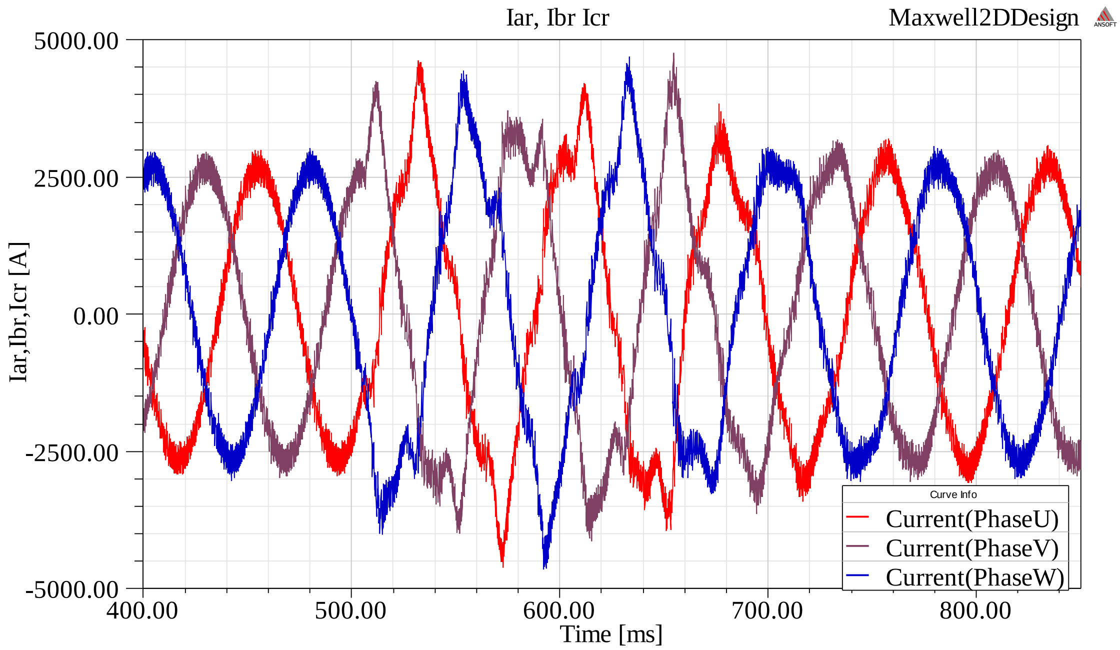

Figure 3.32 Variation of rotor currents in one phase-to-ground fault condition

3.3.2 **Two Phase-to-ground Fault implementation**

Two phase-to-ground fault is implemented by applying zero voltage on secondary side of the phase-B and phase-C. The voltages of primary side of the transformer are given in Figure 3.30 which is also stator winding voltages.

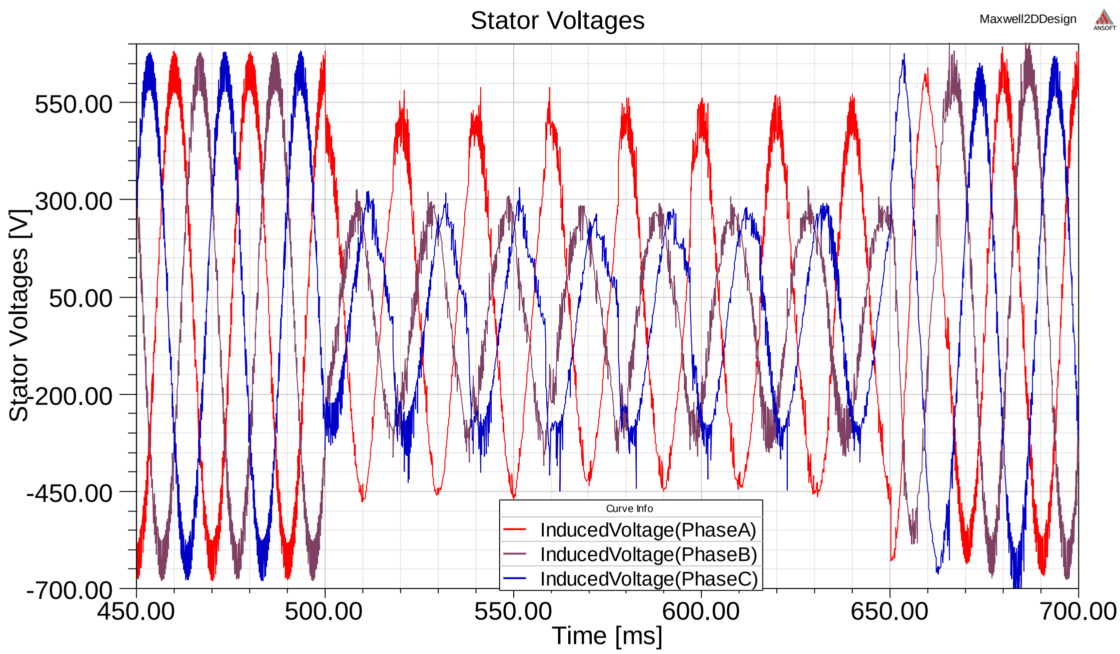

Figure 3.33 Variation of stator voltages in two phase-to-ground fault condition

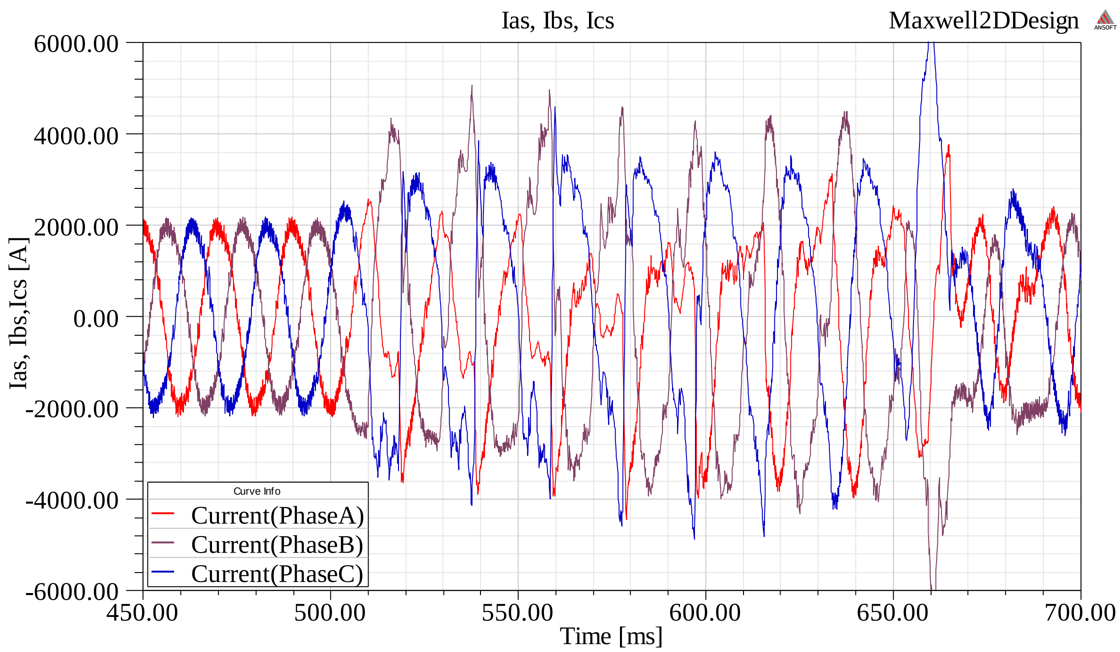

Figure 3.34 Variation of stator currents in two phase-to-ground fault condition

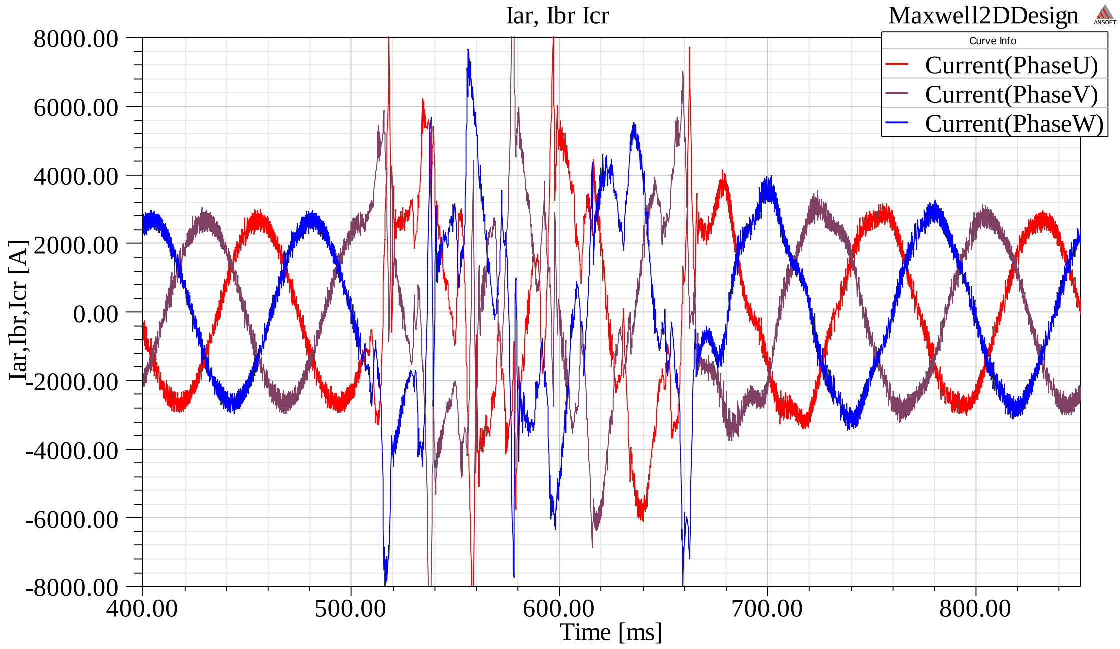

Figure 3.35 Variation of rotor currents in two phase-to-ground fault condition

The stator currents as shown in Figure 3.34 when fault occurs will be almost three times higher than the one flowing during healthy condition. But the current levels in rotor windings are four times high and they are given in Figure 3.35.

3.3.3 **Three Phase-to-ground Fault implementation**

Three phase symmetrical fault is carried out by applying zero voltage on secondary side of the transformer. The stator voltages become as in Figure 3.36.

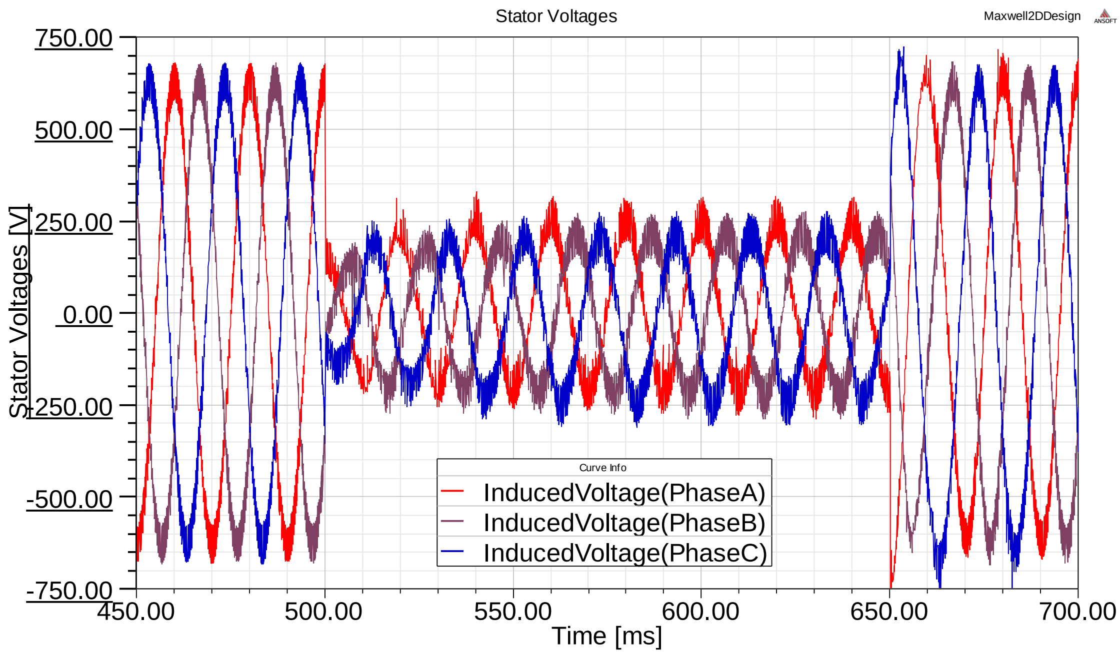

Figure 3.36 Variation of stator voltages in three phase-to-ground fault condition

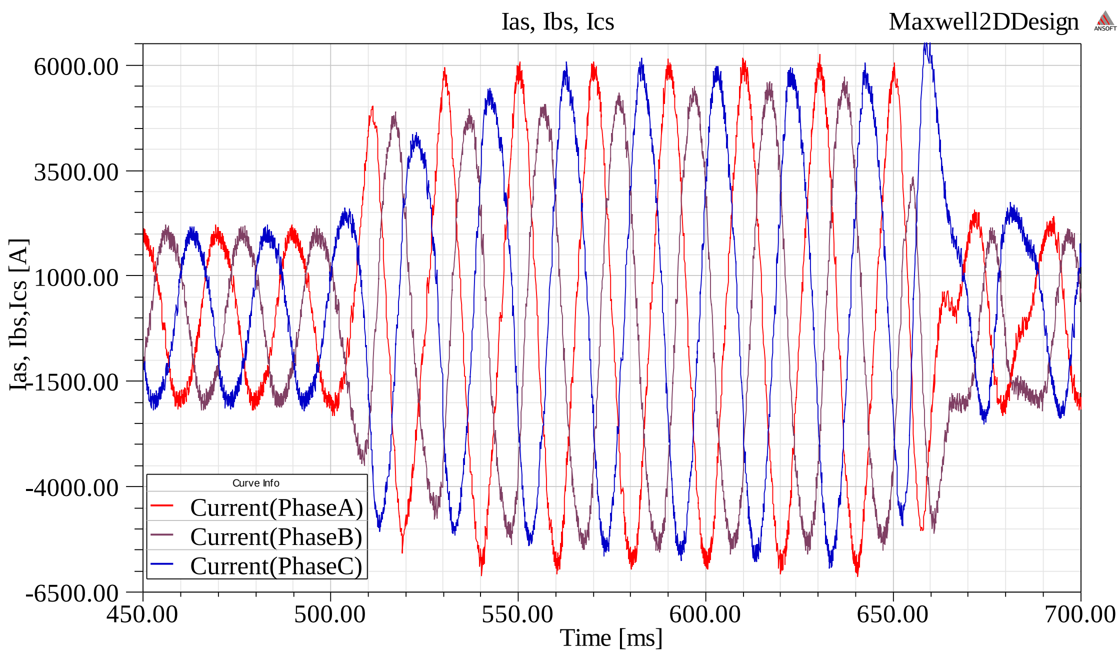

Figure 3.37 Variation of stator currents in three phase-to-ground fault condition

The stator currents and rotor currents are shown in Figure 3.37 and Figure 3.38, respectively. It must be noted here that the algorithm is the same with healthy condition. The goal of this study is to see the effects of fault types on DFIG wind turbine. Power converters, in particular, seem to be weak link in the turbine system and therefore they must be protected during and after the fault occurrence.

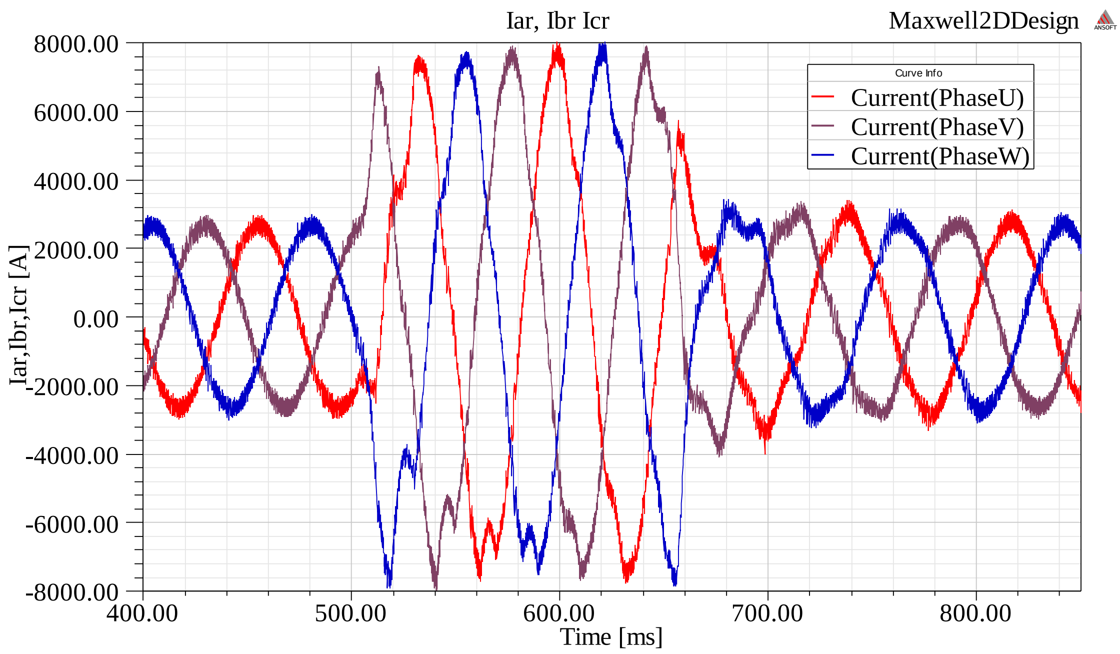

Figure 3.38 Variation of rotor currents in three phase-to-ground fault condition

Consequently, three types of faults are implemented and analyzed. The results have shown that the worst scenarios for the turbine during fault are two phase-to-ground fault and three phase-to-ground fault types as understood from the figures because the power converter currents become very high which could reach as high as three times of healthy condition current.

The analysis results illustrate that the wind turbine cannot remain connected to the grid without solving high current problem. The new control algorithm or additional device/s must be proposed by manufacturers and/or researchers.

3.3.4 **Comparative analysis of fault types**

In this section, the internal parameters variations for three types of faults are analyzed and compared with each other. The aim of this study is to understand the behavior of DFIG during fault. By understanding the behavior, new control algorithms can be developed. The DFIG internal variables such as stator flux and rotor flux, internal parameters such as stator self-inductances and rotor self-inductances are to be analyzed for the prescribed fault conditions.

The stator flux variations for each fault type can be seen from Figure 3.39 to Figure 3.41. The fault occurs at 0.5 sec. and continues up to 0.65 sec. The common point of the results is that all phases during each fault have dc component. The one phase fault is implemented by applying zero to phase-C and the two phase fault is carried out by applying zero volt to phase-B and phase-C on secondary side of the transformer as mentioned before.

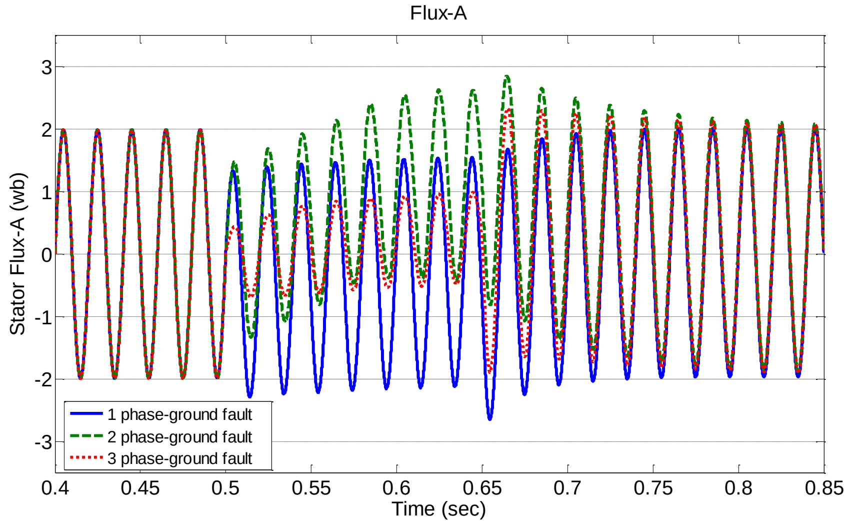

Figure 3.39 Variation of stator phase-A flux for different fault types

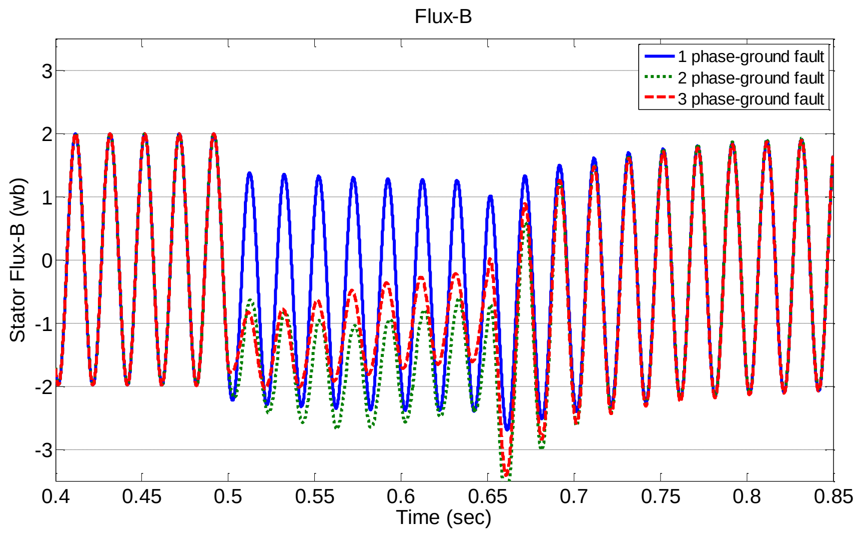

Figure 3.40 Variation of stator phase-B flux for different fault types

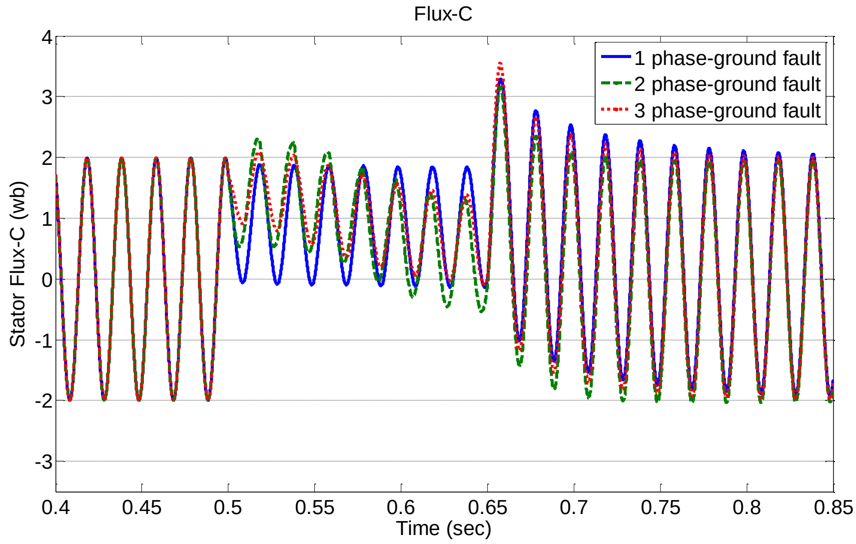

Figure 3.41 Variation of stator phase-C flux for different fault types

In experimental study, the one phase-ground fault type will be implemented. So here, stator fluxes during the similar type of fault condition will be given to compare results with experimental study.

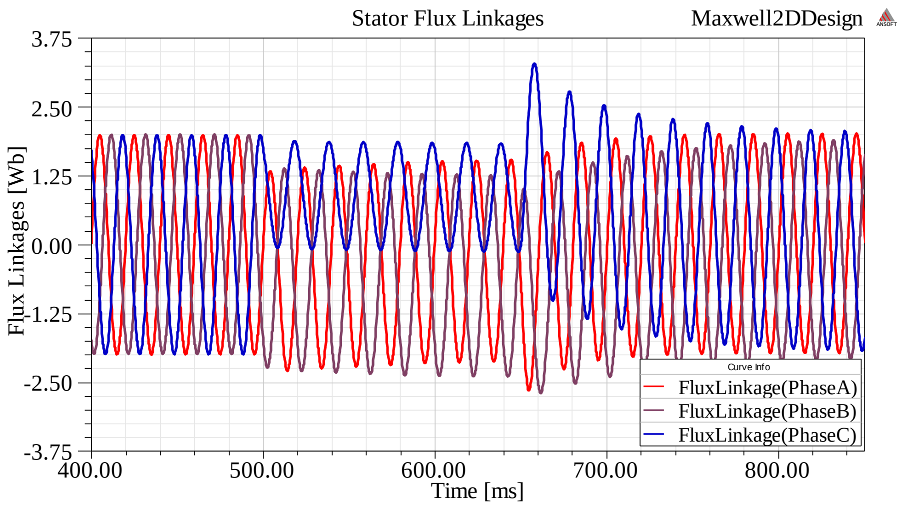

Figure 3.42 Variation of rotor phase-A flux for one phase fault type

Figure 3.42 shows the flux linkages of stator phases during one phase-ground fault. If the Fast Fourier Transform (FFT) analysis is carried out for these wave shapes, the following results in Table 3.3 will be obtained. The most dominant harmonics in stator fluxes are dc and 100 Hz.

TABLE-3.3: Most Dominant Harmonics of stator fluxes during one phase-ground fault

	Phase-A	Phase-B	Phase-C
0 Hz(Dc)	25.72%	25%	93.39%
50 Hz(Fnd)	100%	100%	100%
100 Hz	1.39%	1.63%	1.02%

The rotor flux variations during each fault are shown in Figure 3.43. It has meaningful changes in fault condition. In three types of faults, flux waveforms have the same harmonic contents but different magnitude as noticed in the figure.

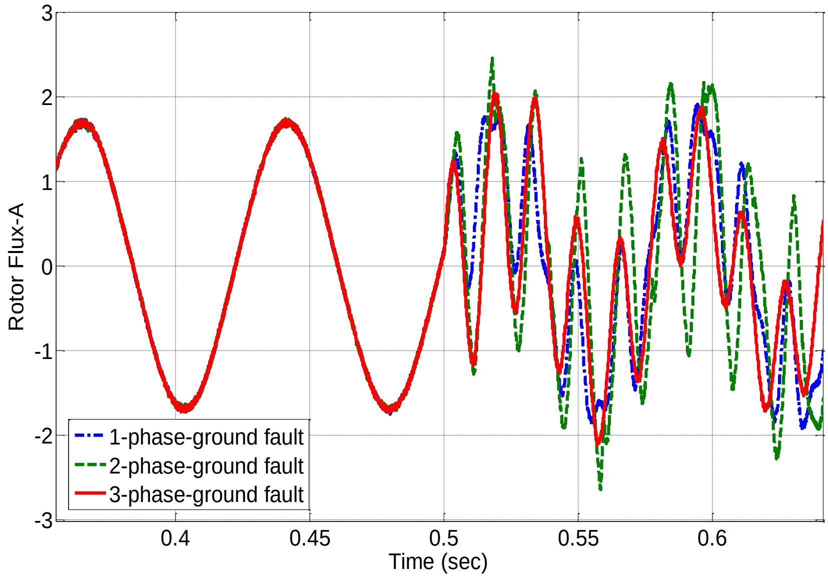

Figure 3.43 Variation of rotor phase-A flux for different fault types

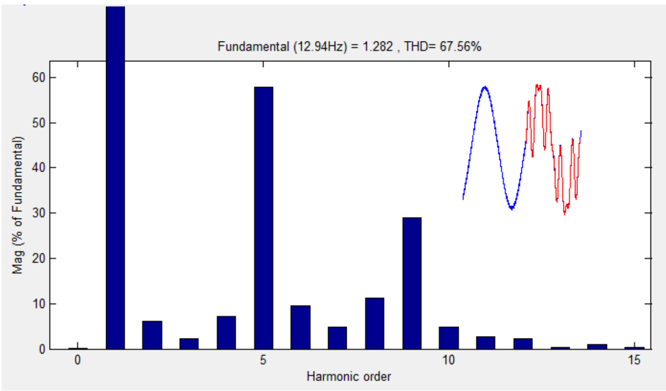

Figure 3.44 The FFT analysis of rotor phase-A flux for one phase fault

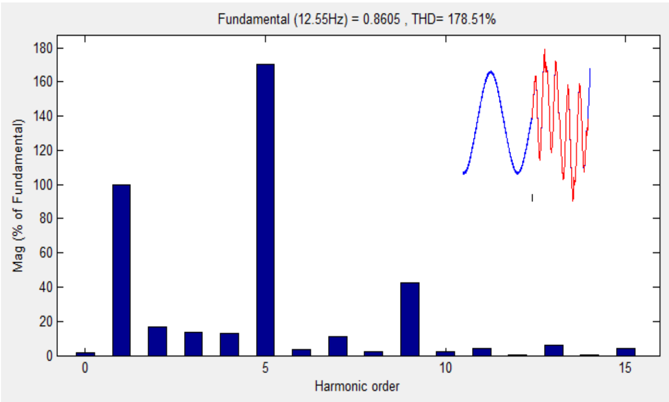

Figure 3.45 The FFT analysis of rotor phase-A flux for two phase fault

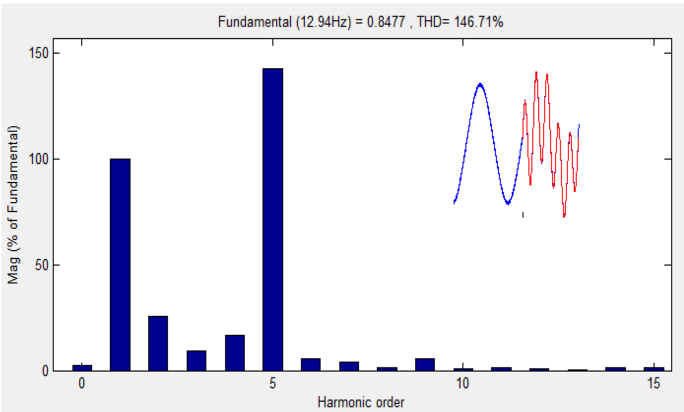

Figure 3.46 The FFT analysis of rotor phase-A flux for three phase fault

The rotor flux-A FFT analysis results are given in Figure 3.44, Figure 3.45 and Figure 3.46 for one, two and three phase fault implementation, respectively. All results show that in asymmetrical fault types, rotor flux has the same most dominant harmonic contents; 5th and 9th harmonics. In particular, two phase-ground fault has much higher 5th harmonic component. In symmetrical three phase-ground fault, 5th harmonic is the most significant component. Harmonic variation for three different fault situations is summarized in Table-3.4. As seen from the Table-3.4, 5^{th} harmonic magnitude is highly affected by the number of phases involved in the fault.

Table-3.4: Most dominant harmonics of rotor fluxes during faults

	Phase-U			Phase-V			Phase-W		
	1p	2p	3p	1p	2p	3p	1p	2p	3p
1. Fund.	100	100	100	100	100	100	100	100	100
5. harmonic	57	170	143	56	166	138	56	159	139
9. harmonic	28	42	6	28	40	5	28	40	4

1p : one phase-ground fault   2p: two phase-ground fault   3p: three phase-ground fault

Initial thought for the reasons of flux harmonic is magnetic saturation and much severer armature reaction during the fault. It can also be concluded that rotor flux harmonics cause high rotor currents with high frequency as shown in Figure 3.47. Using the findings provided by this investigation if the current harmonics are eliminated by changing control strategy, the back-to-back converter can be protected and it can remain connected to the grid during fault conditions.

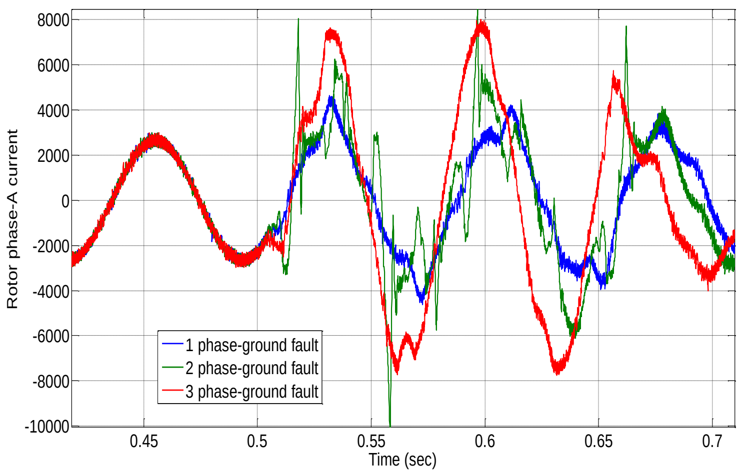

Figure 3.47 The variation of rotor phase-A current under each fault type

The other important parameter to understand the behavior of DFIG is the inductance variation during fault. By means of 2D analysis of DFIG in coupled simulation, inductances can be calculated. Figure 3.48 shows the self-inductance variations of stator phases for 3 phase symmetrical fault. As seen in Figure 3.48, phase shift between inductance waveform is zero during the fault whereas they have 120^{o} phase shift between them during normal operation. Figure 3.48 also implies that linear magnetic circuit assumption and models with invariant inductances is not the most accurate way of DFIG modeling during the fault however many papers in literature take it as an invariant constant.

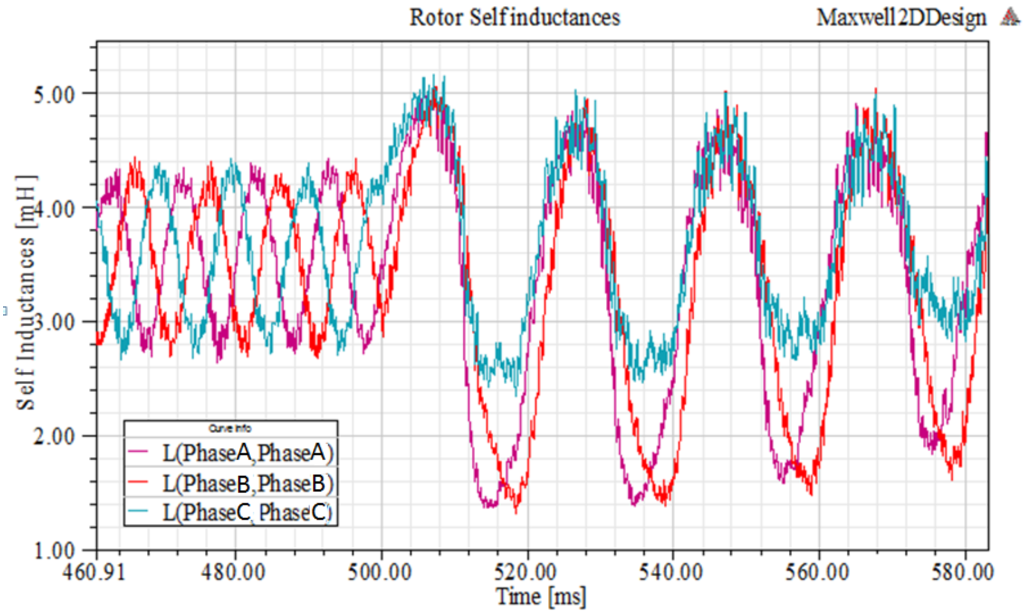

Figure 3.48 The variation of stator self-inductances under three phase ground fault

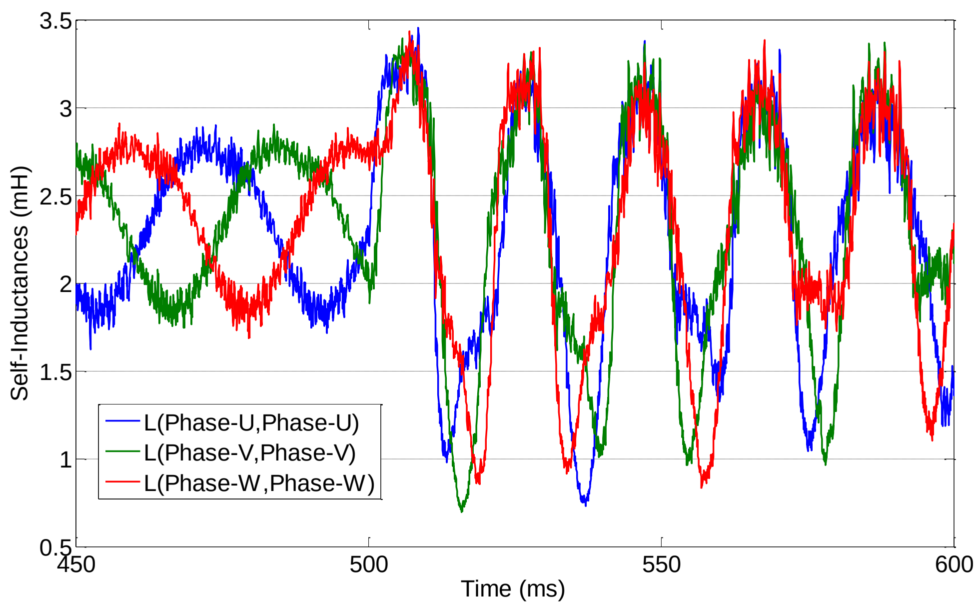

Figure 3.49 The variation of rotor self-inductances under three phase ground fault

The variation of rotor inductances during three phase fault is shown in Figure 3.49. It has also same behavior with stator inductances which the phases shift between phases inductances become zero.

The other one phase-ground and two phase-ground asymmetrical fault types are simulated and inductance variations are analyzed. They have same behavior with three phase-fault type where inductance waveforms are in phase. In order to avoid from confusion they will not be given in this thesis. Only stator phase-A and rotor Phase-U self-inductances variation will be given to compare each fault type effect in Figure 3.50 and Figure 3.51, respectively.

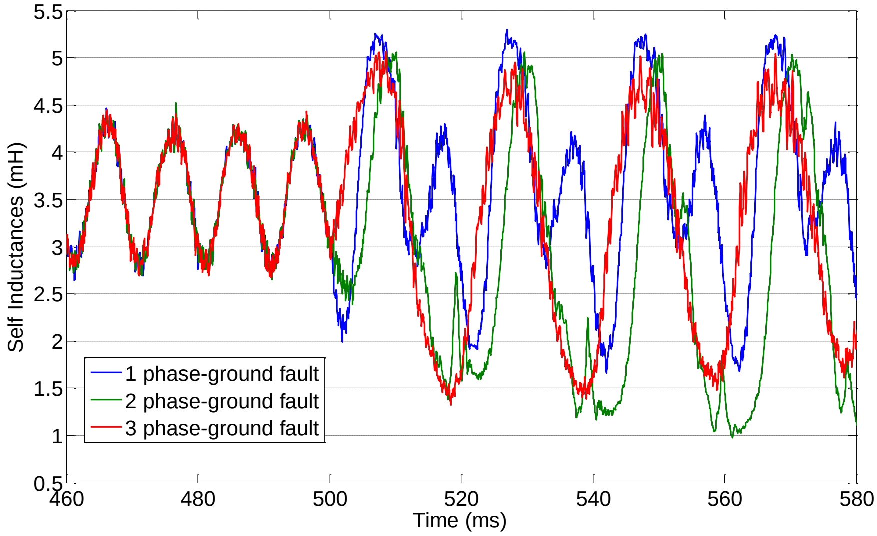

Figure 3.50 The variation of stator phase-A self-inductance for each fault type

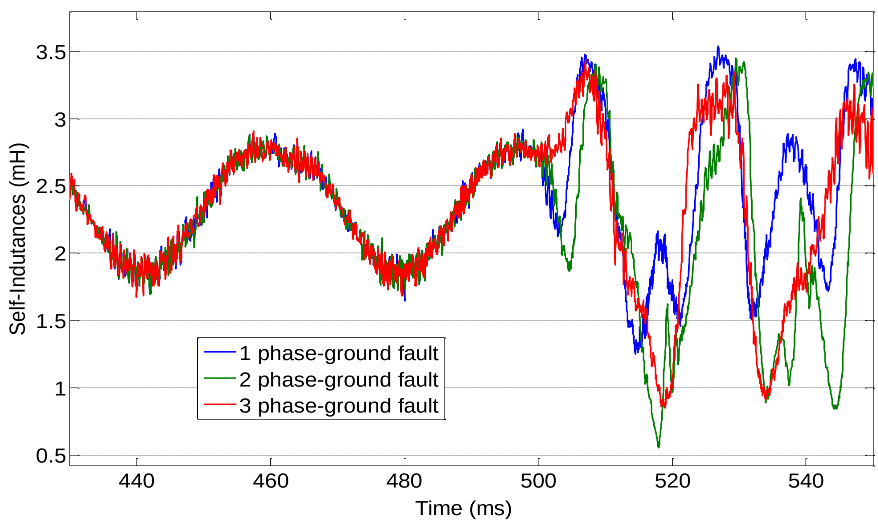

Figure 3.51 The variation of rotor phase-U self-inductance for each fault type

The mechanical speed variation of DFIG is shown in Figure 3.52. This figure is important to understand the faults effects on DFIG mechanical stress in wind turbine. Three phase-ground fault type has the greatest impact on mechanical components in wind turbine as can be seen from the figure. The weakest mechanical stress occurs during one phase-ground fault. This finding is also verified by Aalborg university report [18]. It should be noted here that there is no extra protection algorithm in control stage. So the algorithm in fault condition is same with healthy condition. It can be said from the figure that the controller tries to regulate torque and speed but it cannot succeed due to the big change in electromagnetic torque can be seen from Figure 3.53.

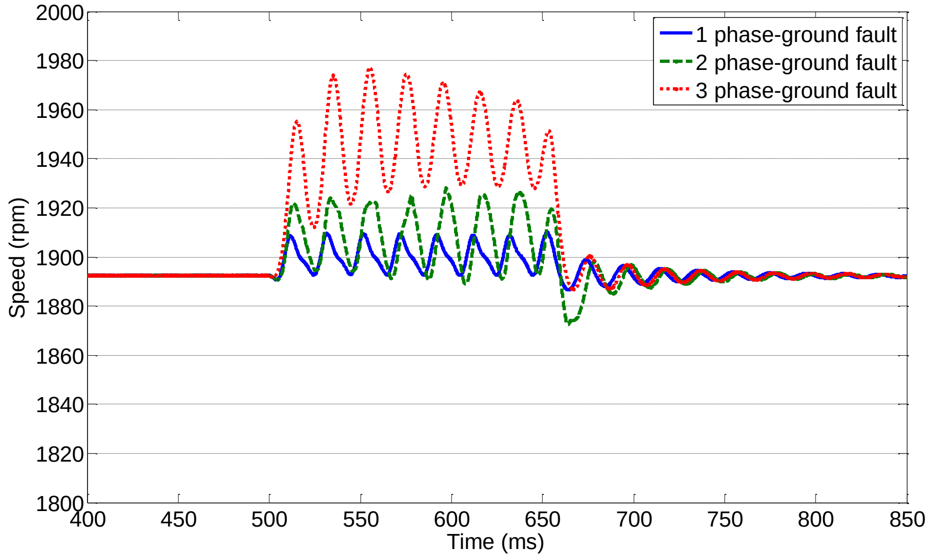

Figure 3.52 The variation of mechanical speed of DFIG during fault

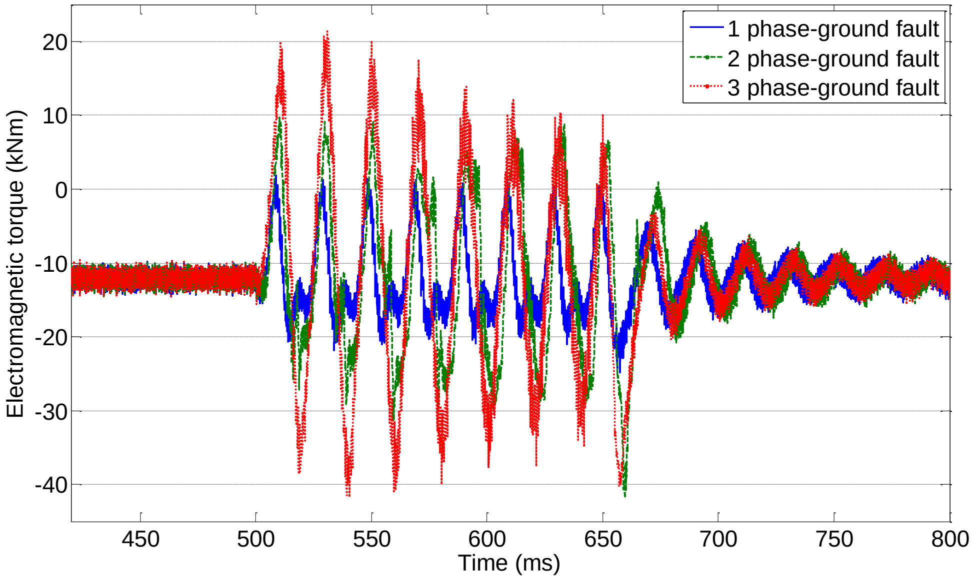

Figure 3.53 The variation of electromagnetic torque of DFIG during fault

In this chapter, the DFIG wind turbine model is simulated for healthy condition and fault condition by using MATLAB-Simulink based model and finite element based coupled simulation model. Because the coupled simulation model is more reliable, only the coupled simulation results are shared for fault analysis. The studies in [32] and [33] create the analytical and finite element based model (FEM) of DFIG to compare these two models. The studies show that there are good agreements in healthy condition with analytical and FEM model. But during the fault some significant differences were noticed especially at the beginning of the fault and at the clearance of the fault. As opposed to many analytical models assuming the magnetic parameters invariable, FEM based co-simulation of DFIG enables the prediction of instant values of the parameter. It clearly shows us that FEM model is more accurate than the analytical model and is inevitable to analyze DFIG with FEM model to analyze fault conditions. Hence the coupled simulation results are evidently promoted in this investigation.

In conclusion there is a need for extended study which takes into account whole wind turbine components such as DFIG with FEA model, power converters, saturable step-up transformer and grid interface during and after the fault to find a key solution for DFIG based wind turbine. This section presented detailed analysis of DFIG wind turbine system components under both symmetrical and asymmetrical type fault conditions. The results were obtained from coupled simulation. Some meaningful results are obtained and can be considered as being presented first time in literature.

CHAPTER 4

EXPERIMENTAL STUDY

The experimental study is carried out to see the effects of grid faults on power converters and on DFIG wind turbine. Another goal is of course verification of simulation results.

In experimental setup, the DFIG is driven by squirrel-cage induction motor. The squirrel-cage induction motor represents wind gives torque to the DFIG. The DFIG was selected 7.5 Hp/1500 rpm for experimental study. The induction motor has a driver. The stator of DFIG is directly connected to the grid which has 380 V line-to-line voltage and 50 Hz frequency. The rotor of DFIG is connected to the back-to-back converter. So the power of rotor flows via rotor side and grid side converters to the grid. The each power converter is designed to provide 18.5 kW power to make sure power converters can still remain connected even if faults occur. Experimental study is carried out for healthy and one phase-ground fault condition. In this section, the experimental setup and PCB design process of power converters will be given. Then experimental results will be shared. Finally some inferences will be provided and the results are discussed.

4.1 Power Converter Design

The PCB design of power converters are created with Proteus PCB software. The converter consists of two PCBs; controller stage and power stage.

4.1.1 Controller PCB

The controller PCB consists of IGBT gate driver circuits, analog digital converter (ADC) signal conditioning circuits, CAN communication circuit, signal inverting and dead time generation circuit, power stage for different voltage levels and error detection circuit.

4.1.1.1 **IGBT Gate Driver Circuit**

The IGBT gate driver circuit used in the converter is shown in Figure 4.1. This gate driver has isolated output from input which is necessary for upper switches of power converter. The npn transistor is used to provide high current to IGBT for fast turning on and the pnp transistor is used to IGBT fast turning off by applying -15 V to the IGBT.

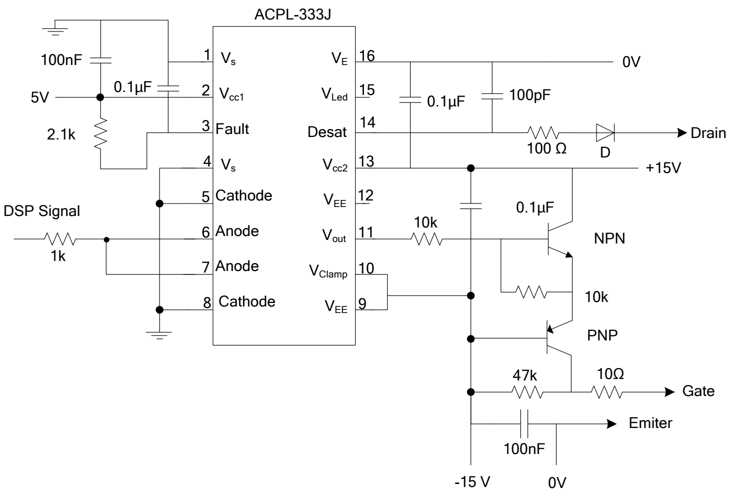

Figure 4.1 The circuit scheme of IGBT driver

4.1.1.2 **ADC Signal Conditioning Circuit**

In experimental study, digital signal processor (DSP) is used for controlling the power converters. Texas Instrument fixed point DSP–TMS320F2812 microprocessor is chosen to implement the study. This DSP has 16 ADC channel to read analog signals between 0 to 3V. To read AC signals those have 0V mean value and has negative voltage, it is required adding offset value. The ADC signal conditioning circuit provides 1.5V offset on AC feedback signals which are the outputs of voltage and current sensors.

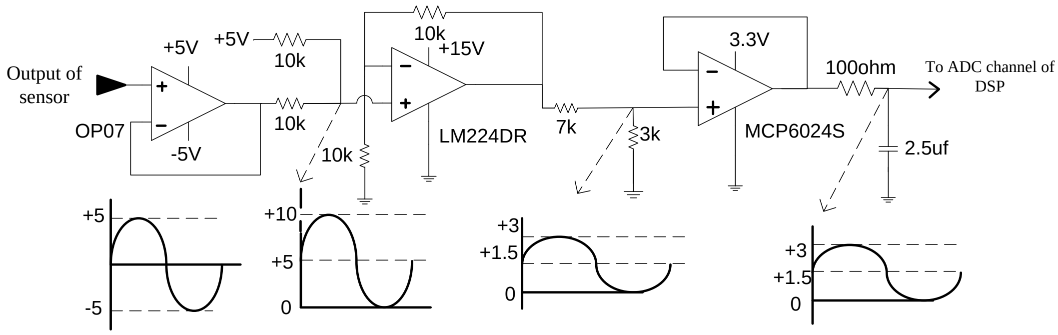

Figure 4.2 The circuit scheme of ADC signal conditioning

Figure 4.2 shows the circuit scheme of ADC signal conditioner. The output voltage of the circuit has 1.5V offset and also ADC channels of DSP are protected from high voltages as can be seen from the figure.

4.1.1.3 **Error Detection Circuit**

The error detection circuit is designed to protect power converters from high currents. The circuit consists of analog ICs which has very fast response time. This feature enables us to protect converters in a very short time from high currents by turning off the all IGBTs. The current sensors output comes to the circuit then it is compared with threshold value. If the current is more than the threshold, the output of the circuit becomes zero and this disables the IGBT driving signal. So all IGBTs will turned off and high currents will be blocked. By using latch, even if the error status ends, the IGBTs will never turn on again without sending reset signal from DSP.

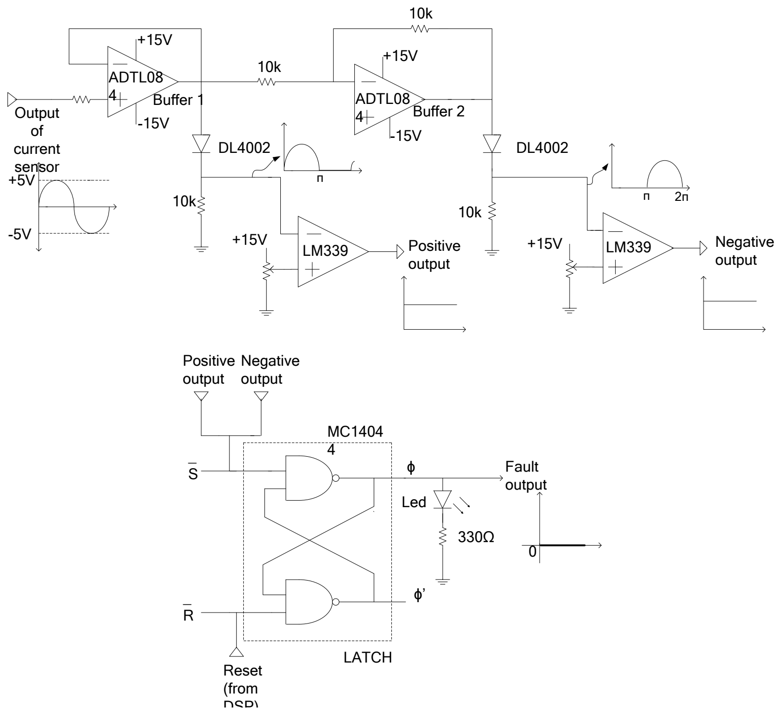

Figure 4.3 The circuit scheme of fault detection

The designed pcb of control stage can be seen from Figure 4.4. Figure 4.5 shows the control stage photo.

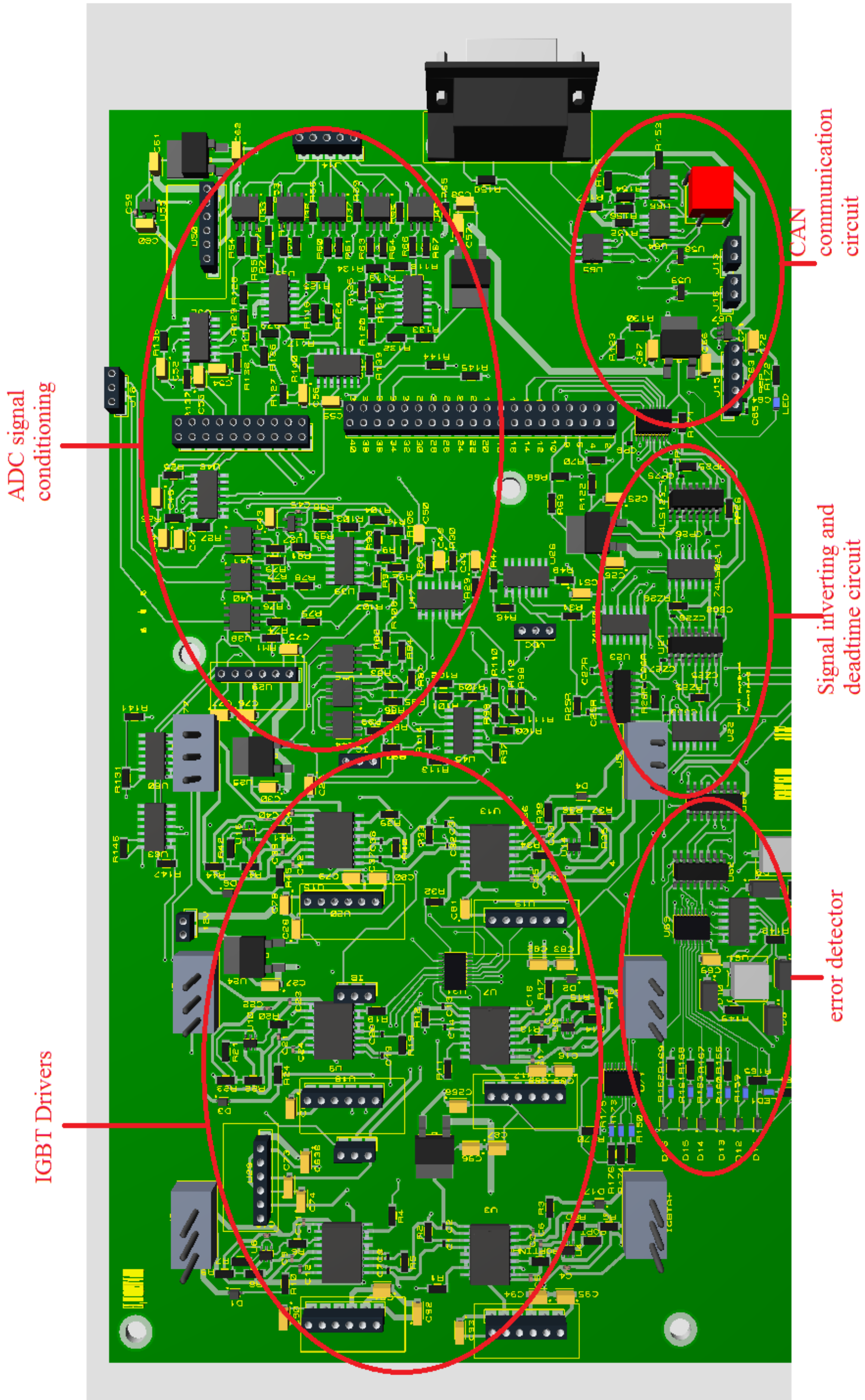

Figure 4.4 The PCB design of control stage

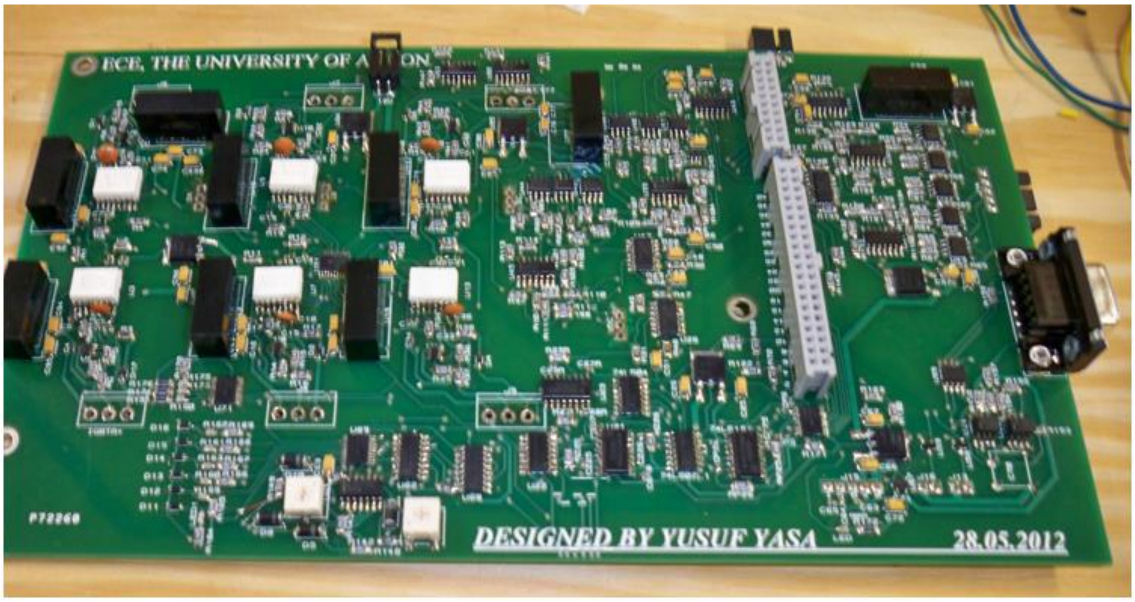

Figure 4.5 The control stage PCB

4.1.2 **Power PCB**

The power stage of the converters is designed with 2-level 6 IGBT topology as mentioned earlier. Figure 2.8 shows the power circuit scheme. Figure 4.6 and Figure 4.7 show the design of power stage which has 6 IGBTs, 8 470uF capacitor (2 groups with 4 parallel), snubber capacitors, current sensors and voltage sensor.

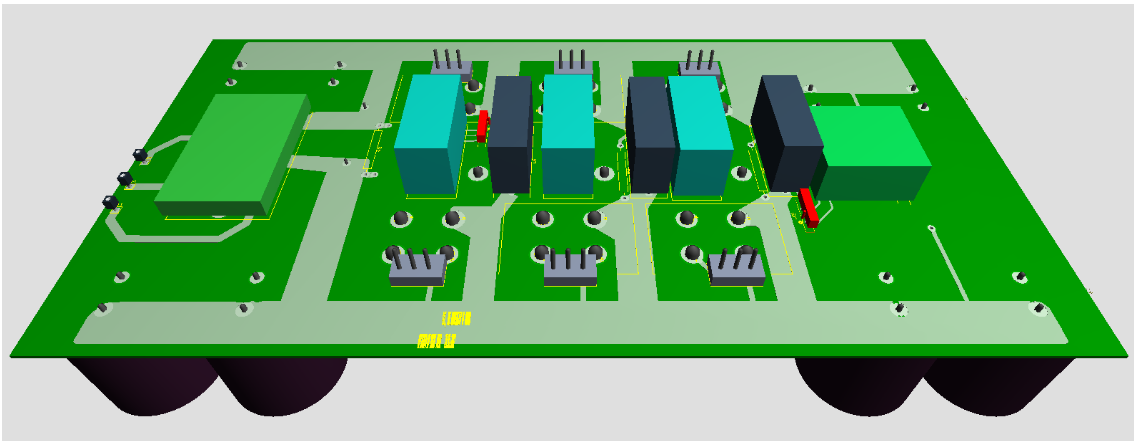

Figure 4.6 The power PCB from top view

There is an additional sensor PCB which is used for synchronization to the grid from stator of DFIG and grid side converter (GSC). In GSC, there are three series inductors to enable current flow from GSC to the grid. Synchronization is very important to work properly in this application. It would be useful to repeat again here that there are two power converters. These are RSC and GSC which are connected each other through DC link.

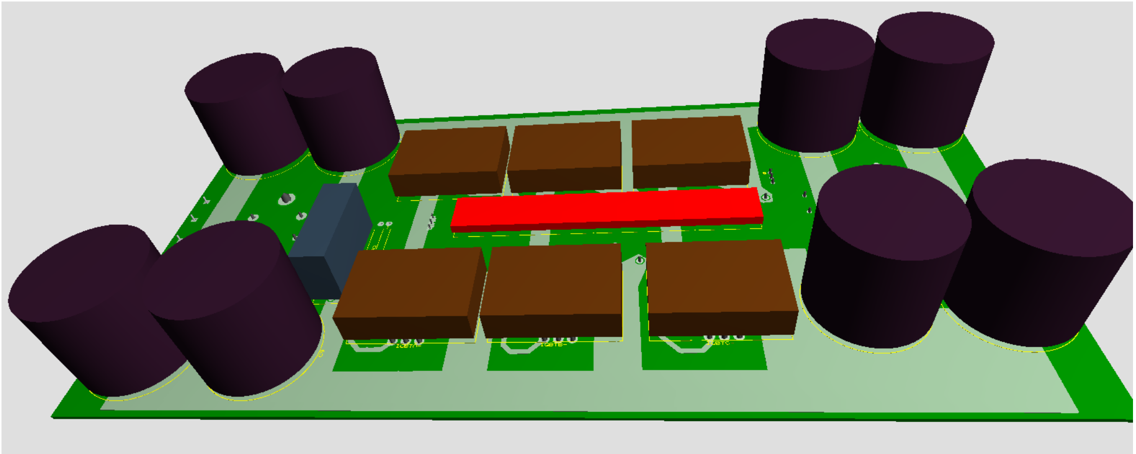

Figure 4.7 The power PCB from bottom view

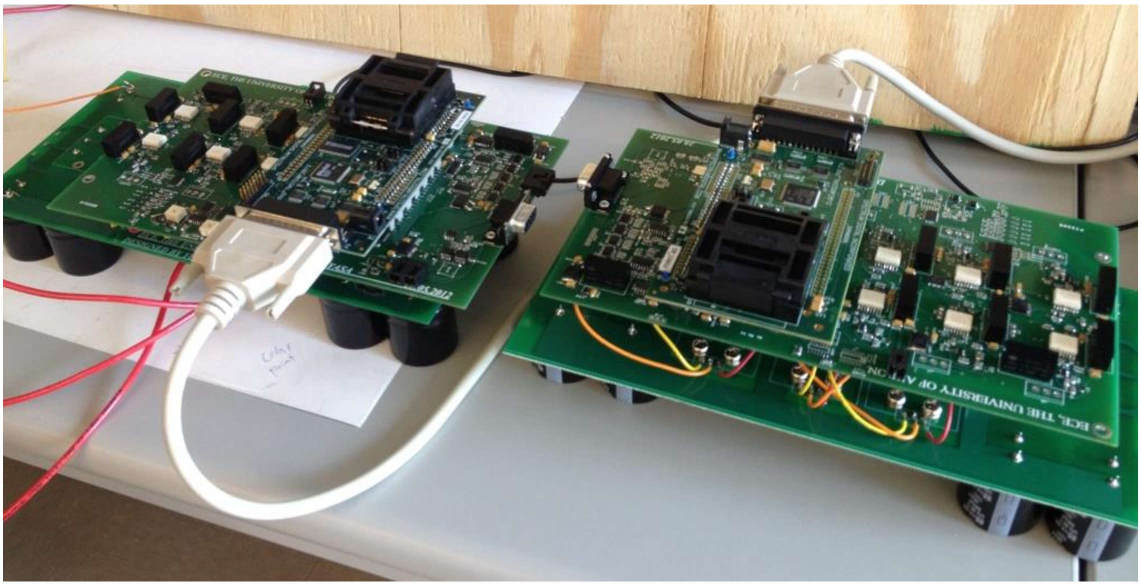

Figure 4.8 The power converters

RSC and GSC power converters are shown in Figure 4.8 which has DSP, control and power PCBs for each side. The experimental setup can be seen from Figure 4.9. The two DSPs for RSC and GSC are controlled with two PCs. The IM represents induction machine and its driver is IM driver. The DFIG and IM can be seen from Figure 4.10

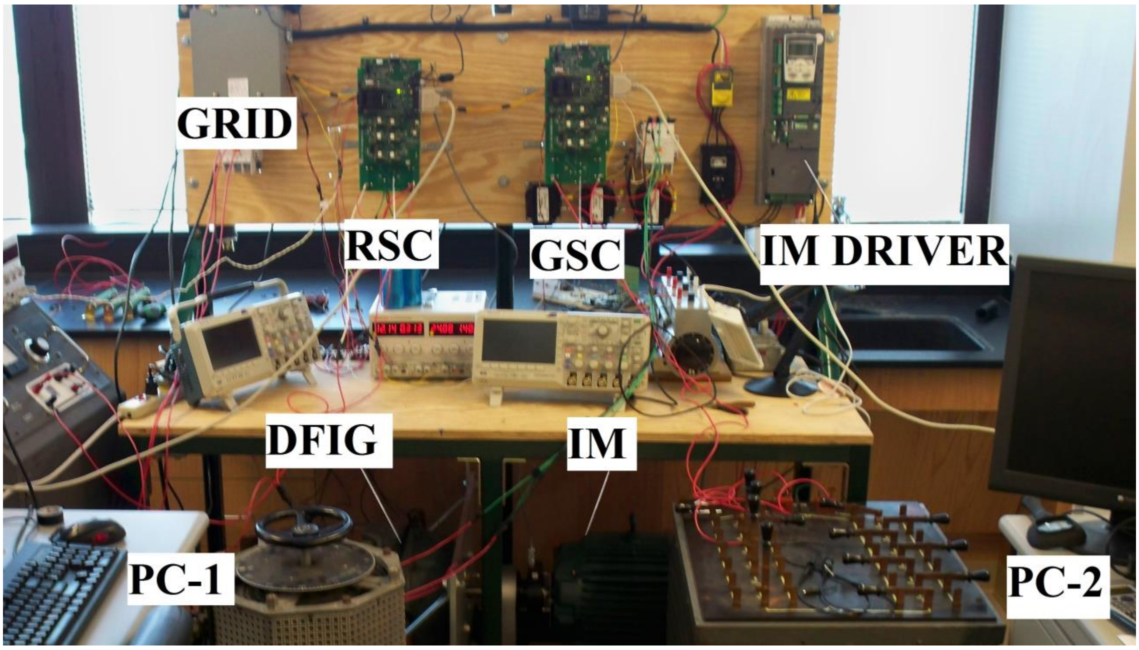

Figure 4.9 The experimental setup

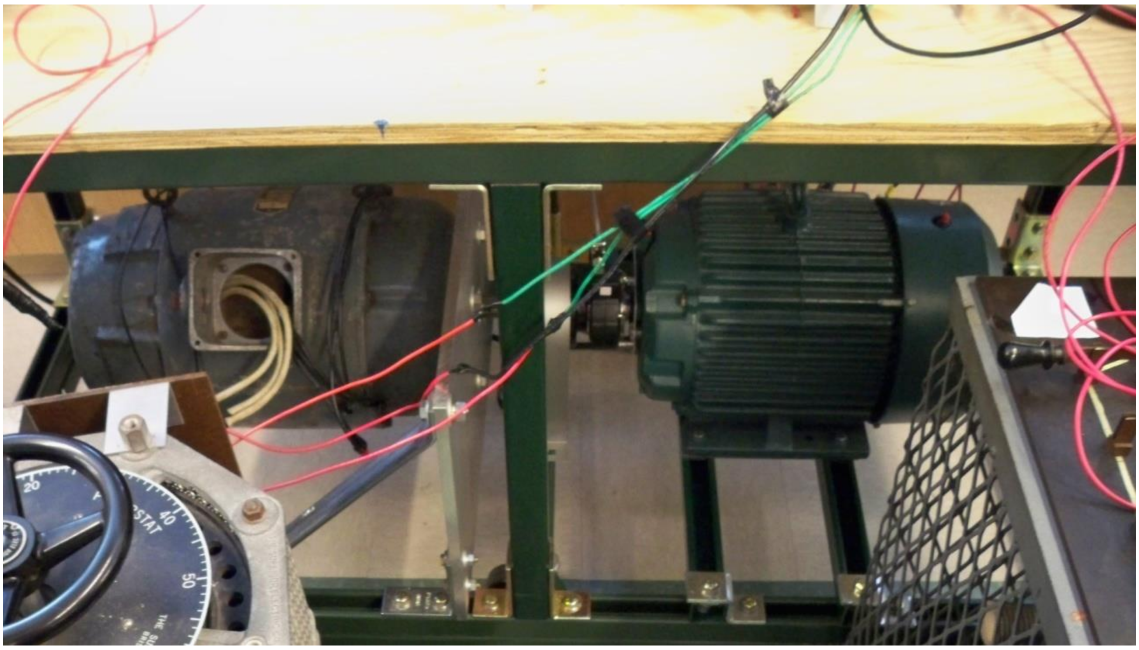

Figure 4.10 The experimental setup-DFIG and IM

4.2 Experimental Results

The experimental results are obtained with two operations; healthy and faulty conditions. One phase-ground fault operation is only implemented because it has the most probability to occur in the grid according to the survey compare to other fault types as mentioned before.

4.2.1 **Healthy Condition**

The experimental setup was programmed to give constant power from DFIG to the grid. Back-to-back converter should give power from rotor to grid or from grid to rotor. Below synchronous speed, rotor takes power from grid. Above synchronous speed, rotor gives power to the grid. Back to back converter is analyzed in these two conditions.

4.2.1.1 **Below synchronous speed (wr<ws)**

Firstly GSC is programmed to regulate DC bus voltage. Grid side converter works as a pwm-rectifier during this operation. The experimental data can be seen from Figure 4.11. DC bus regulation is implemented by q axis reference current. d axis reference is entered at zero as mentioned earlier. DC bus voltage is regulated to 65 V.

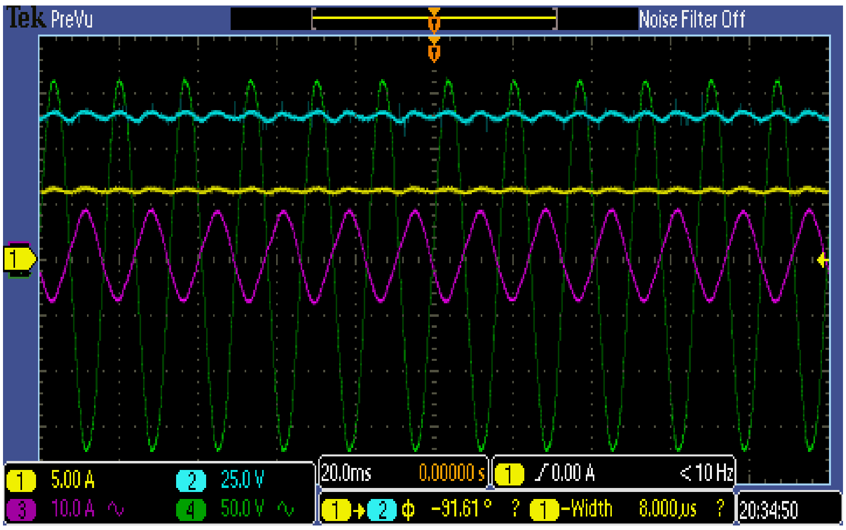

Figure 4.11 DC bus regulation with Grid Side Converter. DC bus voltage (blue), dc output current (yellow), phase A voltage (Green) and phase A current (pink)

As can be seen from Figure 4.11, phase angle between voltage and current of phase-A is around 180°. So this indicates that d axis current is around zero. And the wave shape of the phase current is sinusoidal.

Secondly RSC is programmed to regulate rotor phase currents. The RSC output currents for 15A q axis and 0A d axis references in 1000 rpm mechanical speed are shown in Figure 4.12 [34].

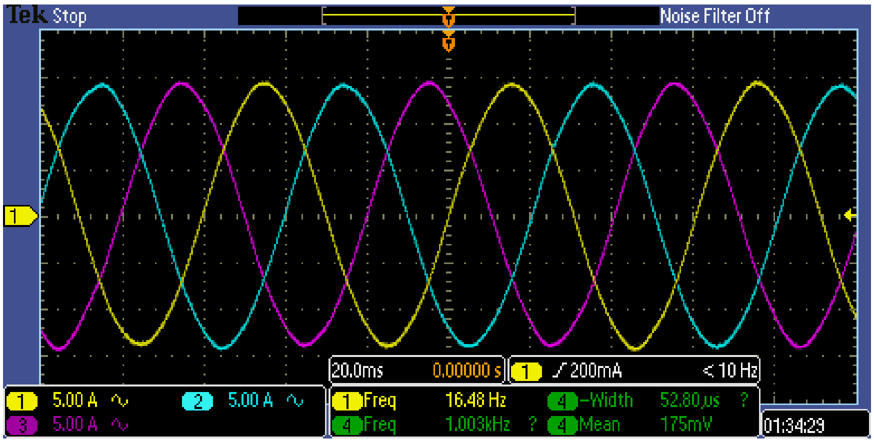

Figure 4.12 Rotor phase currents

4.2.1.2 Above synchronous speed (wr>ws)

Above 1500 rpm, DFIG gives power to grid not only from stator, but also from rotor. During this operation, RSC works as a PWM rectifier and GSC works as an inverter. GSC should have ability to synchronize with grid voltages during this operation. The experimental result for GSC synchronization with grid can be seen from Figure 4.13

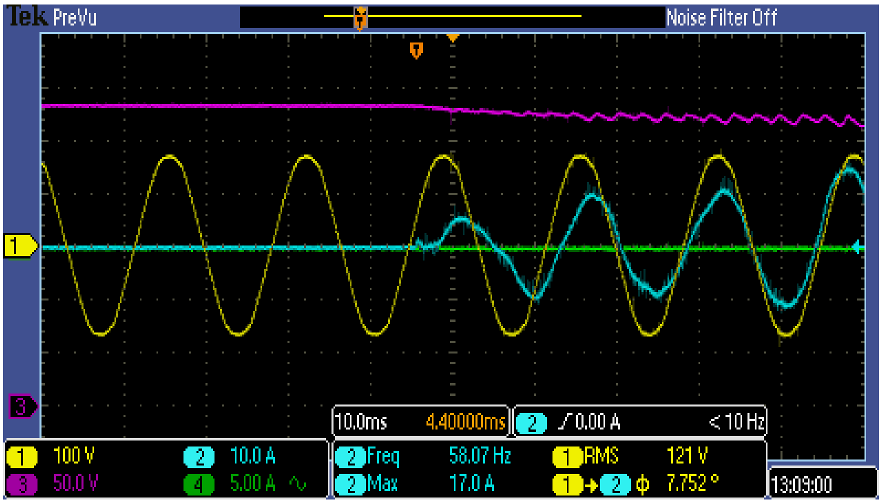

Figure 4.13 Grid synchronization of phase-A with GSC phase-A current (blue), voltage (yellow) and DC bus (pink)

4.2.2 One Phase-Ground Fault Condition

One phase-to-ground fault is a common fault type in grid, as mentioned before. So because of that, one phase-ground fault is implemented in experimental study to see the effect of this fault on RSC that is connected to the rotor windings.

One phase-to-ground fault occurred in Phase-C on secondary side of step-up transformer in coupled simulation study. So the voltage of phase-C on secondary side is considered zero. In that case, the coupled simulation results show that, the voltage level in phase-C on primer side drops to around 40% of healthy condition, as shown in Figure 3.30.

To get realistic results, phase-C is connected to ground with a 10 ohm resistance, while phase-A and phase-B is connected to grid. The circuit scheme is shown in Figure 4.14. To connect 10 ohm resistance and to disconnect phase-C of grid from stator, a proper contactor is used. This contactor has NO (normally open) and NC (normally closed) contacts.

During the experimental study for fault, DC bus is kept constant at 65 V dc. Also speed of generator is kept constant by squirrel-cage induction motor.

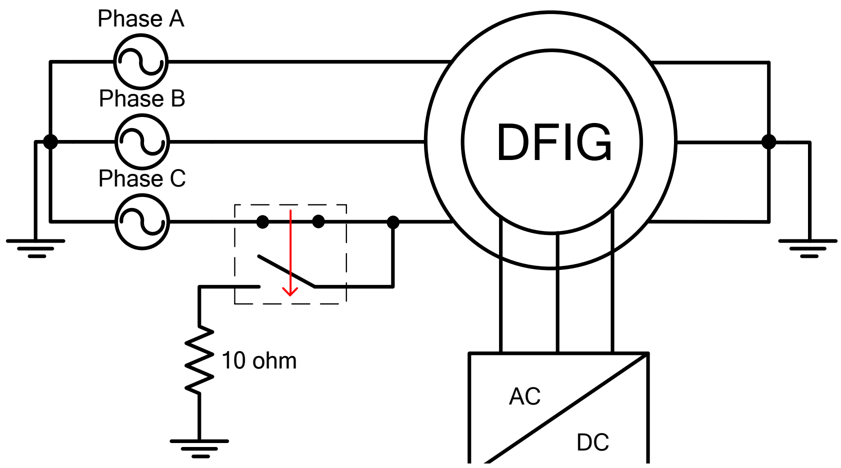

Figure 4.14 A circuit scheme of implementing one phase-ground fault

During fault, phase-C voltage of stator drops to 40% of healthy condition as expected in experimental study, is shown in Figure 4.15. Fault continues upto 6 cycles which is around 120 ms. The rotor phase-A current in this case is shown in Figure 4.16.

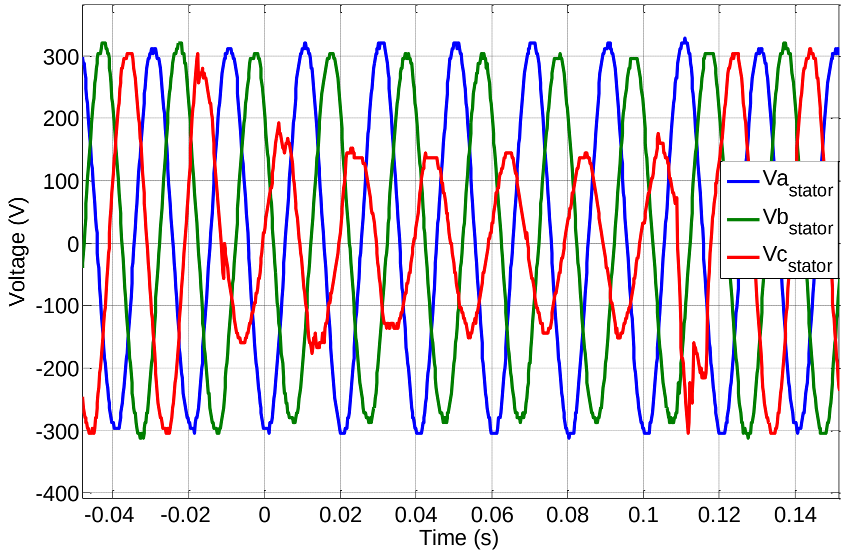

Figure 4.15 Stator voltages during one phase-ground fault in experimental study

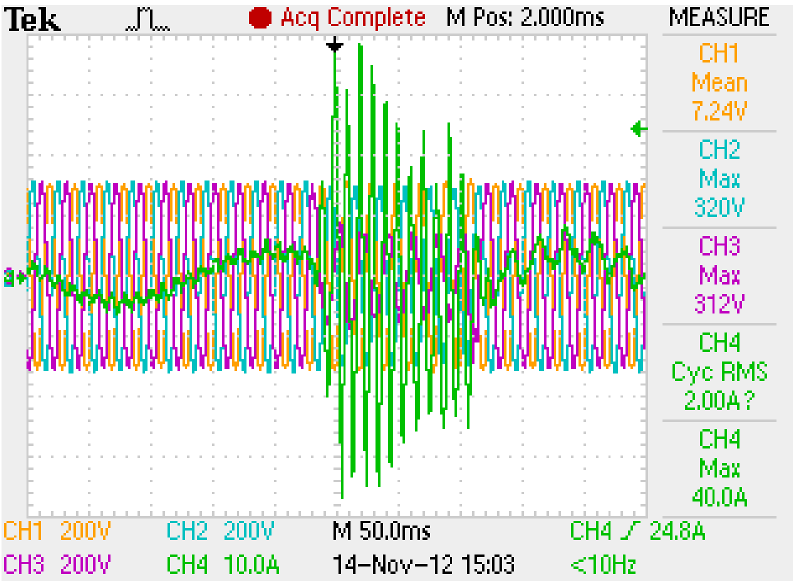

Figure 4.16 Grid voltages and rotor phase-A current (green) during one phase-to-ground fault

It can be obtained from Figure 4.16 and Figure 4.17, the rotor current is affected too much during fault, especially at the beginning of the fault where the current of rotor phase-A reaches to around 40 A, that is four times higher than the current in healhy condition. It can be said, the RSC should be protected from this high current during fault to prevent damaging[35].

Also, the q and d axis of rotor phase currents are obtained by using online data acquisition during fault, as shown in Figure 4.18.

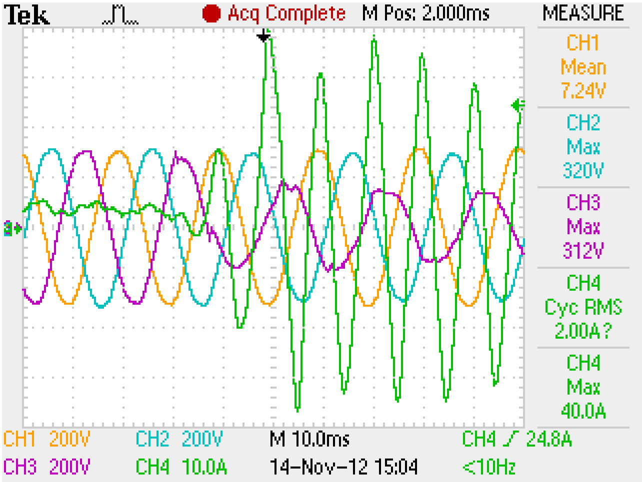

Figure 4.17 Grid voltages and rotor phase-A current (green) during one phase-ground fault

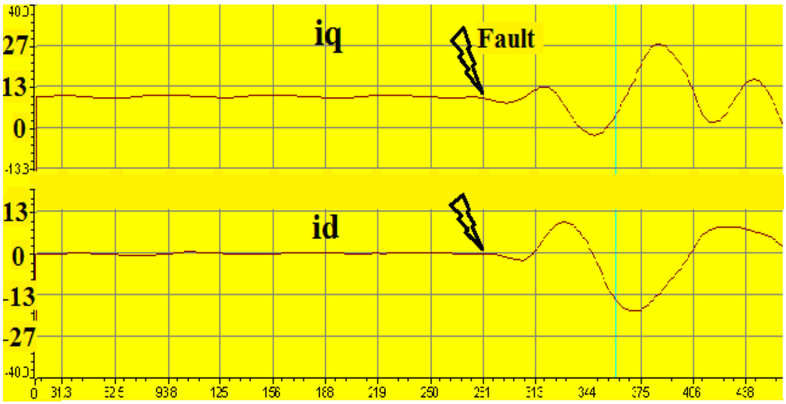

Figure 4.18 Q and d axis current of rotor phases during fault

The flux curves of stator are obtained from stator voltages with (4.1)

$$\psi_s = \int (V_s - i_s R_s) dt \tag{4.1}$$

In (4.1), V_s and i_s are stator phase voltage and stator phase current and R_s is a resistance of the phase. Because of the low voltage drop across the phase resistance even during fault condition, the voltage drop across phase resistance can be neglected. So the q and d axis fluxes of stator can be seen from Figure 4.19. At 0.23 second, the one phase-to-ground fault occurs.

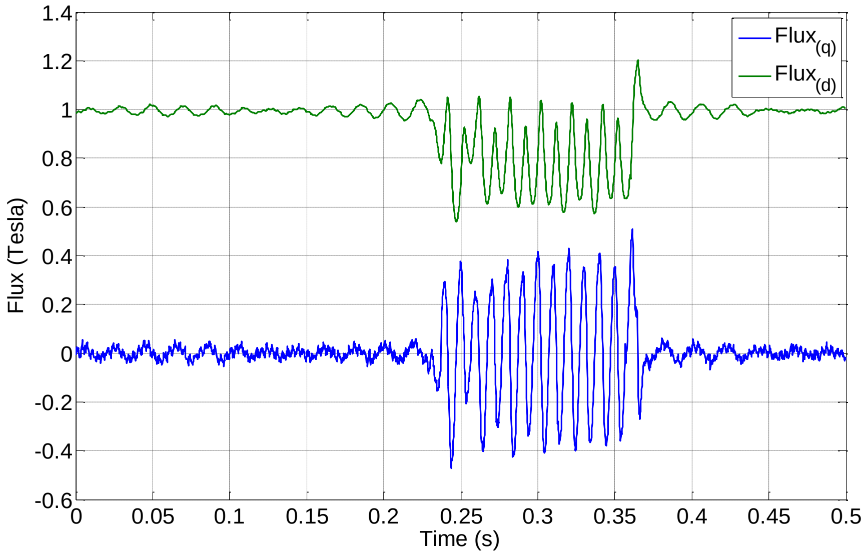

Figure 4.19 Q and d axis fluxes of stator

The FFT analysis of stator flux of phase-C that is obtained from experimental study is shown in Figure 4.20. Table-4.1 shows the FFT analysis results in each phase's fluxes of stator during one phase-ground fault.

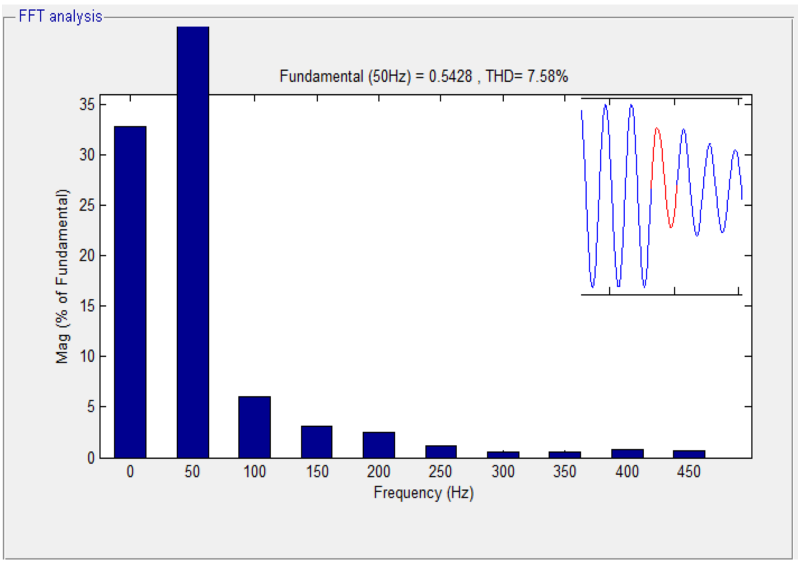

Figure 4.20 FFT analysis of stator phase-C flux during one phase fault

TABLE-4.1: Most dominant harmonics of stator fluxes during one phase fault (estimated from experimental study)

	Phase-A	Phase-B	Phase-C
0 Hz(Dc)	4.56%	4.03%	32.79%
50 Hz(Fnd)	100%	100%	100%
100 Hz	0.64%	1.24%	6.04%

The experimental study for stator fluxes shows that, all phases have same most dominant harmonic frequency with simulation result (Table-3.3 and Table-4.1).

To compare simulation and experimental study for rotor fluxes, some DFIG machine parameters must be known, as suggested by (4.2) and (4.3).

$$\psi_{dr} = \frac{L_r}{L_m}\left[\psi_{ds} - L_s(1-\frac{{L_m}^2}{L_s L_r})I_{dr}\right] \tag{4.2}$$

$$\psi_{qr} = \frac{L_r}{L_m}\left[\psi_{qs} - L_s(1-\frac{{L_m}^2}{L_s L_r})I_{qr}\right] \tag{4.3}$$

Because the inductance parameters are unknown, it is unable to estimate rotor fluxes from stator fluxes. Even if these parameters are known, during fault there might be some saturation in machine, so the machine parameters might be different from healthy condition. To get reliable flux data, only solution is to get these parameters online. There are some techniques to obtain inductance data online in literature, putting magnetic flux sensor in machine is one of these solutions.

The work will be extended in the future to estimate the rotor fluxes during the faults and developing enhanced control algorithms accordingly.

CHAPTER 5

RESULTS AND DISCUSSION

The DFIG wind turbine system is analyzed for both healthy and faulty conditions. The results are provided from MATLAB-Simulink and Coupled Simulation which is used finite element model of DFIG. The healthy condition results of DFIG wind turbine is coherent with MATLAB-Simulink and coupled simulation. But during fault condition, the results become different from each other; the reason of this difference is thought that some system components saturate magnetically under fault condition. MATLAB-Simulink based simulation components of system are created with the linear function or invariable parameters, but coupled simulation uses the finite element model to analyze. The results of the coupled simulation have shown that the behavior of DFIG internal parameters like inductances and fluxes become very different from healthy condition. So DFIG cannot be modeled with the same model with healthy condition, whereas many papers in literature use the DFIG healthy condition model even in fault to analyze fault condition. In addition, it is inferred from the simulations that the step-up transformer has an important role during fault. So it must be taken into account during analysis [36].

Some meaningful variations in internal parameters of DFIG are seen during fault. When the fault occurs, self-inductances of stator and rotor will be in the same phase. For stator fluxes during fault, stator fluxes will have DC component and 2^{th} harmonic in each phase. In rotor fluxes, 5^{th} and 9^{th} harmonic will appear. It would be possible to limit the high currents in the rotor windings during the fault through eliminating harmonics from stator and rotor fluxes. These results were founded for the first time in the literature. It is believed that these findings will contribute to develop new enhanced control techniques which enables the DFIG to remain connected to the grid during fault conditions. Remaining connected to the grid is mandatory in most of countries in

Europe and America. Besides that, some grid codes demand that the grid is supported by providing reactive power from the wind turbines and farms during fault. Experimental setup is developed for the 7.5Hp DFIG. Back to back converters are designed and connected to the rotor of DFIG. Healthy condition and one phase-ground fault condition which has most probability to occur are implemented in the experiment. Some simulation results are verified with experimental results[37].

REFERENCES

[1] World wind energy association (2010), World Wind Energy Report 2010.

[2] TEİAŞ (2012), "Türkiye'de Elektrik Enerjisi Kurulu Gücü" October 2012.

[3] TUREB (2012), "Türkiye Rüzgar Enerjisi İstatistik Raporu" July 2012.

[4] Pannell Graham, Atkinson David J. and Zahawi Bashar (2010), "Analytical Study of Grid-Fault Response of Wind Turbine Doubly Fed Induction Generator", IEEE Transactions on Energy Conversion, 2010, 1081-1091.

[5] Wei Zhang, Peng Zhou and He Yikang (2008), "Analysis of the By-Pass Resistance of an Active Crowbar for Doubly-Fed Induction Generator Based Wind Turbines under Grid Faults", Electrical Machines and Systems Conference, 2008.

[6] Seman Slavomir and Jouko Niiranen (2006), "Ride-Through Analysis of Doubly Fed Induction Wind-Power Generator under Unsymmetrical Network Disturbance", IEEE Transactions on Power Systems, 2006, 1782-1789.

[7] Wessels Christian, Gebhardt Fabian and Friedrich Fuchs Wilhelm (2011), "Fault Ride-Through of a DFIG Wind Turbine Using a Dynamic Voltage Restorer During Symmetrical and Asymmetrical Grid Faults", IEEE Transactions on Power Electronics, 2011, 807 – 815.

[8] Morren Johan and W. H. de Haan Sjoerd (2005), "Ridethrough of Wind Turbines With Doubly-Fed Induction Generator During a Voltage Dip," IEEE Transactions on Energy Conversion,2005, 435-441.

[9] Abbey Chad and Joos Géza (2007), "Supercapacitor Energy Storage for Wind Energy Applications," IEEE Transactions on Industry Applications, 2007, 776-769.

[10] Flannery Patrick S. and Venkataramanan Giri (2009), "Unbalanced Voltage Sag Ride-Through of a Doubly Fed Induction Generator Wind Turbine with Series Grid-Side Converter," IEEE Transactions on Industry Applications, 2009, 1879 – 1887.

[11] Xiang Dawei, Ran Li, Tavner J. Peter and Yang Shunchang (2006), "Control of a Doubly Fed Induction Generator in a Wind Turbine During Grid Fault Ride-Through," IEEE Transactions on Energy Conversion, 2006, 652.

[12] Lima Francisco K. A., Luna Alvaro, Rodriguez Pedro, Watanabe Edson H. and Blaabjerg Frede (2010), "Rotor Voltage Dynamics in the Doubly Fed Induction

Generator during Grid Faults," IEEE Transactions on Power Electronics, 2010, 130-118.

[13] Santos-Martin David, Rodriguez-Amenedo Jose Luis, Arnaltes Santiago (2009), "Providing Ride-Through Capability to a Doubly Fed Induction Generator under Unbalanced Voltage Dips" IEEE Transactions on Power Electronics, 2009, 1747-1756.

[14] Gomis-Bellmunt Oriol, Junyent-Ferre Adria (2008), "Ride-Through Control of a Doubly Fed Induction Generator under Unbalanced Voltage Sags," IEEE Transactions on Energy Conversion, 2008, 1036-1045.

[15] Rodriguez Pedro, V. Timbus Adrian, Teodorescu Remus, Liserre Marco, and Blaabjerg Frede (2007), "Flexible Active Power Control of Distributed Power Generation Systems During Grid Faults," IEEE Transactions on Industrial Applications, 2007, 2583-2592.

[16] Mullane Alan, Lightbody Gordon and Yacamini R. (2005), "Wind-Turbine Fault Ride-Through Enhancement (2005)," IEEE Transactions on Power Systems, 2005, 1937-1929.

[17] Mohseni Mansour, Masoum Mohammad A.S. and Islam Syed (2011), "Emergency Control of DFIG-Based Wind Turbines to Meet New European Grid Code Requirements," IEEE PES, Innovative Smart Grid Technologies, 2011,1-6.

[18] Iov Florin, Hansen Anca Daniela, Sørensen Poul and Cutululis Nicolaos Antonio (2007), "Mapping of Grid Faults and Grid Codes," Risø-r-Report, July 2007, 7-6.

[19] Tsili M. and Papathanassiou S. (2009), "A Review of Grid Code Technical Requirements for Wind Farms," IET Renewable Power Generation 2009, 308-332

[20] Erlich I., Winter W. and Dittrich A. (2006), "Advanced Grid Requirements for the Integration of Wind Turbines nto the German Transmission System," Power Engineering Society General Meeting 2006, 1-7.

[21] Kasem A.H., El-Saadany E.F., El-Tamaly H.H. and Wahab M.A.A. (2008), "An Improved Fault Ride-Through Strategy for Doubly Fed Induction Generator-Based Wind Turbines," IET Renewable Power Generation, 2008, 214-201.

[22] Erlich I. and Bachmann U. (2005), "Grid Code Requirements Concerning Connection and Operation of Wind Turbines in Germany", Power Engineering Society General Meeting 2005, 1253-1257.

[23] Mohseni Mansour, Islam Syed M. and Masoum Mohammad A. S. (2011), "Impacts of Symmetrical and Asymmetrical Voltage Sags on DFIG-Based Wind Turbines Considering Phase-Angle Jump, Voltage Recovery and Sag Parameters," IEEE Transactions on Power Electronics, 2011, 1587-1598.

[24] Krause P.C, Thomas C. H. (1965) "Simulation of Symmetrical Induction Machinery," IEEE Transactions on Power Apparatus and Systems, 1965, 1038-1053.

[25] Krause P.C, Wasynczuk Oleg and Sudhoff Scott D. (2002) Analysis of Electric Machinery and Drive Systems, A John Wiley & Sons, Inc. Publication.

[26] Sarul Hadi (2010), Elektrik Makinalarının Endüstriyel Uygulamaları, lecture notes.

[27] Texas Instruments Europe (1998), Field Orientated Control of 3-Phase AC-Motors, Literature Number BPRA073.

[28] Texas Instruments Europe (1998), Field Orientated Control of 3-Phase AC-Motors, Literature Number BPRA073.

[29] Bellini A. and Bifaretti S. (2005), "Comparison between Sinusoidal PWM and Space Vector Modulation Techniques for NPC Inverters," Power Tech, 2005, 1-7.

[30] Boldea Ion (2005), Variable Speed Generators, CRC Press.

[31] European Committee of Manufacturers of Electrical Machines and Power Electronics: http://www.cemep.org/

[32] Seman Slavomir, Niiranen Jouko and Arkkio Antero (2006), "Ride-Through Analysis of Doubly Fed Induction Wind-Power Generator Under Unsymmetrical Network Disturbance," IEEE Transactions on Power Systems, 2006, 1782-1789.

[33] Seman Slavomir, Niiranen Jouko, Kanerva Sami and Antero Arkkio (2006), "Performance Study of a Doubly Fed Wind-Power Induction Generator under Network Disturbances," IEEE Transactions on Energy Conversion, 2006, 883-890.

[34] Yasa Y., Yılmaz S. and Mese E. (2013), "Unbalanced Fault Analysis of Doubly Fed Induction Generator Drive System for Wind Turbine Applications," IEEE Applied Power Electronics Conference (APEC), 2013.

[35] Yasa Y., ISEN E., Sozer Y. and Mese E. (2013), "Analysis of Doubly Fed Induction Generator Wind Turbine System During One Phase-to-Ground Fault," IEEE European Conference on Power Electronics and Applications (EPE), 2013.

[36] Gürleyen H., Mese E. and Yasa Y. (2013), "Fault Ride Through of DFIG-Based Wind Turbine with Saturable Transformer Model," IEEE European Conference on Power Electronics and Applications (EPE), 2013.

[37] Yasa Y., Sozer Y. and Mese E. (2013), "Harmonic Analysis of Doubly Fed Induction Generator Based Utility Interactive Wind Turbine Systems during Fault Conditions," IEEE Energy Conversion Congress and Exposition (ECCE), 2013.

APPENDIX-A

APPENDIX-B

CURRICULUM VITAE

PERSONAL INFORMATION

Name Surname	: YUSUF YAŞA
Date of birth and place	: 1st August 1989 – Erzurum
Foreign Languages	: English
E-mail	: yasa@yildiz.edu.tr

EDUCATION

Degree	Department	University	Date of Graduation
Undergraduate	Electrical Engineering	Yıldız Technical University	28.07.2010
High School	Maltepe Lisesi		19.06.2006

WORK EXPERIENCE

Year	Corporation/Institute	Enrollment
2010	Yıldız Technical University	Research Assistant

PUBLICATIONS

Conference Papers

1. Yasa Y., Yılmaz S. and Mese E. (2013), “Unbalanced Fault Analysis of Doubly Fed Induction Generator Drive System for Wind Turbine Applications,” IEEE Applied Power Electronics Conference (APEC), 2013.

2. Yasa Y., ISEN E., Sozer Y. and Mese E. (2013), “Analysis of Doubly Fed Induction Generator Wind Turbine System During One Phase-to-Ground Fault,” IEEE European Conference on Power Electronics and Applications (EPE), 2013.

3. Yasa Y., Sozer Y. and Mese E. (2013), “Harmonic Analysis of Doubly Fed Induction Generator Based Utility Interactive Wind Turbine Systems during Fault Conditions,” IEEE Energy Conversion Congress and Exposition (ECCE), 2013.

4. Gürleyen H., Mese E. and Yasa Y. (2013), “Fault Ride Through of DFIG-Based Wind Turbine with Saturable Transformer Model,” IEEE European Conference on Power Electronics and Applications (EPE), 2013.

5. Mese E., Yasa Y., Akca H., Aydeniz M.G. and Garip M. (2012) “A new electric accessory drive system for hybrid electric vehicles”, IEEE Energy Conversion Congress and Exposition (ECCE), 2012.

6. Mese E., Tezcan M., Ayaz M., Yasa Y. and Yilmaz K. (2012), “Design Considerations for Dual Winding Permanent Magnet Synchronous Machines,” IEEE Energy Conversion Congress and Exposition (ECCE), 2012.

7. Yasa Y., Sahin E., Acar C., Gozutok R. A., Fırat E. and Mese E. (2013), “The Driver Design and Implementation of Electric Motor for High Performance Servo Applications,” EVK2013.

8. Yasa Y. and Mese E. (2011), “Charge Balancing Systems for Serial Connected Lithium Ion Battery Cells,” EVK2011.

Projects

1. “Design and Control of Dual Winding Electrical Machine for Hybrid Electric Vehicle,” TUBİTAK-110E111.

2. “Investigating Battery and Capacitor Sizing Problems with More Efficient Power Flow Control Techniques for Sustainable Hybrid Electric Vehicle Development,” European Union Marie Curie Project.